Summer 8-19-2022

A Study of Red Snapper (Lutjanus Campechanus) Ecology in the Northern Gulf of Mexico and the Effect of Variable River Outflow Using Stable Isotope Analysis of the Food Web and Eye Lenses

Caitlin C. Slife
University of Southern Mississippi

A STUDY OF RED SNAPPER (LUTJANUS CAMPECHANUS) ECOLOGY IN THE NORTHERN GULF OF MEXICO AND THE EFFECT OF VARIABLE RIVER OUTFLOW USING STABLE ISOTOPE ANALYSIS OF THE FOOD WEB AND EYE LENSES

by

Caitlin Slife

A Dissertation
Submitted to the Graduate School,
the College of Arts and Sciences
and the School of Ocean Science and Engineering
at The University of Southern Mississippi
in Partial Fulfillment of the Requirements
for the Degree of Doctor of Philosophy

Approved by:

Dr. Kevin Dillon, Committee Chair
Dr. Wei Wu
Dr. Frank Hernandez
Dr. Kelly Robinson

August 2022

Published by the Graduate School

ABSTRACT

In the Mississippi Bight and surrounding waters, river outflow impacts the basal resources of the Red Snapper food web, altering carbon sources and impacting prey and predator isotopes. In this study, the impact of riverine outflow on nutrients, particulate organic matter (POM), and physical water parameters on Red Snapper and their food web was analyzed using stable isotope and stomach content analysis over 5 years. The Mississippi, Pearl, Pascagoula, and Mobile rivers were included in the analysis of river impact. The Mississippi and Mobile rivers were found to significantly impact nutrients and POM in the region. River outflow was also broken out by high, medium, and low outflow regimes. Trends found in POM and zooplankton isotopes related to river outflow reflected the isotope values of Red Snapper and their prey, and Red Snapper body condition improved under moderate to low outflow regimes. Under these conditions diet changed enough to reflect in the isotopes of Red Snapper muscle tissue, though different diet analysis techniques did not agree on how diet changed. With increased river outflow due to climate change and more frequent and longer openings of river diversions, managers must understand how Red Snapper habitat use and dietary shifts change. Red Snapper eye lenses were compared to otoliths to determine if they could be used as an aging tool, and individual lamina of the eye lenses were analyzed for stable isotopes. Though eye lenses were not particularly useful as a primary aging tool, the successive layering of lens lamina over time was consistent enough to determine a general age. Stable isotope analysis of eye lens lamina captured ontogenetic shifts prevalent in the literature. The use of eye lenses provides the opportunity to use a single fish instead of

many from different cohorts to study changes in diet and habitat use at ecologically and ontogenetically important time periods, under different outflow regimes.

ACKNOWLEDGMENTS

There are many people without whom which this dissertation would not have come to fruition. I would like to thank, first and foremost my advisor Dr. Kevin Dillon who has provided constant support throughout this process and had helped me grow in confidence and self-reliance. Under his guidance I have learned to trust myself and ask better questions. I would also like to thank Dr. Frank Hernandez and Dr. Kelly Robinson for their kindness and willingness to discuss any and all issues or questions I had when planning various projects and making them actually doable. I would like to than Dr. Wei Wu for her help with modeling, and coding. Under her tutelage, my knowledge of statistics and models has vastly expanded. I would also like to thank Gary Grey for taking much more time that anticipated helping me determine how to age Red Snapper eye lenses and for being my second eye lens reader.

I also want to thank the various graduate students and technicians who put in extensive time and work on this project. Paul Grammar, Chris Lapniewski, Trevor Moncrief, Jennifer Green, Angie Hoover, Andrea Leontiou, Gary Grey, Dyan Gibson, and Anna Millender for their tireless collection and processing of fish and prey samples; Andrew Evans, Laura Stewart, Stephanie Lorenze, and Jeremy Johnson for DNA processing and barcoding analysis; Captain Rick Block and the crew of the R/V Jim Franks for providing vessel support; Jim Franks, Amanda McGehee, Patrick Graham, and the project's lead investigators Read Hendon and Jill Hendon; and most especially Morgan Frank for running all my isotope samples, keeping the whole lab organized and on track, and providing a friendly face at the lab every day.

Lastly, I would like to thank my family. This dissertation has been a long time coming and has not been an easy road. You all have provided me with constant emotional support, made sure I stayed afloat, and never complained when I needed a sounding board to bounce ideas off of. Thank you, Dad, especially, for taking the time to read through my drafts and provide feedback when I needed a fresh set of eyes, and Mom for making sure I didn't forget to be a human while also being a graduate student. Last but not least, I want to thank my fiancé, Michael Hill. Even though you have no idea what I'm talking about, you are always willing to let me go on about fish eyes or my most recent plot, and you always ask good questions. You are a never ending source of love, patience, and support and have made the end of this process much less stressful than it could have been.

FUNDING

Funding for this project was provided by the National Fish and Wildlife Foundation through the Mississippi Department of Marine Resources and the Mississippi Department of Environmental Quality and the University of Southern Mississippi. The Funding sources were not involved in design or completion of the study and the views and conclusions contained herein are those of the author and should not be interpreted as representing the options, views or policies of the National Fish and Wildlife Foundation or the University of Southern Mississippi.

DEDICATION

I would like to dedicate this work to my parents Harry and Leslie Slife, and my fiancé Michael Hill, who have kept me afloat, and provided constant patience, love, and support.

TABLE OF CONTENTS

LIST OF TABLES

LIST OF FIGURES

CHAPTER I – INTRODUCTION

1.1 River impact on the Northern Gulf of Mexico

The Mississippi River delta and Mississippi Sound are biologically productive ecosystems due to extensive wetlands and estuaries along the coast and high freshwater and nutrient delivery from several major rivers that flow into the region. The Mississippi River, the largest contributor of fresh water to the area, is the largest source of nutrients and organic material to the Northern Gulf of Mexico (NGOM) and is estimated to have the seventh largest particulate load in the world (Milliman 2001; Santschi et al. 2007; Hypoxia Task Force 2016). However, there are several smaller rivers that contribute to the north central GOM, including the Pearl and Pascagoula rivers which lie between the Mobile Bay system and the Mississippi River delta. Recent studies have shown that these smaller more regional rivers may have a greater contribution to the north central NGOM than the Mississippi river, despite its significantly larger outflow (Sanial et al. 2019) (Fig. 0.1). The terrestrially derived nutrients delivered via these rivers into the NGOM fuel high wetland and phytoplankton productivity, in turn supporting expansive fisheries which earned the region the moniker “the fertile fisheries crescent” in the 1960’s (Gunter 1963).

The amount of nitrogen and phosphorus input to the NGOM from the Mississippi River and coastal watersheds during seasonal outflow is positively correlated with the percent of land used as cropland and population density in the drainage area, as these nutrients are primarily derived from nonpoint pollution sources from fertilizer and waste (Mitsch et al. 2005; Turner et al. 2007). As of 2007, the average annual total nitrogen and phosphorus fluxes from the Mississippi River are over 1.4 million and 140,000

metric tons respectively (Aulenbach et al. 2007). Nitrate (NO3) flux to the coastal zone tripled from 1970-2000 due to intensified agricultural activity (Goolsby et al. 2001; Goolsby et al. 2000). The dissolved nitrogen delivered by the Mississippi River has a very high concentration of nitrate (typically over 100 μM at the mouth of the Southwest Pass) (Goolsby et al. 2001; Dagg and Breed 2003); however, contributions of waters from the Pearl and Pascagoula rivers, which have much lower dissolved inorganic nitrogen concentrations, result in much lower nutrient concentrations in the region than would be anticipated by impacts purely from the Mississippi River (Dortch et al. 2007). Preliminary analyses of nutrients in NGOM have shown increased fluxes of nutrients from these rivers during periods of high outflow directly influencing surface waters with decreasing impacts with distance from shore, similar to previous studies (Turner et al. 2007; Lohrenz et al. 2008; Rabalais and Turner 2019) but increasing concentrations of nitrate with increasing depth, likely due to nutrient remineralization from microbial respiration fueled by sinking particulate organic matter (Rahav et al. 2013).

The particulate organic matter (POM) pool is primarily composed of plankton cells and waste from organisms produced in estuarine and marine environments, and detritus from riverine sources (Kendall et al. 2001; Wang et al. 2004). In summer months, high phytoplankton productivity in surface waters fertilized by riverine nutrients, coupled with strong water column stratification can result in hypoxic bottom waters (dissolved oxygen concentration <2 mg/L) due to bacterial decomposition of sinking organic matter from the upper water column (Trefry et al. 1994; Bianchi et al. 2010; Rahav et al. 2013). This seasonal pattern of hypoxia creates a dead zone during most summers along the Louisiana shelf, extending from the Mississippi River delta west to

Texas (Bianchi et al. 2010; Sanial et al. 2019). Similarly, nutrients from the various rivers east of the Mississippi River delta as well as some input from the Mississippi River itself cause hypoxic conditions in the Mississippi Bight (Dzwonkowski et al. 2018). Bottom water hypoxia in the Mississippi Bight may be further exacerbated by sporadic freshwater releases through river diversions and flood control structures along the Mississippi River such as the Bonnet Carré Spillway (Parra et al. 2020). Riverine outflow exerts control on water residence times, salinity, turbidity, temperature, nutrient concentrations and phytoplankton community assemblages (both size and composition) in estuarine and coastal waters (Day et al. 2016; Bargu et al. 2019). Therefore, freshwater input has a significant effect on biogeochemical processes and net ecosystem metabolism of the water bodies they flow into (Hoellein et al. 2013; Odum 1980; Russell and Montagna 2007). Seasonal phytoplankton blooms, which occur during peak flow periods in the late spring through early fall when nutrient delivery is high (Fig. 0.1), can shift the POM pool from being dominated by terrestrial detrital material to being primarily phytoplankton-based (Lohrenz et al. 2008). Delivery of riverine nutrients and POM to coastal waters is essentia to understand when modeling food webs in the NGOM as their variability strongly impacts biogeochemical cycling and hypoxic events (Dzwonkowski et al. 2017; Dzwonkowski et al. 2018).

1.2 Red Snapper in the NGOM

Across the NGOM, NOAA and the GOM Fishery Management Council manage reef associated fisheries in order to sustain recreational and commercial stocks. They currently manage 31 reef fish species in six families including Triggerfish (Balistidae),

Jacks (Crangidae), Wrasses (Labridae), Tilefish (Malacanthidae), Groupers (Serranidae), and Snappers (Lutjanidae). Of these species, Gray Triggerfish, Greater Amberjack, and Red Snapper were classified as overfished stocks in 2017 (Gulf of Mexico Fishery Management Council 2017). Stock assessments are based on data collected by Southeast Area Monitoring and Assessment Program (SEAMAP) surveys and state trawls. The Reef Fish Survey component of this assessment is conducted by the National Marine Fisheries Service (NMFS) in Texas, Louisiana, and Alabama while the state of Florida monitors reef fish independently (Fig. 0.2). The state of Mississippi does not routinely monitor reef fish populations and is not included in SEAMAP surveys, leaving data gaps for reef fish in Mississippi waters (Rester 2015).

Red Snapper mature around age two and have a lifespan of up to 50 years, during which time they have high fecundity that increases with increased size (Gallaway et al. 2009). Red Snapper spawn from April through September in the NGOM and produce buoyant eggs, which hatch into pelagic larvae (~2.2 mm total length) within a day. At approximately 16-19 mm (26 to 30 days old), larvae metamorphose and settle on low relief hardened habitat such as oyster reefs, shell hash, rock outcroppings or other small reefs. Once they reach ~50 mm total length (1-2 years), Red Snapper are often caught as bycatch by the penaeid shrimp trawl fishery until approximately Age-2 when they recruit into the adult population (Gallaway et al. 2009). Once juveniles reach approximately 100-200 mm total length (2-3 years) they leave the protection of shallow, small, low-relief reefs, and move to larger more complex and deeper reefs, exhibiting an ontogenetic shift in diet and habitat use with increased size and age (Szedlmayer and Lee 2004; Jaxion-Harm and Szedlmayer 2015). Tagging studies have shown that adult Red Snapper

exhibit high site fidelity. Fish move <5 km from their home site when feeding around their home reef and only move significantly longer distances to avoid disturbances such as hurricanes and hypoxia (Gallaway et al. 2009; Everett et al. 2020).

The primary Red Snapper fishery extends from Panama City, Florida to Galveston, Texas with the majority of commercial and recreational fish harvested from the area south and west of the Mississippi River delta (Goodyear 1993). Red Snapper fishing efforts in the NGOM vastly increased in the late 1950's and early 1960's due to gear improvements after World War II which made fishing more efficient and offshore sites easier to access, resulting in a larger catches and corresponding declines in reef fish abundances (Carpenter 1965; Macpherson 2001; Fitzhugh et al. 2019). To better manage declining fishery stocks, the United States Congress passed the 1976 Magnuson-Stevens Act (MSA) to address the issues of increased fishing pressure, a lack of fisheries resource management and conservation, and direct or indirect habitat loss. The law aimed toward developing better management strategies to protect fish stocks while providing optimum yields for commercial and recreational fisheries. It also required monitoring and conservation of fishery resources. The Gulf of Mexico Red Snapper stock was listed as overfished in 1977 and under the MSA, NOAA Fisheries began conducting stock assessments.

In 1984, the Gulf of Mexico Fishery Management Council (GMFMC) began conservation efforts for Red Snapper under the Environmental Impact Statement and Fishery Management Plan for the Reef Fish Resources of the Gulf of Mexico. The plan's aim was to manage stocks to provide the optimum yield for domestic user groups by setting catch, size, and gear limits, and limiting the number of fishing licenses available

to both charter and commercial harvesters. However, in 1990, the population of Red Snapper declined to a minimum, with a low spawning potential (the number of eggs a fish may produce in its lifetime in an exploited population versus an unexploited population) of 2% which is far below the required 20% to maintain the fishery (Gulf of Mexico Fishery Management Council 2004). Strict management strategies such as reef fish permits, seasonal catch limits, creel limits, and size restrictions were set a year later, and the fishing season was drastically shortened to reduce fishing pressure in hopes the population would rebound (Fischer et al. 2004). A 26% spawning potential was set as a target for the stock with a 20% minimum required by the Reef Fish Fishery Management Plan (Goodyear 1993; Porch et al. 2013; Szedlmayer and Brewton 2019). Red Snapper stocks have thus been managed since 2007 under various GMFMC amendments designed to decrease bycatch by the shrimp trawling fishery, decrease overfishing, and increase spawning stock (Gulf of Mexico Fishery Management Council 2007).

1.3 Study Region

As part of a National Fish and Wildlife Foundation grant focused on quantifying reef fish abundances and trophic dynamics, we collected water and fish samples from bare bottom water control sites and reef fish habitats (artificial reefs and oil/gas platforms). The study region encompasses 7,095 km^2 of state and federal waters south of the Mississippi barrier islands including continental shelf waters south to the 100m depth contour, in an area bound by MS/AL state line and west to the MS River and Chandeleur Islands (Fig. 0.3). The sampling area fills the gap in the SEAMAP vertical line survey of the NGOM and is split into three depth strata: shallow (<20 m), mid (20-50 m), and deep

(50-100 m). Within each depth strata, we collected samples at three active oil/gas platforms, two non-structure controls, and either one fish haven and two rigs-to-reef sites, or three rigs-to-reef sites, depending on availability. Sites were randomly selected from a set number of sites chosen during mapping of the region in 2015.

1.4 Stable Isotopes

Stable isotopes are used throughout this study to determine dietary and movement information. They are non-radioactive forms of the same element where atoms of the two forms have the same number of protons and electrons but different numbers of neutrons giving the rarer heavier isotope a slightly increased atomic mass relative to the much more abundant lighter isotope. Carbon and nitrogen have two stable isotopes each, ^{12}C and ^{13}C, and ^{14}N and ^{15}N. These isotopes are measured as ratios (R) of the heavy isotope to the lighter isotope of a sample relative to the R of a known standard. In this case carbon is measured as a ratio of $^{13}C/^{12}C$ and nitrogen is measured as $^{15}N/^{14}N$. Isotope ratios are expressed as delta (δ) values (eq.1)(Fry 2006).

Equation 1. $$\delta X = \left[\frac{R_{sample}}{R_{standard}} - 1\right] \times 1000$$

The internationally agreed upon standards for carbon and nitrogen stable isotope values are PeeDee beleminite and atmospheric dinitrogen gas. Isotope fractionation is a partitioning of the different isotopes that occur due to physical processes or chemical reactions which thermodynamically favor the lighter isotope (Fry 2006). In ecological

studies, the mixing and fractionation of $\delta^{13}C$ and $\delta^{15}N$ are used to identify basal resource contributions and trophic position of organisms within food webs.

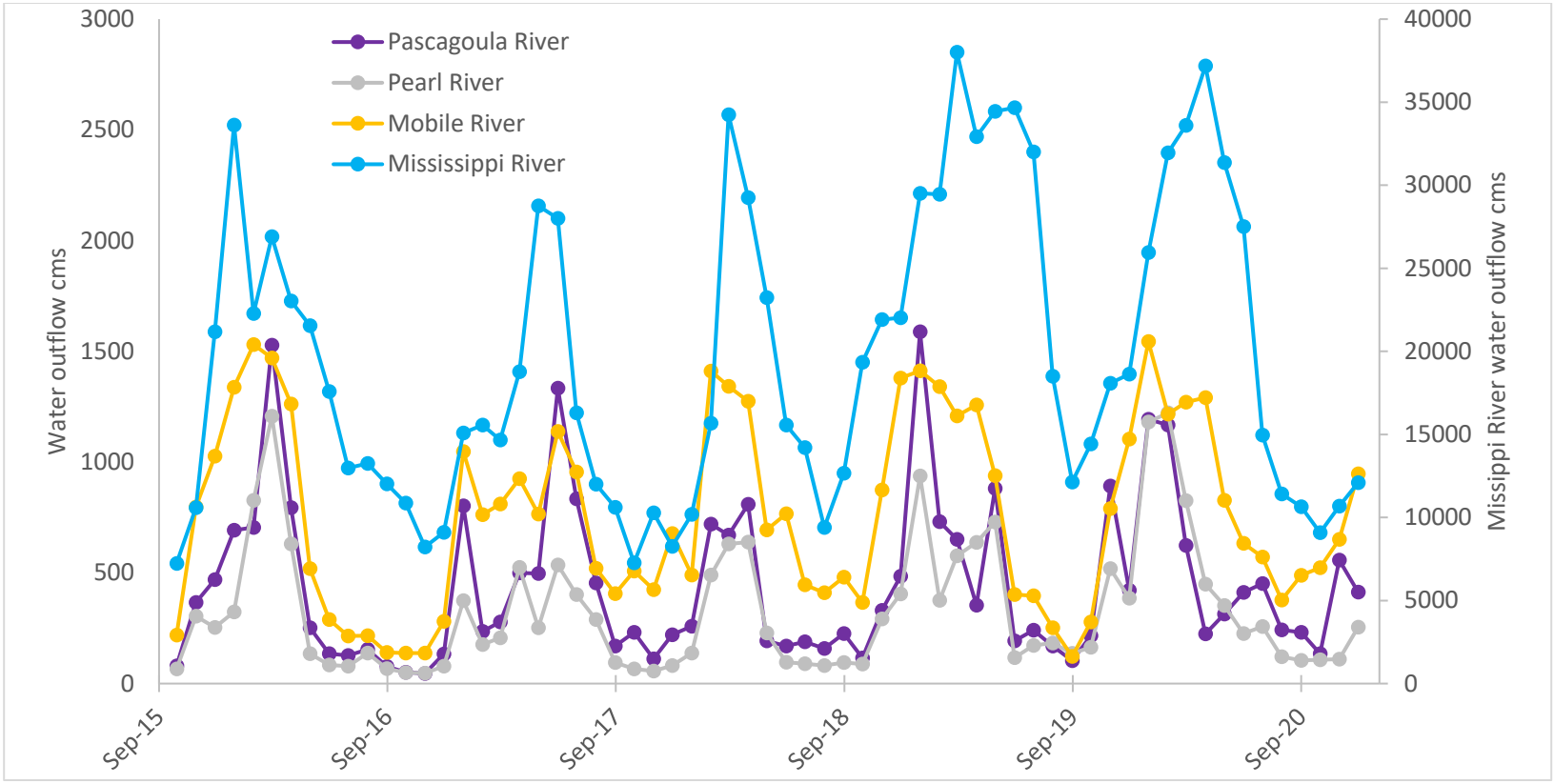

Figure 1.1 Monthly average water outflow in cubic feet per second from the major rivers entering waters off Mississippi. Data from USGS stream gauges (Mississippi River site 07374000, Pascagoula River site 02479310, Pearl River site 02492620, and Mobile River site 02470629).

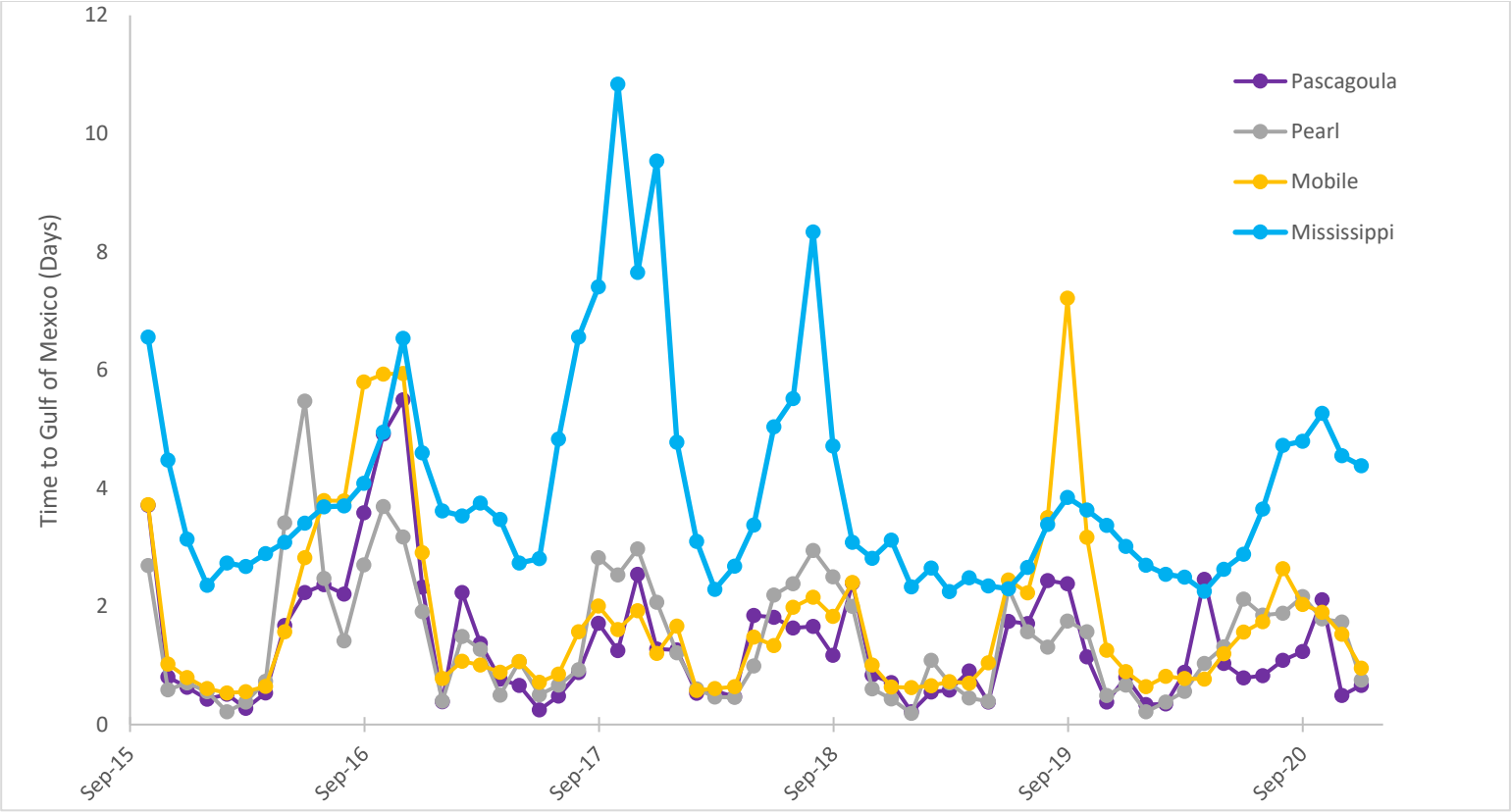

Figure 1.2 Average monthly time for river water to move from stream gauge to the NGOM.

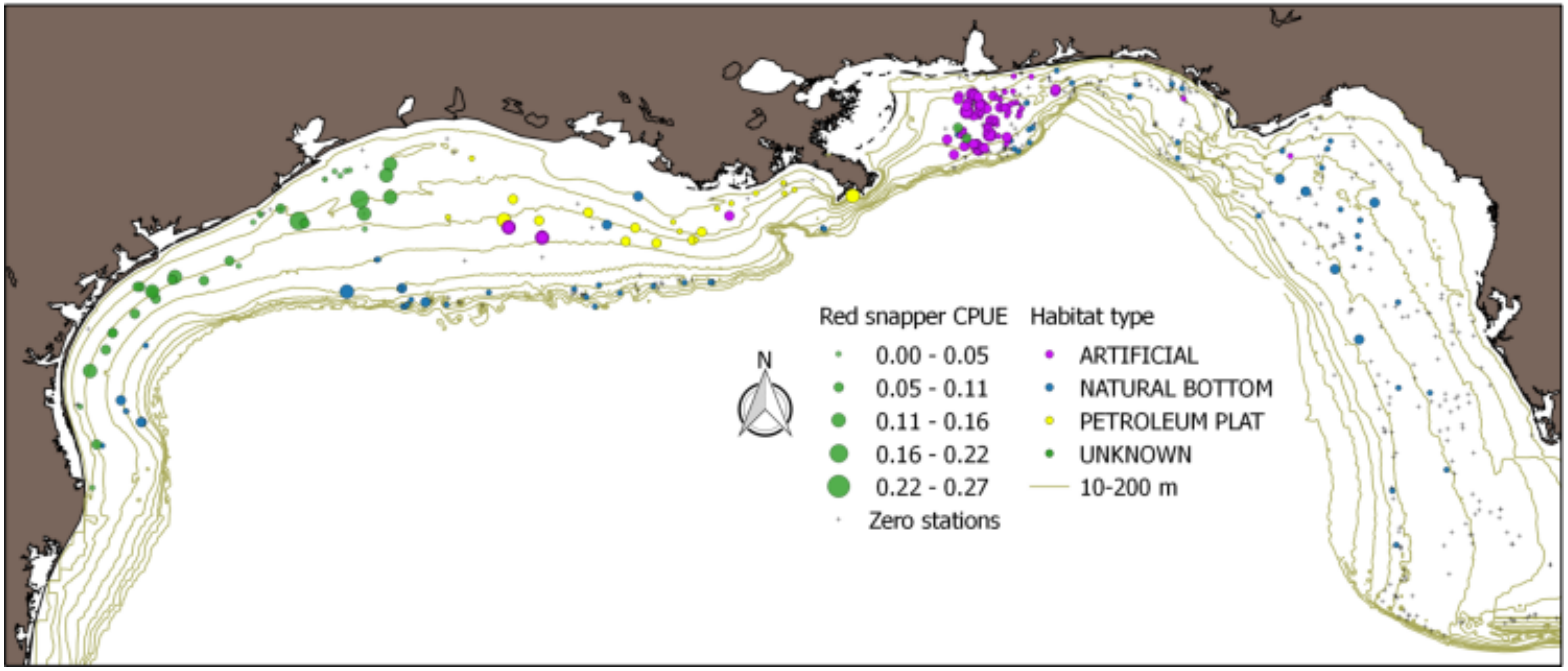

Figure 1.3 Vertical line reef fish studies completed prior to 2016.

From: Campbell MD, Switzer T, Mareska J, Hendon J, Rester J, Dean C, Martinez-Andrade F (2017) SEAMAP Vertical Line Survey: Relative Indices of Abundance of Gulf of Mexico- Red Snapper. SEDAR, North Charleston, SC.

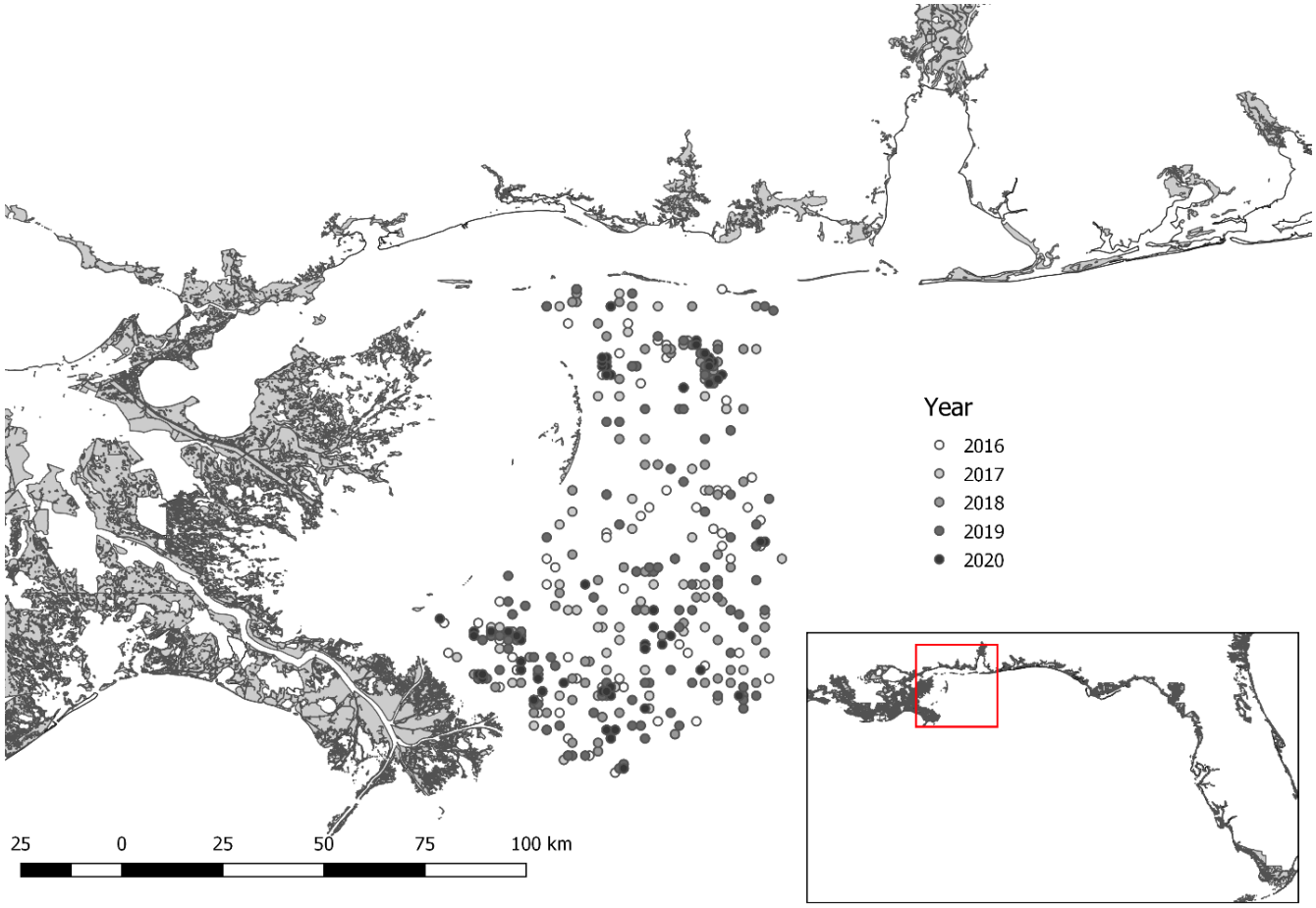

Figure 1.4 Reef survey area with stations sampled colored by year.

CHAPTER II – RIVERINE IMPACT ON MISSISSIPPI STATE AND ADJACENT STATE WATERS

2.1 Abstract

The Mississippi River is the largest freshwater source to the northern Gulf of Mexico and can influence nutrient concentrations, phytoplankton production and food web structure seasonally and across years. However, recent studies have shown that smaller local rivers also have a structuring effect that controls particulate organic material (POM) and nutrient patterns in the Mississippi Bight and surrounding areas. Analysis of nutrient concentrations, salinity, and POM carbon and nitrogen content and stable isotope values was used to analyze riverine impact in Mississippi state and adjacent federal waters, to determine the extent to which the Mississippi, Pearl, and Pascagoula rivers, and the Mobile River impact the region. Multiple linear modeling of physical water, water quality, and POM parameters were used to determine which rivers at which lag times had the greatest effect. These results were used to inform kreiging models that illustrate the impact over the study region. Significant impacts by fresh water delivered from smaller more regional rivers were shown to strongly impact the region, despite the much larger outflow from the Mississippi. The riverine inputs were shown to not just physically stratify the water column, but also alter the amount of refractory carbon present, and the amount of *in situ* production occurring in the region.

2.2 Introduction

The impact of rivers in the NGOM significantly impacts the physical and chemical parameters of the water column. Fresh, nutrient rich water stratifies the water

column and promotes *in situ* production as well as increased bacterial respiration. Much previous work has been focused on the Mississippi River's impact on the region due to its extremely high outflow in comparison to other areas, but wind, bottom topography, and local currents cause much of the Mississippi River plume to move westward along the Louisiana-Texas shelf, rather than up into the Mississippi Bight except during episodic northeastward spreading (Schiller et al. 2011). Many other significant rivers also contribute to the region of fresh water influence east of the Mississippi River Delta (Dzwonkowski et al. 2018), most significantly, the Mobile, Pearl and Pascagoula rivers (Sanial et al. 2019). All of these rivers impact nutrient dynamics, biological production, and particulate organic matter composition in the area of the Mississippi shelf however little is known about varying freshwater influences to the region in terms of nutrient delivery, subsequent changes in primary production and bottom up effects on marine food webs.

The particulate organic matter (POM) pool is assumed to be dominated by phytoplankton and is often used as an isotopic proxy for phytoplankton, but in regions with large terrestrial inputs from rivers this may not be a valid assumption. Phytoplankton cells in most regions have a somewhat predictable ratio of carbon to nitrogen to phosphorus (C:N:P). Termed the Redfield ratio, C:N:P of phytoplankton is 106:16:1 (Redfield 1958). The average N:P in the lower Mississippi river has historically been greater than the Redfield ratio varying from 10:1, below the Redfield ratio in the 1970's, to 40:1 in the 1980's, and dropping to 20:1 by the 2000's (Bargu et al. 2019). This variability has also been shown to vary seasonally (Cai et al. 2012). The outflow from the rivers in the area fertilize the NGOM with increased nitrogen, typically during the

spring, causing increases in phytoplankton production (Turner et al. 2007). Determining the sources of POM as either terrestrial or marine can give insight into biological processes occurring in the area. A shift between terrestrial and riverine basal resources may be traced using stable isotope values of the POM as well as its carbon to nitrogen concentration ratios. In Bay St. Louis the $\delta^{13}C$ of POM increased from -28.51‰ to -23.79‰ as sampling moved from estuarine to more marine waters (Cai et al. 2012). This is consistent with work done at the mouth of the Mississippi and onto the continental shelf which found $\delta^{13}C$ of POM values to vary between -23.8‰ to -26.8‰, with a strong seasonal variability related to riverine discharge of terrestrial POM (Wang et al. 2004). Therefore, stable carbon isotope analysis of ^{13}C may be used to determine shifts in dominant basal resources in coastal pelagic ecosystems if there is a large enough difference between the terrestrial and marine isotope values (Dorado et al. 2012). By measuring $\delta^{13}C$ and $\delta^{15}N$ of POM as well as its carbon to nitrogen ratio, we may be able to determine the relative contribution of riverine vs. marine derived carbon and nitrogen sources to the POM pool in the area of study. We hypothesized that with increasing river output, concentrations of nutrients, DOC, DON, and the carbon content of POM would increase and POM $\delta^{13}C$ values would decrease.

2.3 Methods

2.3.1 Sample collection and Nutrient analysis

Water and particulate organic matter samples were collected from control sites and reef fish habitats (artificial reefs and oil/gas platforms). Vertical profiles at a 0.25m resolution were obtained for water temperature, salinity, density, dissolved oxygen, and

chlorophyll a florescence via Conductivity-Temperature-Depth (CTD) recorder casts using a Sea Bird Electronics model SBE 25plus CTD which was calibrated prior to each 1-2 day sampling trip. Water samples were collected at the surface (approximately 1m below surface) with a 4 L horizontal Wildco niskin bottle, and bottom (approximately 1 m above bottom) a 10 L vertical Goflo niskin bottle. Water from each sampling event was then analyzed for dissolved inorganic nutrients (nitrate, nitrite, ammonium, and phosphate), dissolved organic C (DOC), total dissolved nitrogen (TDN), and particulate C and N (POC and PON) concentrations and stable isotope values ($\delta^{13}C$ and $\delta^{15}N$) at each depth.

Water samples for 1 day sampling events were collected whole and placed into triplicate 1L acid washed polyethylene bottles which were stored on ice and in the dark until being filtered after return to the laboratory whereas water samples collected on multiple day trips were filtered at sea. Triplicate water samples for nutrient analysis were filtered through muffled (500°C for 2 hours) GF/F filters (0.7 μm nominal pore size) either in the field or at the end of a sampling day. Filtered nutrient samples were stored in clean and acid washed polypropylene bottles while DOC/TDN samples were stored in muffled 22 ml glass vials with precleaned TFE lined caps. Samples processed in the field were placed on dry ice immediately after collection. For POM samples, a known amount of water was filtered in triplicate onto 25-mm GF/F filters (0.7-μm) for analysis of and carbon and nitrogen content and stable isotope values. Filters were frozen in petri dishes immediately after sample filtration. Once back in the lab, samples were stored frozen at -20°C until being slowly thawed and analyzed. Dissolved PO_4, NH_4, and NO_2 concentrations were analyzed with standard colorimetric techniques (Strickland and

Parsons 1972; Nielsen 1998) while NO_3 concentrations were measured with an acidic vanadium reaction vessel plumbed into a Thermo NOx Model 42i chemiluminescent analyzer (Braman and Hendrix 1989). The lower limits of detection for NH_4, PO_4, NO_3+NO_2 and NO_2 were: 0.5, 0.5, 1.0 and 0.1 µM, respectively. A Shimadzu TOC-V analyzer equipped with a TN unit was used to measure DOC and total dissolved nitrogen (TDN) concentrations. Concentrations of DON were calculated as the difference between TDN and DIN concentrations ([DIN]=[NH_4] + [NO_2] +[NO_3]). Particulate filters were acid fumed for 24 hours with concentrated HCl vapor to remove inorganic carbonates (Cai et al., 2015), then C and N concentrations and $\delta^{13}C$ and $\delta^{15}N$ values of the POM were analyzed using a Thermo Delta V Advantage stable isotope ratio mass spectrometer coupled to a Costech 4010 elemental combustion system via a Thermo Conflo IV interface. A secondary working acetanilide lab standard that was calibrated against primary NIST certified standards (USGS-40, USGS-41 and urea) was analyzed daily to ensure accurate results.

2.3.2 River outflow data

River outflow from the four major sources of freshwater input to the study region were obtained from the USGS. River outflow data (m^3/sec) of the Mississippi River (USGS Baton Rouge station 07374000), Pearl River (USGS Pearl River Bogalusa, LA station 02489500), Pascagoula River (USGS Grams Ferry station 02479310) and the Mobile River (USGS Mobile River at river mile 31.0 at Bucks, AL station 02470629) were obtained from October 1, 2015, through December 31, 2020, and averaged by month. As flow from the Pearl and Pascagoula rivers were determined to be highly correlated, these two rivers were combined for analysis. River discharge was converted

to velocity using cross sectional area at the stream gauge which was irregularly updated by the USGS throughout the study period (Fig. 1.1). Updates ranged from multiple times a month to once every few years. Velocity of the river at the stream gauge was used to calculate an average monthly time for a parcel of water to move from the stream gauge to the NGOM. Time to the NGOM was never more than 15 days, less than the month being averaged. Therefore, no initial lag was used to correct current discharge into the NGOM.

2.3.3 Statistical analysis

Surface and bottom water DIN, PO_4, DOC, TDN, DON, POC, PON, and C:N were plotted for each month during sampling across all five years using box plots to visualize the variation across the study area. Pairwise Pearson correlation was used to analyzed linear relationships between water quality (PO_4, DIN, DOC, and DON), POM ($\delta^{13}C$, $\delta^{15}N$, POC, and C:N) and physical water parameters (temperature, DO mg/L, depth, and salinity) from surface and bottom waters, using the function rcorr in the R package Hmisc.

Those parameters that had a significant correlation with total outflow from the rivers, or total outflow from the rivers lagged by three months were used for further analysis. In the surface water PO_4, DIN, and DON, were included as water quality parameters, POC, PON, $\delta^{13}C$, and C:N, as POM parameters, and temperature, and salinity as physical water parameters. In the bottom water PO_4, DIN, and DON, were included as water quality parameters, $\delta^{13}C$, and C:N, were included as POM parameters, and temperature, and DO were included as physical water parameters. A Kaiser-Meyer-Olkin (KMO) test of sampling adequacy (Psych package in R) and Bartlett's test of sphericity (parameters package in R) were performed to determine if a factor analysis would be

appropriate for the data. A principal component analysis (PCA) was then performed using the FactoMine package in R. Eigenvalues were extracted and dimensions with eigenvalues over 1 were kept for further analysis. Dimensions with eigenvalues below one were also used if the cumulative percent variance explained had not reached 70% and the eigenvalue was still close to one. An initial linear regression was performed using all relevant dimensions to determine overall impact of the Mississippi River, Mobile River, Pearl River plus Pascagoula River, and all of these with a three month lag, on the surface and bottom water.

After the initial PCA was completed, the loading matrices of the extracted PCA dimensions were obliquely, rather than orthogonally rotated due to correlations between the factors, to equalize the relative importance of the dimensions and determine the optimum parameter structure for each dimension that maximized loading variance (promax function stats package in R). All loadings less than |0.4| were suppressed and the parameters most impacting each dimension were determined. Those dimensions including the most water quality, POM, and physical water parameters were assigned to water quality, POM and physical parameter groups respectively, and used as dependent variables in multiple linear regression to determine riverine impact for each parameter grouping. When only two parameters of two different groups had loadings over |0.4|, the parameter with the stronger loading determined the placement of the dimension.

Current river output and a three-month lag were used to analyze river impact on water quality, POM, and physical parameters, as a one-month lag was determined to be an inadequate amount of time to separate riverine effects (Turner et al. 2005). The lowest

AIC and highest adjusted coefficient of determination (R^2) was used to select which rivers under which lag conditions were to be used for linear modeling.

2.3.4 Visualization via Universal Kriging

River outflow from the Pearl, Pascagoula, Mississippi, and Mobile rivers were summed to determine high (>28317 m^3/s), mid (16990 – 28317 m^3/s), and low (<16990 m^3/s) outflow conditions over time (Fig 1.2). A finer resolution of 5 outflow groupings was attempted but due to uneven distributions of river outflow groups during the sampling periods, there was not enough statistical power to determine outflow effects at this level. Under each of the three outflow conditions salinity, $\delta^{13}C$, and C:N were visualized using universal kriging to see the spatial impacts at the surface and bottom of the water column of rivers on the parameters (Murphy et al. 2010). After division into outflow groups, the data were transformed (normalized) using the Box and Cox maximum likelihood approach in the R package car (Box and Cox 1964; Osborne 2010). Before plotting, the data were back transformed for easier visualization and interpretation.

2.4 Results

2.4.1 Parameter concentrations

Nutrient concentrations plotted by month and year display classic seasonal stratification patterns between surface and bottom waters (Fig. 1.3 & 1.4). The highest dissolved inorganic nitrogen (DIN) concentrations were in bottom waters in summer and into fall excluding times when the Bonnet Carré Spillway was open (March 8th-March 30th, 2018; Feb 27th–April 11th and May 10th-July 27th, 2019). Measured DIN

concentrations ranged from below detection to 92 μM. Phosphate (PO_4) concentrations were typically higher in the bottom waters and declined across the 5 years (Fig. 1.4) and ranged from below detection to 2.0 μM in the surface waters with two outliers in 2016 surface waters that reached 3.0 and 3.2 μM, and below detection to 2.1 μM in the bottom waters. Observed peaks in both surface and bottom water were present in mid to late summer.

Dissolved organic carbon (DOC) concentrations ranged from 1.2 μM to 2217.1 μM but were typically below 500 μM. Concentrations tended to be higher in surface waters (Fig 1.5). Total dissolved nitrogen (TDN) tended to increase in the summer months with comparable concentrations in the surface and bottom waters (Fig. 1.6). Concentrations of TDN ranged from 3.8 μM to 124.7 μM. Dissolved organic nitrogen, the organic fraction of the TDN, ranged from below detection to 119.5 μM and made up the majority of the TDN measurement. It therefore also tended to peak in the summer months (Fig. 1.7).

Concentrations of particulate organic carbon (POC) and nitrogen (PON) ranged from 0 to 523.7 μM and 0 to 66.4 μM respectively. POC was higher in the surface waters where it tended to peak in the summer months. In the bottom waters it was relatively stable across seasons (Fig. 1.8). PON showed similar patterns to POC (Fig. 1.9). The POM C:N across the sampling years and seasons ranged from 0.7 to 20 and was consistently higher in bottom waters than in surface waters (Fig. 1.10). The slope of carbon vs. nitrogen for all five years was near the Redfield ratio of 6.7 (Fig. 1.11). While the Bonnet Carré Spillway was open during 2019, there was a significant increase in C:N

in bottom waters. The POM $\delta^{13}C$ ranged from -53.1 to -11.5 ‰ (Fig. 1.12) and $\delta^{15}N$ ranged from -36.7 to 69.6 ‰ (Fig. 1.13).

2.4.2 Pairwise Correlations

Pairwise Pearson correlation between dependent variables measured across the study area determined that there were many significant correlations (Table. 1.1 & 1.2), however few were ecologically significant. Correlations with r values between 0 and 0.39 were classified as weak, 0.4-0.69 were moderate, and over 0.7 were strong. All correlations were weak, with some moderate exceptions.

Water depth had no significant correlation with any water quality parameters for surface water samples, but all water quality parameters except DIN and $\delta^{15}N$ were significantly correlated with depth in bottom water samples. Phosphate and DIN concentrations were moderately positively correlated in surface waters ($r=0.46$, $p<0.00$) and weakly in bottom waters ($r=0.16$, $p<0.00$). Inorganic nutrients were not correlated with DOC while DON was weakly positively correlated with DOC (surface $r=0.16$, $p<0.00$; bottom $r=0.14$, $p<0.00$). Carbon concentrations of POC were weakly correlated with both DOC (surface $r=0.22$, $p<0.00$; bottom $r=0.11$, $p=0.01$) and DON concentrations (surface $r= 0.17$, $p<0.00$; bottom $r= 0.10$, $p=0.03$). Surface water PO_4 was weakly negatively correlated with salinity ($r=-0.20$, $p<0.00$) and DIN concentration was moderately negatively correlated with salinity ($r=-0.44$, $p<0.00$). DIN was also weakly negatively correlated with temperature ($r=-0.11$, $p=0.02$), and weakly positively correlated with DO ($r=0.15$, $p<0.00$). In the bottom waters PO_4 concentrations were moderately negatively correlated with DO ($r=-0.38$, $p<0.00$), and weakly with depth ($r=-0.22$, $p<0.00$), but weakly positively correlated with temperature ($r=0.28$, $p<0.00$).

Concentrations of DIN in the bottom water was weakly negatively correlated with temperature ($r=-0.19$, $p<0.00$) and moderately with DO ($r=-0.53$, $p<0.00$).

Isotope values of POM were variably correlated with other water quality parameters. In surface water samples, $\delta^{13}C$ was weakly positively correlated with DO ($r=0.26$, $p<0.00$), and more weakly, salinity ($r=0.10$, $p=0.03$), but weakly negatively correlated with PO_4 ($r=-0.17$, $p<0.00$), and DIN ($r=-0.21$, $p<0.00$). Bottom water $\delta^{13}C$ was weakly correlated with depth and temperature ($r=-0.18$, $p<0.00$; $r=0.11$, $p=0.02$) and weakly positively correlated with PO_4 ($r=0.18$, $p<0.00$) and DOC ($r=0.12$, $p<0.00$). Surface water $\delta^{15}N$ was very weakly positively correlated with DO ($r=0.10$, $p=0.02$) and negatively correlated with PO_4 ($r=-0.14$, $p<0.00$) and DON ($r=-0.21$, $p<0.00$). Carbon to nitrogen ratios (C:N) of POM in surface water were very weakly negatively correlated with temperature ($r=-0.11$, $p=0.01$) but moderately positively correlated with salinity ($r=0.30$, $p<0.00$). In the bottom water, C:N was also weakly correlated with depth ($r=0.20$, $p<0.00$). In the surface water C:N was weakly negatively correlated with PO_4 ($r=-0.14$, $p<0.00$), DIN ($r=-0.17$, $p<0.00$), and DON ($r=-0.11$, $p=0.01$), and weakly positively correlated with $\delta^{13}C$ ($r=0.13$, $p<0.00$) and $\delta^{15}N$ ($r=0.17$, $p<0.00$). In the bottom water, C:N was weakly negatively correlated with PO_4 ($r=-0.19$, $p<0.00$) and moderately negatively correlated with $\delta^{13}C$ ($r=-0.57$, $p<0.00$), but weakly positively correlated with DIN ($r=0.14$, $p<0.00$) and $\delta^{15}N$ ($r=0.13$, $p<0.00$).

2.4.3 Moderate correlations by year

In the surface waters, the moderate correlation between PO_4 and DIN had an increasing slope over the 5 years, indicating more DIN was present per amount of PO_4 (Fig. 1.14). The concentration of DIN was also moderately correlated with salinity, with

steeper slopes during 2017, 2018, and 2020 (Fig 1.15). The correlation of C:N of the POM with salinity in the surface water also showed a trendline that crossed the Redfield ratio C:N of 6.7 at lower salinities in later years (Fig 1.16). Salinity and POC were moderately negatively correlated, with the highest POC concentrations present in the surface water at the lowest salinities (Fig 1.17). The shallowest slopes between the POC and salinity relationship were found in 2019, followed by 2016, with the other three years all having slopes below -4. Concentrations of POC and DO were moderately positively correlated with the highest POC concentrations found at the highest DO (Fig 1.18). Hypoxic conditions were only present when POC was low.

In bottom waters, the moderate negative correlations of PO_4 and DIN with DO showed a distinct relationship between higher concentrations of nutrients and lower DO in the bottom water, often reaching hypoxic levels (Fig 1.19 & 1.20). The relationship between PO_4 and DO also had a decreasing slope with successive years (Fig. 1.19). The C:N in the bottom water also was moderately negatively correlated with $\delta^{13}C$, but this relationship across the 5 years was often unclear with most C:N values grouping around the Redfield ratio (Fig 1.21). During 2019 when C:N had a large range, there is a more clear declining relationship, indicating that with increasing $\delta^{13}C$ values, C:N ratios increased.

2.4.4 Principle Components Analysis and Linear Regression

Surface water KMO test of sampling adequacy and Bartlett's test of sphericity showed enough partial correlation and variable relationship strength to perform a factor analysis (Table 1.3). Principal component analysis resulted in 4 dimensions with eigenvalues over 0.97, resulting in 73.7% of the variance explained (Table 1.4).

Loadings of parameters for the rotated PCA scores for these dimensions resulted in Dimensions 1 and 4 being labeled as POM dimensions including parameters POC, PON, $\delta^{13}C$, and C:N. Dimensions 2 and 3 were labeled as water quality dimensions including parameters PO_4, DIN, and DON (Table 1.5). The two physical water parameters that were correlated with outflow in the surface water (temperature, and salinity) did not group out into separate dimensions. Salinity, despite being correlated with outflow, did not have a strong loading on any dimension, while temperature was included in dimension 2, with water quality parameters.

Linear modeling of all four dimensions by the monthly averaged outflow from the Mississippi, Mobile, and Pearl plus Pascagoula rivers, as well as outflow from these rivers lagged by three months indicated that three month lagged outflow from the Mobile River, had the strongest impact on the surface waters of the region. This was followed by current outflow from the Mobile River, current outflow from the Mississippi River, current outflow from the Pearl plus Pascagoula rivers, and three month lagged outflow from the Pearl plus Pascagoula Rivers (Table 1.6 & 1.16). The inclusion of the current outflow from the three month lagged Pearl plus Pascagoula rivers also improved the model but did not have a significant impact on the parameters.

Linear regression of surface water quality dimensions (dimensions 2 and 4) by river outputs showed that the current outflow from the Mississippi River, had the strongest impact on the PO_4, DIN, DON concentrations and temperature. This was followed by the three month lagged outflows from the Mobile and Mississippi rivers, and the current outflows from the Pearl plus Pascagoula rivers and Mobile River (Table 1.7 & 1.16). POM dimensions (including POC, PON, $\delta^{13}C$, and C:N parameters) were by far

most impacted by the three month lag outflow from the Mobile River, followed by the current outflow from the Mississippi River, and the three month lagged outflow from the Pearl plus Pascagoula rivers (Table 1.8 & 1.16).

Bottom water KMO and Bartlett's tests also showed enough partial correlation and variable relationship strength to perform a factor analysis (Table 1.9). Principal component analysis resulted in 4 dimensions with eigen values over 0.92, resulting in 81.02% of the variance explained (Table 1.10). Loadings of parameters for the rotated PCA scores for these dimensions resulted in Dimension 1 being labeled as the only POM dimension, including $\delta^{13}C$ and C:N. Dimensions 2 and 4 were labeled as water quality dimensions, including DIN, DO, and DON. Dimension 3 was labeled as the only physical water parameter dimension including PO_4 and temperature (Table 1.11). As only two parameters were included in dimension 3 and they were from different grouping, the parameter with the strongest loading on the dimension (temperature), was used as the grouping parameter.

Linear modeling of all four dimensions by the monthly averaged outflow showed that the current outflow from the Mobile River, the three month lagged outflow from the Mobile River, and the current outflow from the Pearl plus Pascagoula rivers had the most significant impacts on all measured parameters analyzed together (Table 1.12 & 1.17). Bottom water quality dimensions (including DIN, DON, and DO parameters) were most impacted by both current and three month lagged outflow from the Mobile River (Table 1.13 & 1.17). Water quality parameters were also impacted by current outflow from the Pearl and Pascagoula rivers, and the current and three month lagged outflow from the Mississippi River. Bottom water POM dimensions (including $\delta^{13}C$ and C:N parameters)

were impacted by all outflow sources with both current and three month lag excluding the current outflow from the Mobile River (Table 1.14 & 1.17). The physical water dimension (including PO_4 and temperature parameters) in the bottom water were most impacted by the current outflows from the Mobile and Mississippi rivers, followed by the three month lagged outflows from the Mississippi River and Pearl plus Pascagoula rivers (Table 1.15 & 1.17). The three month lagged outflows however were just barely non-significant, with p-values of 0.053 and 0.055 respectively.

2.4.5 Visualization via Universal Kriging

Salinity was consistently lower in the surface water than in the bottom water (Fig 1.22 & Fig. 1.23). Overall, surface salinity was lower in the southwest by the Mississippi River delta and in the northwest by the western side of the Mississippi Sound and northern side of the Chandeleur Sound (Fig 1.22, panel A). Salinity gradually increased toward the eastern side of the study region. The low outflow regime (panel B) closely reflected patterns seen in the overall plot but without the lower salinity in the northwest seen in the overall plot. In the mid outflow regime (panel C), lower salinity was more prevalent in the northwest with the highest salinity in the south. In the high outflow regime (panel D), low salinity radiated north from the Mississippi River delta northwards, causing general overall freshening of the study region. In the bottom waters (Fig 1.22) salinity remained relatively constant above 34 psu, with some occurrences of lower salinity in the northwest under the high outflow regime.

Consistently higher (less negative) POM $\delta^{13}C$ was measured in surface waters than in bottom waters (Fig. 1.23 & 1.24). Overall, $\delta^{13}C$ values were variable but lower in the western region in the low outflow (Fig 1.23 panel B). Under the mid outflow (panel

C), $\delta^{13}C$ values were consistent across the study region and higher than under any other hydrological condition. Under the high outflow conditions however (panel D), variability across the study region was high with generally lower $\delta^{13}C$ values.

In the bottom waters (Fig 1.24), $\delta^{13}C$ values tended to be lower toward the southeast and higher in the west overall (panel A). The low outflow (panel B) also reflected this pattern but less strongly than in the overall plot. In the mid outflow regime (panel C), the lower $\delta^{13}C$ values previously seen in the low outflow disappeared and POM $\delta^{15}N$ increased across the entire study area. In the high outflow however (panel D), this trend reversed, and POM $\delta^{15}N$ decreased, with the lowest values measured across the entire southern region of the study area and increasing northward.

Lower POM C:N were measured in surface waters than in bottom waters (Fig 1.25 & 1.26). In the surface water (Fig 1.25), C:N was somewhat consistent overall with the highest values being found in the central and eastern areas of the study region and the lowest values in near the Mississippi River delta in the south west, and the western Mississippi Sound in the northwest (panel A). This pattern is reflected to a greater extent in the low outflow regime (panel B). In the mid outflow regime (panel C), C:N tended to be lower throughout the western side of the study region and increased toward the southeast. In the high outflow regime (panel D), C:N tended to generally increase throughout the region with the highest values in the northwest. In the bottom water (Fig 1.26), the generally higher C:N of the POM was greater in the southeast and lower in the northwest overall. This trend is reflected in the low (panel B) and mid (panel C) outflow regimes, with the mid outflow C:N being higher in the south east than under the low outflow condition. The mid outflow regime also showed a stronger gradient from

northwest to southeast than was present under the low outflow. Under the high outflow regime (panel D), this gradient shifted from northwest to southeast, to southwest to northeast, with the highest values being present near the mouth of the Mississippi River and the lowest up toward the eastern side of the Mississippi Sound.

2.5 Discussion

2.5.1 Correlations

As the Mississippi, Pearl, Pascagoula, and Mobile rivers flow out into the Gulf of Mexico, they deliver nutrient rich fresh water, which impacts the biological processes occurring in the water column of the central northern Gulf of Mexico. There is often strong stratification of the water column due to this fresh water, which also causes differences in the concentrations of nutrients and oxygen between the two water masses. Eutrophication of the upper water column has long been documented as a cause of decreased DO in the bottom waters. This process is due to raining down of POM from phytoplankton detritus and/or increased delivery of terrestrial organic material delivered by rivers, increasing bacterial respiration in the bottom waters of a thermally stratified water column which commonly causes hypoxic and anoxic conditions along the Louisiana shelf. (Goolsby et al. 1999; Childs et al. 2002; Quiñones-Rivera et al. 2007; Turner et al. 2007; Lohrenz et al. 2008). This study captured the DO response to increased nutrients fertilizing the bottom water as a moderate negative correlation between DO and both phosphate and DIN concentrations in the bottom water (Fig. 1.19 & 1.20). With higher concentrations of PO_4 or DIN, DO was more likely to be lower. The slope of the relationship in bottom waters of PO_4 and DO also declined over the

years, suggesting that less PO_4 was required for DO to reach hypoxia over the course of the study. We can relate this back to decreased salinity in the surface water, indicating higher outflow from the rivers in the region. Figure 1.15 shows that higher amounts of DIN were common when salinity was lower, and this relationship had a steeper slope in 2017, 2018, and 2020. These were years when the Bonnet Carré Spillway was not open, indicating that this Mississippi river diversion delivers higher concentrations of DIN in 2016 and 2019 to the study region. Bargu et al. (2011) found that when the Bonnet Carré Spillway was opened in 2008, concentrations of nitrate (the dominate form of DIN in this study) and PO_4 reached more than 5 times the background levels, causing cyanobacterial blooms and nutrient limitation in the surface water following closure of the spillway. In 2019, Bargu et al. found the same occurred during the 2011 opening of the Bonnet Carré Spillway as well as increased sediment loading which delivered large amounts of dissolved inorganic phosphorous to Lake Pontchartrain. Both Bargu studies showed that increases in nutrients drove phytoplankton production. In the surface water POC also positively correlated with DO and negatively correlated with salinity in the surface waters, with the highest POC concentrations being present at lower salinities and high DO concentrations (Fig. 1.17 & 1.18). Cai et. al. (2015) showed that POC concentrations increased with increasing river outflow, peaking during medium flooding events and the beginning of large flooding events, and Bianchi et.al. (2010) as well as Turner et. al. (2007) have suggested that increased erosion of marshes may be causing an increase in the amount of particulate carbon being delivered to the NGOM by the rivers, further fueling hypoxic events (Fry et al. 2015). The decreased processing and absorption of particulates and nutrients as they move through marshes caused by the diversion of the

Mississippi River therefore was captured in this study as an increase in DO with increased delivery of POC at low salinities and a decrease in the dissolved oxygen in the bottom water.

The isotope values of the POM between the surface and bottom waters also support the results from the previous correlations. The $\delta^{13}C$ of POM is generally indicative of terrestrial vs marine primary production. Lower values tend to be terrestrial (-34 to -23 ‰) indicating C3 and C4 plant sources, while higher values tend to be more marine or indicative of phytoplankton sources (-18 to -22 ‰) (Thayer et al. 1983; Cai et al. 2015; Lee et al. 2020). The negative correlation between $\delta^{13}C$ and C:N in the bottom water suggests that during periods when POC had more terrestrial sources, C:N was higher (Fig. 1.21). This was also found in the Bay of St. Louis in the Northern Gulf of Mexico wherein POC also tended to decrease with increasing salinity as shown in this study (Fig1.17) (Cai et al. 2012). Cai et al. (2012) also found that there was a general positive correlation between C:N and $\delta^{13}C$ with increasing salinity as was also found in this study. This was attributed to the predominance of terrestrial organic material in the water column with increasing amounts of diagenically altered POM from sediment resuspension in the lower bay, with about one third of the POM in the lower bay coming from autotrophic production. Diagenesis is the combination of biological, chemical, and physical processes that change the chemical makeup of organic matter in marine sediments (Henrichs 1992). Initially when organic matter is first deposited on the sediment surface, organic material is remineralized by microbes. We can see these initial changes in our study when C:N tends to increase in the bottom water due to uptake of nitrogen by microbes as particulates sink (Fig. 1.10) (Cowie and Hedges 1994). With

increased POM output from the rivers and increased flow rate causing greater resuspension near river mouths, we can expect more diagenically altered POM in the bottom waters driving up C:N in the bottom waters, which is supported by this and previous studies.

2.5.2 Riverine influences

Several models and studies have shown that delivery of nutrient rich fresh water carrying terrestrially derived carbon from rivers has driven hypoxic events and alters NGOM nutrient concentrations and physical water parameters (Rabalais et al. 1996; Rabalais et al. 2002; Justić et al. 1996; Justić et al. 2005; Fry et al. 2015), and this has been supported by the correlations previously discussed. Most of these studies however have been focused on the impact of the Mississippi River on the Louisiana shelf while more recent studies have shown that more regional rivers such as the Pearl, Pascagoula, and Mobile have a more consistent impact in the Mississippi Bight and on the Mississippi shelf (Schiller et al. 2011; Dzwonkowski et al. 2018; Sanial et al. 2019). As this study covered 5 years, an average impact of all of the rivers on the Mississippi shelf water column can be determined from the results. In the surface water, PCA of various water quality parameters resulted in four dimensions which were grouped according to parameter loadings. Dimensions 1 and 4 were labeled as POM dimensions including parameters POC, PON, $\delta^{13}C$, and C:N. Dimensions 2 and 3 were labeled as water quality dimensions including parameters PO_4, DIN, and DON (Table 1.5). No dimensions were included as physical water dimensions. In the bottom water PCA of water quality parameters were again grouped according to their loadings. Dimension 1 was labeled as the only POM dimension, including $\delta^{13}C$ and C:N. Dimensions 2 and 4 were labeled as

water quality dimensions, including DIN, DO, and DON. Dimension 3 was labeled as the only physical water parameter dimension including PO_4 and temperature (Table 1.11).

When all surface water dimensions were analyzed together the current outflow from the Mobile River was determined to be the most impactful, however, when only nutrient water quality dimensions were included, the Mississippi River dominated. Parameters of POM, when analyzed alone, were primarily impacted by the Mobile River. In these cases, larger rivers with larger basins (the Mississippi and Mobile Rivers) played a more prolonged role in nutrient and particulate delivery. Work by Sanial et al. (2019) and Dzwonkowski et al. (2018) suggest that the smaller more regional rivers have a more significant impact than the much larger Mississippi in the NGOM east of Louisiana, as the Mississippi River plume tends to advect to the west to LA/TX shelf rather than north east to the Mississippi Bight. These results are supported by our study, with the Mississippi River only being prominent in linear models where nutrients are the only parameters. This is likely due to the much higher concentrations of inorganic nutrients in the Mississippi making partitioning of nutrient contributions from smaller rivers more difficult to distinguish. However, the Mobile River also tends to flow primarily westward into the Mississippi Bight as a buoyant plume, remaining on the surface due to lower salinity of the river water and delivering sediment and nutrients to the shelf (Stumpf et al. 1993; Dzwonkowski et al. 2015). The size of the plume from the Mobile Bay was determined to be dependent on Mobile River discharge, increasing with increasing discharge and with ~75% going out to the shelf instead of into the Mississippi Sound (Dinnel et al. 1990). The more consistent outflow from the Mobile plume into the region is likely why it was determined by the model to have the greatest overall impact

over the Mississippi, and its larger outflow relative to the Pearl and Pascagoula rivers likely make its outflow more dominant. Surface water kriged plots allow us to visualize the impact of these rivers on the surface water of the study region. While the impact of the Mississippi River is often visible in the south west, especially in plots of salinity and $\delta^{13}C$, contributions from the northern and eastern rivers can be seen extending away from the source under high outflow regimes, and from the Mobile River in higher C:N in the central east during low outflow.

Riverine impact on bottom waters is more difficult to discern. This study also did not take into account any impacts caused by other sources of particulates or nutrients such as resuspensions of particulates, submarine ground water discharge or diffusion of nutrients from the sediments which may be delivering nutrients and POM into the study region. However, linear models were highly significant and showed that when all bottom water dimensions were included, the Mobile River system current outflow had the most significant impact on the region. The Mobile River also had the most significant impact when only dimensions with water quality or physical parameters were analyzed. When only POM dimensions were included in the analysis, the Mississippi River had the most significant impact on bottom water. This was supported by the kriged plots and changes in carbon isotopes over time. The $\delta^{13}C$ of bottom water POM had a much lower value similar to more terrestrial C3 values under both low and high outflows. There was also an increase in C:N in the bottom waters relative to the surface water due to preferential utilization of POM N by microbes, and the kriged plots show the areas of highest C:N were near the Mississippi River Delta. These results suggest that the current outflow from the Mobile strongly structures the dissolved and physical water quality parameters

of the bottom waters, while the particulate fraction is primarily structured by the Mississippi. This may be due to distance from the study area. The Mobile River plume, though more constant than the Mississippi, cannot carry large amounts of POM from the Alabama coast into the Mississippi Bight, while advection of the Mississippi plume can deposit river derived POM directly into the study area. The Mobile plume, like most river plumes, is also buoyant and so has a more direct effect on the surface water rather than the bottom water. Dissolved nutrients therefore may be able to reach the study area with little issue. The Mobile may have the greatest impact on temperature in the bottom waters due to the winter plume (Dzwonkowski et al. 2011). During winter months (defined as November through February) Dzwonkowski et al. (2011) found that the Mobile River plume extends ~40 km offshore mixing down to mid depth, (~30 m), just east of the Mississippi Alabama state line. This result may also be an artifact of seasonal variation that coincides with outflow from the Mobile River more closely than the Mississippi. To determine the true method of impact, further water quality testing would be required.

2.6 Conclusions

On the Louisiana shelf where bottom water has been extensively studied due to issues with hypoxia, POM C has been shown to be largely from terrestrial sources (Bianchi et al. 2002; Turner et al. 2007; Fry et al. 2015). But these sources appear to be more than just the Mississippi River delivering large amounts of nutrients and causing phytoplankton blooms. Multiple rivers in the region have been shown by previous studies to be significant contributors to various parameters in the NGOM and these water

quality parameters appear to interact in highly dynamic ways. For example, the strong correlation between particulate and dissolved fractions of organic carbon and nitrogen become much weaker in the bottom waters, indicating various processes may be occurring including the dissolved fraction being taken up by organisms, breakdown of the particulate material sinks, or undergoes various diagenic processes, resuspension of previously processed particulates from the sediments, etc. The particulates in the bottom water however, seem to be primarily impacted by Mississippi River outflow while in the surface water they are primarily impacted by the delayed outflow from the Mobile, whereas when considering nutrients, this is reversed with the Mississippi River impacting nutrients in the surface waters and the Mobile impacting them in the bottom. The dynamics of nutrient uptake and recycling under different oxygen conditions and the flux of particulates between different water layers are all highly dynamic and until recently have been primarily studied under the lens of the Mississippi alone (Rabalais et al. 1996; Turner et al. 2007; Nunnally et al. 2013), but our study shows that other more regional rivers must be considered in order to better understand the processes occurring in the study region and the impact of various rivers under different outflow conditions.

Table 2.1 Pearson correlations between surface water quality variables.

		PO_4 µM	DIN µM	DOC µM	DON µM	POC µM	$\delta^{13}C$	$\delta^{15}N$	C:N	Temp	DO mg/L	Depth m
Water quality	PO_4 µM											
	DIN µM	**** 0.46										
	DOC µM	0.02	* 0.10									
	DON µM	** 0.13	-0.09	*** 0.16								
POM	POC µM	-0.01	**** 0.27	**** 0.22	0.17***							
	$\delta^{13}C$	*** -0.17	**** -0.21	0.08	0.09*	** 0.14						
	$\delta^{15}N$	** -0.14	-0.07	0.02	**** -0.21	* 0.11	0.00					
	C:N	** -0.14	*** -0.17	-0.07	-0.11*	*** -0.16	** 0.13	*** 0.17				
Physical water quality parameters	Temp	-0.08	* -0.11	* 0.10	** 0.14	**** 0.32	0.07	0.06	* -0.11			
	DO mg/L	0.03	*** 0.15	0.08	0.04	**** 0.43	**** 0.26	* 0.10	0.08	-0.01		
	Depth m	-0.03	-0.02	-0.01	-0.01	-0.03	0.06	-0.02	0.00	0.06	-0.05	
	Salinity	**** -0.20	**** -0.45	**** -0.29	**** -0.32	**** -0.47	* 0.10	0.02	**** 0.30	**** -0.22	** -0.14	-0.06

$p < .0001$ '****'; $p < .001$ '***', $p < .01$ '**', $p < .05$ '*'

Table 2.2 Pearson correlations between bottom water quality variables.

		PO_4 µM	DIN µM	DOC µM	DON µM	POC µM	$\delta^{13}C$	$\delta^{15}N$	C:N	Temp	DO mg/L	Depth m
Water quality	PO_4 µM											
	DIN µM	*** 0.16										
	DOC µM	-0.02	-0.05									
	DON µM	0.07	-0.05	** 0.14								
POM	POC µM	**** 0.28	0.02	* 0.11	* 0.10							
	$\delta^{13}C$	**** 0.18	**** -0.24	** 0.12	**** 0.21	**** 0.25						
	$\delta^{15}N$	-0.04	-0.02	0.06	* -0.12	** 0.14	** -0.14					
	C:N	**** -0.19	** 0.14	-0.03	-0.05	**** -0.21	**** -0.57	** 0.13				
Physical water quality parameters	Temp	**** 0.28	**** -0.19	* 0.10	**** 0.19	**** 0.31	* 0.11	0.06	-0.08			
	DO mg/L	**** -0.38	**** -0.53	-0.06	** -0.12	**** -0.18	0.03	-0.07	0.06	* -0.11		
	Depth m	**** -0.22	0.06	*** -0.16	**** -0.18	**** -0.37	*** -0.17	-0.09	**** 0.20	**** -0.49	**** 0.21	
	Salinity	-0.06	** 0.13	* -0.11	**** -0.24	**** -0.23	-0.06	-0.06	0.06	**** -0.52	0	**** 0.38

$p < .0001$ '****'; $p < .001$ '***', $p < .01$ '**', $p < .05$ '*'

Table 2.3 Surface water KMO and Bartlett's tests summary.

Kaiser Meyer Olkin Measure of Sampling Adequacy		0.5
Bartlett's Test of Sphericity	approx. Chi Square	2388.05
	Df	36
	Sig.	<0.001

Table 2.4 Eigenvalues and variance explained for by each dimension of Principal component analysis for surface water.

	Eigenvalue	% Variance	Cumulative % Variance
Dim.1	2.8922318	32.2028587	32.202859
Dim.2	1.68972835	18.81387353	51.016732
Dim.3	1.07075751	11.92209174	62.938824
Dim.4	0.96930771	10.79252332	73.731347
Dim.5	0.78588046	8.750196767	82.481544
Dim.6	0.70665714	7.868103756	90.349648
Dim.7	0.54273228	6.042921965	96.39257
Dim.8	0.31026194	3.454536926	99.847107
Dim.9	0.01373179	0.1528933	100

Table 2.5 Component matrix of surface water loadings following promax rotation.

	Dim1	Dim 2	Dim3	Dim4
POC	0.652			
PON	0.622			
PO4		-0.591		
DIN		-0.644		
Temp		0.413		
DON			0.880	
d13C				0.761
CN				0.603
Sum of squared loadings	1.058	1.008	1.046	1.069
Proportion variance	0.118	0.112	0.116	0.119
Cumulative variance	0.118	0.23	0.346	0.465
Dimension group	POM	Water Quality	Water Quality	POM

* Salinity did not significantly contribute to any dimension and so was not included here

Table 2.6 Surface water forward stepwise linear regression of all rotated PCA dimension groups. Table a is models run by analysis, Table b is results of regression for each model in table a.

Table a.

Model	Predictors					
1	Mobile 3					
2	Mobile	Mobile 3				
3	MS	Mobile	Mobile 3			
4	MS	Mobile	Mobile 3	PP		
5	MS	Mobile	Mobile 3	PP	PP 3	
6	MS	MS 3	Mobile	Mobile 3	PP	PP 3

MS = Mississippi River
Mobile = Mobile River
PP = Pearl and Pascagoula Rivers
no number = no lag included
3 = three month lag

Table b.

Model	Adj. R-Square	Pred R-Square	R-Square	C(p)	AIC	SBIC	SBC	MSEP	FPE	HSP	APC
1	0.108	0.1061	0.1007	66.8915	2225.3444	859.8362	2237.872	2853.1486	5.9564	0.0124	0.8995
2	0.1647	0.1612	0.1544	34.3306	2195.7655	830.4067	2212.469	2677.4501	5.6011	0.0117	0.8458
3	0.1838	0.1787	0.1703	24.6416	2186.5981	821.3094	2207.477	2621.4993	5.4954	0.0114	0.8299
4	0.2162	0.2096	0.2006	6.9106	2169.1385	804.1842	2194.194	2522.8597	5.2995	0.011	0.8003
5	0.2212	0.213	0.2023	5.8317	2168.0297	803.1664	2197.261	2511.8946	5.2873	0.011	0.7984
6	0.2226	0.2128	0.2003	7	2169.1864	804.3739	2202.593	2512.796	5.3	0.011	0.8004

AIC: Akaike Information Criteria
SBIC: Sawa's Bayesian Information Criteria
SBC: Schwarz Bayesian Criteria
MSEP: Estimated error of prediction, assuming multivariate normality
FPE: Final Prediction Error
HSP: Hocking's Sp
APC: Amemiya Prediction Criteria

Table 2.7 Surface water forward stepwise linear regression of rotated water quality PCA dimension groups. Table a is models run by analysis, Table b is results of regression for each model in table a

Table a.

Model	Predictors					
1	MS 3					
2	MS	MS 3				
3	MS	MS 3	Mobile 3			
4	MS	MS 3	Mobile	Mobile 3		
5	MS	MS 3	Mobile	Mobile 3	PP	
6	MS	MS 3	Mobile	Mobile 3	PP	PP3

MS = Mississippi River
Mobile = Mobile River
PP = Pearl and Pascagoula Rivers

no number = no lag included
3 = three month lag

Table b.

Model	Adj. R-Square	Pred R-Square	R-Square	C(p)	AIC	SBIC	SBC	MSEP	FPE	HSP	APC
1	0.08	0.08	0.08	69.50	1803.87	438.34	1816.40	1187.89	2.48	0.01	0.92
2	0.15	0.14	0.14	33.74	1771.43	406.08	1788.13	1108.13	2.32	0.00	0.86
3	0.18	0.17	0.17	16.60	1754.98	389.82	1775.86	1068.67	2.24	0.00	0.84
4	0.18	0.18	0.17	15.90	1754.33	389.18	1779.38	1065.02	2.24	0.00	0.83
5	0.20	0.20	0.19	5.01	1743.42	378.57	1772.65	1039.01	2.19	0.00	0.82
6	0.20	0.19	0.18	7.00	1745.41	380.60	1778.82	1041.19	2.20	0.00	0.82

AIC: Akaike Information Criteria
SBIC: Sawa's Bayesian Information Criteria
SBC: Schwarz Bayesian Criteria
MSEP: Estimated error of prediction, assuming multivariate normality
FPE: Final Prediction Error
HSP: Hocking's Sp
APC: Amemiya Prediction Criteria

Table 2.8 Surface water forward stepwise linear regression of rotated POM PCA dimension groups. Table a is models run by analysis, Table b is results of regression for each model in table a.

Table a.

Model	Predictors					
1	Mobile 3					
2	MS	Mobile 3				
3	MS	Mobile 3	PP 3			
4	MS	Mobile	Mobile 3	PP	PP 3	
5	MS	Mobile	Mobile 3	PP	PP 3	
6	MS	MS 3	Mobile	Mobile 3	PP	PP 3

MS = Mississippi River
Mobile = Mobile River
PP = Pearl and Pascagoula Rivers

no number = no lag included
3 = three month lag

Table b.

Model	Adj. R-Square	Pred R-Square	R-Square	C(p)	AIC	SBIC	SBC	MSEP	FPE	HSP	APC
1	0.08	0.07	0.07	32.36	1768.39	403.14	1780.92	1103.42	2.30	0.00	0.93
2	0.11	0.11	0.10	14.89	1751.64	386.51	1768.34	1063.46	2.22	0.00	0.90
3	0.14	0.13	0.12	3.78	1740.60	375.65	1761.48	1037.19	2.17	0.00	0.88
4	0.14	0.13	0.12	5.24	1742.05	377.13	1767.11	1038.19	2.18	0.00	0.88
5	0.14	0.13	0.12	5.56	1742.36	377.50	1771.59	1036.72	2.18	0.00	0.88
6	0.14	0.13	0.12	7.00	1743.79	378.97	1777.19	1037.68	2.19	0.00	0.88

AIC: Akaike Information Criteria
SBIC: Sawa's Bayesian Information Criteria
SBC: Schwarz Bayesian Criteria
MSEP: Estimated error of prediction, assuming multivariate normality
FPE: Final Prediction Error
HSP: Hocking's Sp
APC: Amemiya Prediction Criteria

Table 2.9 Bottom water KMO and Bartlett's tests summary.

Kaiser Meyer Olkin Measure of Sampling Adequacy		0.54
Bartlett's Test of Sphericity	approx. Chi Square	614.85
	Df	21
	Sig.	<0.001

Table 2.10 Eigenvalues and variance explained for by each dimension of Principal component analysis for bottom water.

	Eigenvalue	% Variance	Cumulative % Variance
Dim.1	1.894009641	27.11329981	27.11329981
Dim.2	1.744101632	24.96732298	52.08062279
Dim.3	1.106519121	15.84014358	67.92076637
Dim.4	0.915387196	13.1040344	81.02480077
Dim.5	0.562179623	8.047765085	89.07256585
Dim.6	0.39515687	5.656785721	94.72935157
Dim.7	0.368183106	5.270648427	100

Table 2.11 Component matrix of bottom water loadings following promax rotation.

	Dim1	Dim 2	Dim3	Dim4
d13C	0.674			
CN	-0.713			
DIN		0.697		
DO		-0.648		
PO4			0.494	
Temp			0.840	
DON				0.963
Sum of squared loadings	1.02	1.039	1.039	1.013
Proportion variance	0.146	1.148	1.148	1.145
Cumulative variance	0.146	0.294	0.443	0.588
Dimension group	POM	Water Quality	Physical Water Parameters	Water Quality

Table 2.12 Bottom water forward stepwise linear regression of all rotated PCA dimension groups. Table a is models run by analysis, Table b is results of regression for each model in table a.

Table a.

Model	Predictors					
1	Mobile					
2	Mobile	Mobile 3				
3	Mobile	Mobile 3	PP			
4	MS 3	Mobile	Mobile 3	PP		
5	MS	MS 3	Mobile	Mobile 3	PP	
6	MS	MS 3	Mobile	Mobile 3	PP	PP 3

MS = Mississippi River
Mobile = Mobile River
PP = Pearl and Pascagoula Rivers

no number = no lag included
3 = three month lag

Table b.

Model	Adj. R-Square	Pred R-Square	R-Square	C(p)	AIC	SBIC	SBC	MSEP	FPE	HSP	APC
1	0.11	0.11	0.11	33.63	2160.83	787.06	2173.37	2441.74	5.07	0.01	0.90
2	0.14	0.13	0.13	21.31	2149.13	775.41	2165.86	2378.58	4.94	0.01	0.87
3	0.17	0.17	0.16	3.69	2131.73	758.27	2152.64	2289.90	4.77	0.01	0.84
4	0.17	0.17	0.16	3.81	2131.83	758.43	2156.92	2285.68	4.77	0.01	0.84
5	0.18	0.17	0.16	5.38	2133.40	760.03	2162.67	2288.43	4.79	0.01	0.85
6	0.18	0.17	0.15	7.00	2135.01	761.69	2168.47	2291.41	4.80	0.01	0.85

AIC: Akaike Information Criteria
SBIC: Sawa's Bayesian Information Criteria
SBC: Schwarz Bayesian Criteria
MSEP: Estimated error of prediction, assuming multivariate normality
FPE: Final Prediction Error
HSP: Hocking's Sp
APC: Amemiya Prediction Criteria

Table 2.13 Bottom water forward stepwise linear regression of rotated water quality PCA dimension groups. Table a is models run by analysis, Table b is results of regression for each model in table a.

Table a.

Model	Predictors					
1	MS 3					
2	Mobile	Mobile 3				
3	Mobile	Mobile 3	PP			
4	Mobile	Mobile 3	MS 3	PP		
5	Mobile	Mobile 3	MS	MS 3	SM	
6	Mobile	Mobile 3	MS	MS 3	SM	SM 3

MS = Mississippi River
Mobile = Mobile River
PP = Pearl and Pascagoula Rivers

no number = no lag included
3 = three month lag

Table b.

Model	Adj. R-Square	Pred R-Square	R-Square	C(p)	AIC	SBIC	SBC	MSEP	FPE	HSP	APC
1	0.07	0.07	0.07	77.07	1779.41	405.31	1791.95	1110.33	2.30	0.00	0.93
2	0.13	0.13	0.12	42.78	1748.80	374.84	1765.53	1040.16	2.16	0.00	0.88
3	0.19	0.19	0.18	10.94	1718.29	344.71	1739.20	974.61	2.03	0.00	0.82
4	0.2005	0.1938	0.1854	7.1476	1714.4947	341.0215	1739.587	965.0272	2.014	0.004	0.816
5	0.207	0.1987	0.1881	5.1963	1712.5036	339.1418	1741.778	959.1087	2.006	0.004	0.813
6	0.21	0.20	0.19	7.00	1714.30	340.98	1747.76	960.73	2.01	0.00	0.82

AIC: Akaike Information Criteria
SBIC: Sawa's Bayesian Information Criteria
SBC: Schwarz Bayesian Criteria
MSEP: Estimated error of prediction, assuming multivariate normality
FPE: Final Prediction Error
HSP: Hocking's Sp
APC: Amemiya Prediction Criteria

Table 2.14 Bottom water forward stepwise linear regression of rotated POM PCA dimension groups. Table a is models run by analysis, Table b is results of regression for each model in table a.

Table a.

Model	Predictors					
1	MS 3					
2	MS 3	Mobile 3				
3	MS	MS 3	Mobile 3			
4	MS	MS 3	Mobile 3	PP		
5	MS	MS 3	Mobile 3	PP	PP 3	
6	MS	MS 3	Mobile	Mobile 3	PP	PP 3

MS = Mississippi River
Mobile = Mobile River
PP = Pearl and Pascagoula Rivers

no number = no lag included
3 = three month lag

Table b.

Model	Adj. R-Square	Pred R-Square	R-Square	C(p)	AIC	SBIC	SBC	MSEP	FPE	HSP
1	0.09	0.09	0.09	141.76	1577.74	203.22	1590.29	731.97	1.52	0.00
2	0.22	0.21	0.21	58.32	1508.19	134.05	1524.92	632.70	1.32	0.00
3	0.28	0.27	0.27	20.05	1472.42	98.69	1493.33	586.42	1.22	0.00
4	0.29	0.29	0.28	11.46	1463.97	90.41	1489.06	575.10	1.20	0.00
5	0.30	0.29	0.28	6.69	1459.17	85.77	1488.44	568.26	1.19	0.00
6	0.30	0.30	0.28	7.00	1459.46	86.13	1492.92	567.45	1.19	0.00

AIC: Akaike Information Criteria
SBIC: Sawa's Bayesian Information Criteria
SBC: Schwarz Bayesian Criteria
MSEP: Estimated error of prediction, assuming multivariate normality
FPE: Final Prediction Error
HSP: Hocking's Sp
APC: Amemiya Prediction Criteria

Table 2.15 Bottom water forward stepwise linear regression of physical water PCA dimension groups. Table a is models run by analysis, Table b is results of regression for each model in table a.

Table a.

Model	Predictors					
1	Mobile					
2	Mobile	PP 3				
3	MS	MS 3	Mobile			
4	MS	MS 3	Mobile	PP 3		
5	MS	MS 3	Mobile	PP	PP 3	
6	MS	MS 3	Mobile	Mobile 3	PP	PP3

MS = Mississippi River
Mobile = Mobile River
PP = Pearl and Pascagoula Rivers

no number = no lag included
3 = three month lag

Table b.

Model	Adj. R-Square	Pred R-Square	R-Square	C(p)	AIC	SBIC	SBC	MSEP	FPE	HSP
1	0.19	0.18	0.18	24.04	1424.41	50.71	1436.95	533.22	1.11	0.00
2	0.21	0.21	0.20	9.98	1410.73	37.15	1427.46	517.30	1.08	0.00
3	0.22	0.22	0.21	4.78	1405.54	32.06	1426.45	510.74	1.06	0.00
4	0.23	0.22	0.22	3.10	1403.82	30.43	1428.91	507.89	1.06	0.00
5	0.23	0.22	0.21	5.00	1405.72	32.36	1434.99	508.85	1.06	0.00
6	0.23	0.22	0.21	7.00	1407.72	34.39	1441.17	509.92	1.07	0.00

AIC: Akaike Information Criteria
SBIC: Sawa's Bayesian Information Criteria
SBC: Schwarz Bayesian Criteria
MSEP: Estimated error of prediction, assuming multivariate normality
FPE: Final Prediction Error
HSP: Hocking's Sp
APC: Amemiya Prediction Criteria

Table 2.16 Final Surface water models determining riverine contribution to environmental parameters. Rivers are in order of statistical importance.

Dimension groups and parameters included	linear model *p* value	Rivers included in final model	*p* values of ANOVA for each river	0.5% CI	99.5% CI
All Parameters	< 2.2E-16				
		Mobile River lagged 3 months	< 2.00E-16	7.80E-05	1.42E-04
		Mobile River	2.64E-07	-1.38E-04	-4.65E-05
		Mississippi River	1.42E-05	-3.42E-06	-8.83E-07
		Pearl + Pascagoula Rivers	6.85E-05	1.99E-05	9.17E-05
		Pearl + Pascagoula Rivers lagged 3 months	0.07991	-3.48E-05	6.66E-06
Water quality	<2.2E-16				
PO4, DIN, Temp, DON		Mississippi River	1.05E-09	-2.83E-06	-1.17E-06
		Mobile River lagged 3 months	4.73E-08	1.75E-05	4.80E-05
		Mississippi River lagged 3 months	1.37E-06	6.28E-07	2.04E-06
		Pearl + Pascagoula Rivers	3.59E-04	8.85E-06	5.42E-05
		Mobile River	1.29E-04	-7.49E-05	-1.48E-05
POM	5.12E-15				
POC, PON, d13C, C:N		Mobile River lagged 3 months	3.97E-14	4.15E-05	8.27E-05
		Mississippi River	2.51E-05	-1.80E-06	-4.39E-07
		Pearl + Pascagoula Rivers lagged 3 months	3.25E-04	-3.13E-05	-5.22E-06
Physical Water Quality	NA				

Table 2.17 Final bottom water models determining riverine contribution to environmental parameters. Rivers are in order of statistical importance.

Dimension groups and parameters included	linear model *p* value	Rivers included in final model	*p* values of ANOVA for each river	0.5% CI	99.5% CI
All Parameters	< 2.2E-16				
		Mobile River	4.12E-16	-1.80E-04	-9.57E-05
		Mobile River lagged 3 months	4.87E-06	1.47E-05	5.21E-05
		Pearl + Pascagoula Rivers	1.17E-05	2.35E-05	8.94E-05
Water quality	< 2.2E-16				
DIN, DO, DON		Mobile River	3.22E-15	-1.19E-04	-6.15E-05
		Mobile River lagged 3 months	3.50E-07	1.46E-05	4.39E-05
		Pearl + Pascagoula Rivers	7.65E-06	1.70E-05	6.23E-05
		Mississippi River lagged 3 months	0.034	-1.19E-07	1.20E-06
		Mississippi River	0.047	-1.85E-07	1.42E-06
POM	< 2.2E-16				
d13C, C:N		Mississippi River lagged 3 months	< 2E-16	-2.47E-06	-1.49E-06
		Mississippi River	5.02E-13	-2.46E-06	-1.19E-06
		Mobile River lagged 3 months	2.83E-10	2.12E-05	4.95E-05
		Pearl + Pascagoula Rivers	2.64E-04	4.70E-06	2.70E-05
		Pearl + Pascagoula Rivers lagged 3 months	9.58E-03	5.05E-08	1.76E-05
Physical Water Quality	<2.2E-16				
PO4, Temp		Mobile River	3.37E-09	-4.30E-05	-1.72E-05
		Mississippi River	0.024	-1.05E-06	6.89E-08
		Mississippi River lagged 3 months	0.053	-8.17E-07	1.16E-07
		Pearl + Pascagoula Rivers lagged 3 months	0.055	-1.06E-05	1.55E-06

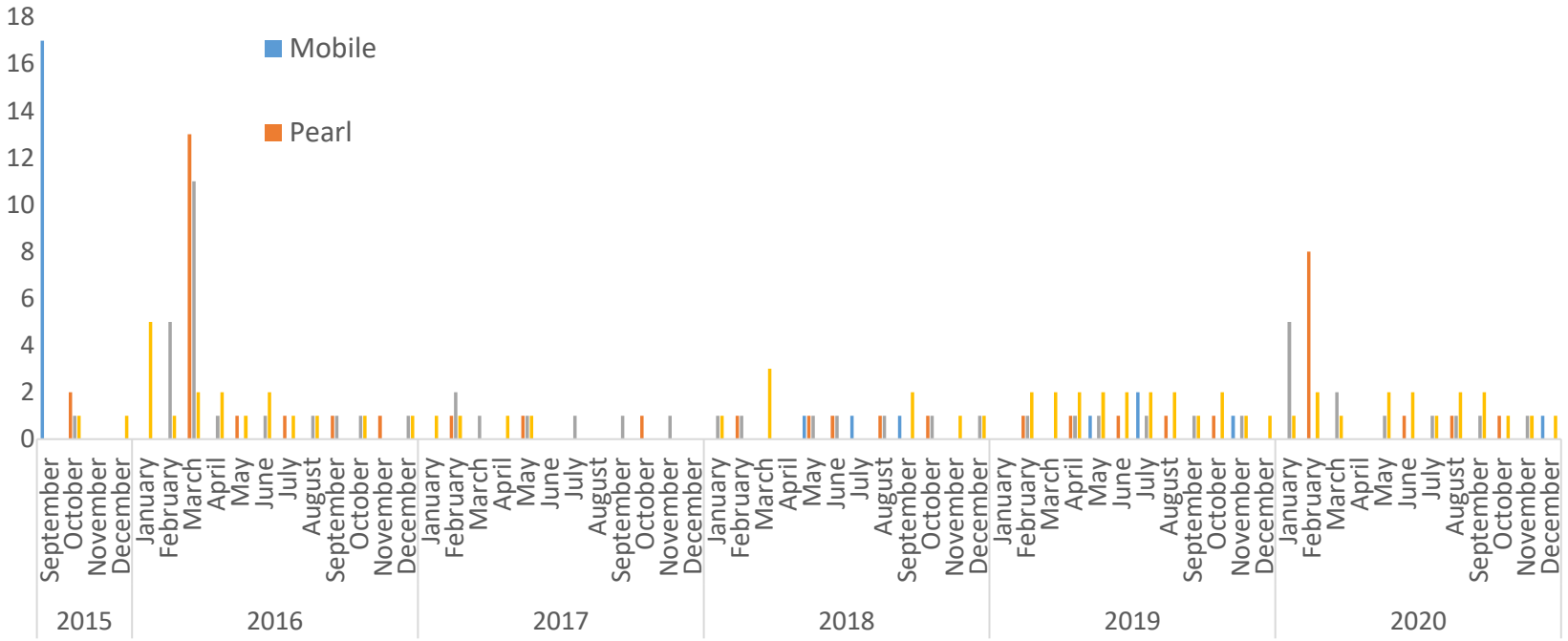

Figure 2.1 Count of number of times stream channel area was measured by the USGS during outflow periods relevant to the study for each river included in the study.

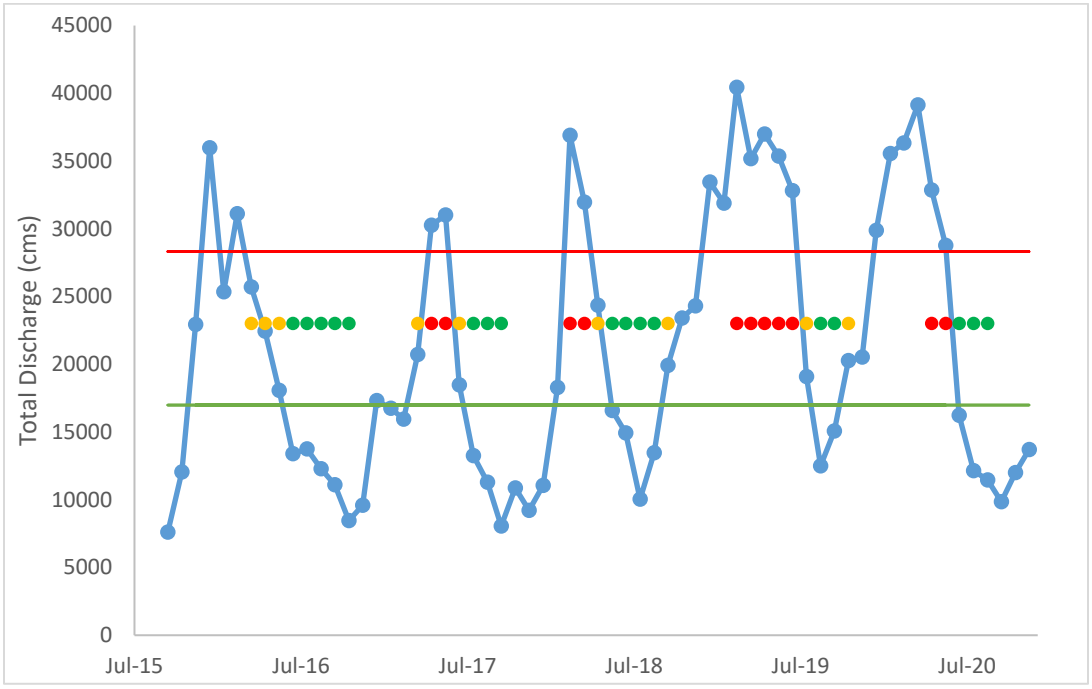

Figure 2.2 Average monthly total discharge from the Mississippi, Pearl Pascagoula, and Mobile rivers with outflow periods marked. Above red line indicates high outflow, between lines indicates mid outflow, and below green line indicates low outflow. Months when sampling occurred are marked by dots. Green dots indicate the month was coded as low outflow, orange indicates mid outflow, and red indicates high outflow.

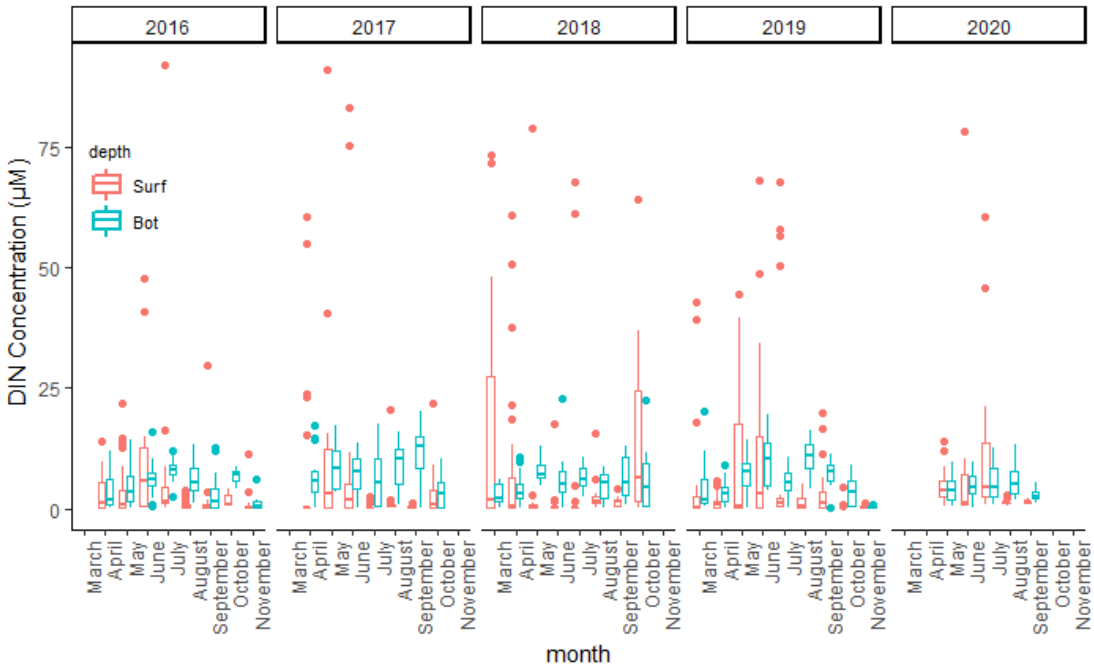

Figure 2.3 Dissolved inorganic nitrogen concentrations by depth across all sampling months and years.

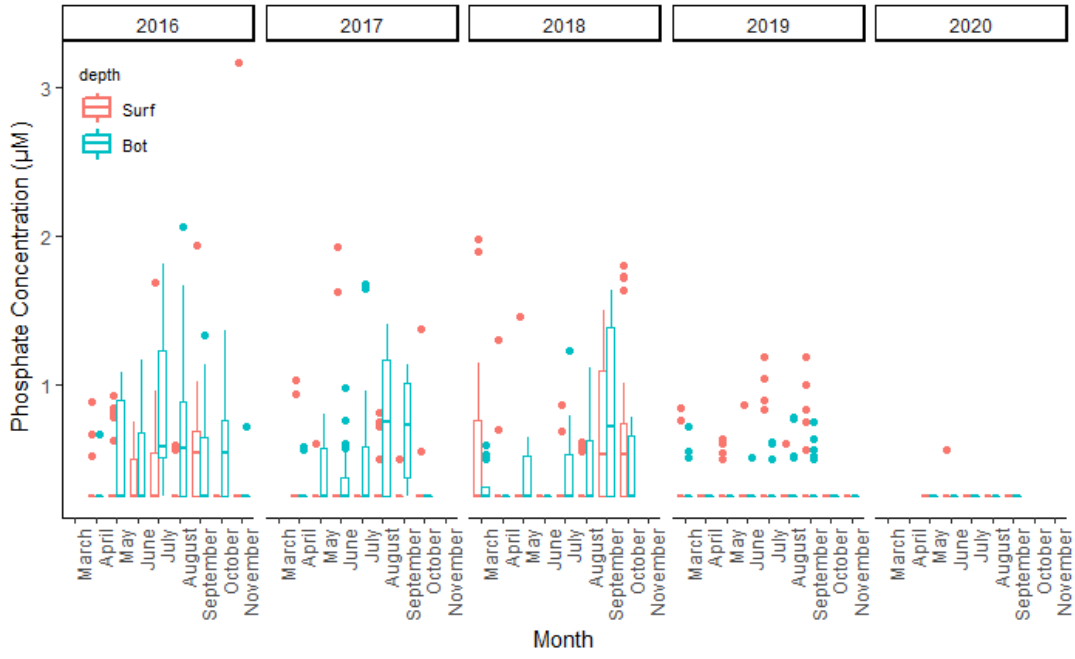

Figure 2.4 Phosphate concentration by depth across all sampling months and years.

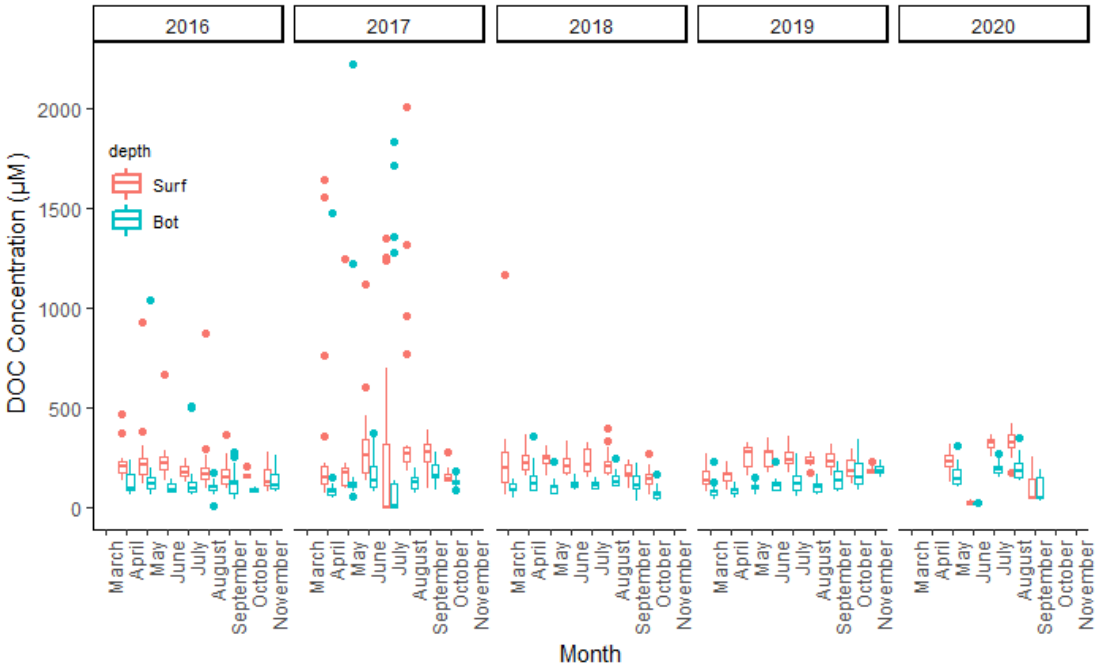

Figure 2.5 Dissolved organic carbon concentrations across all sampling months and years.

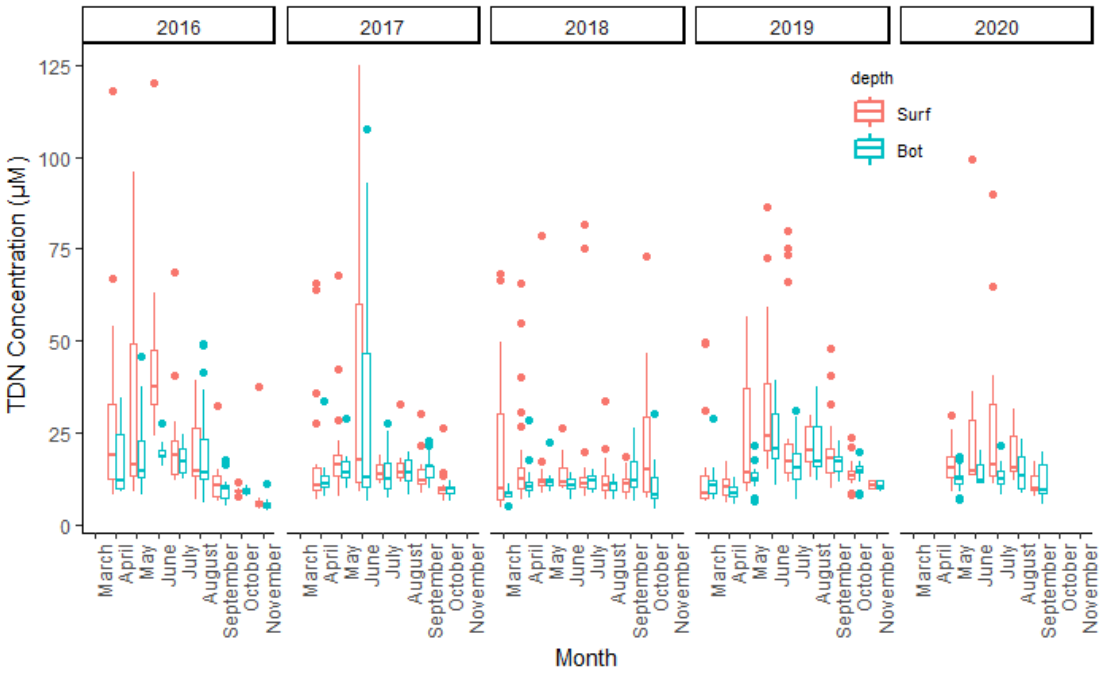

Figure 2.6 Total dissolved nitrogen concentrations across all sampling months and years.

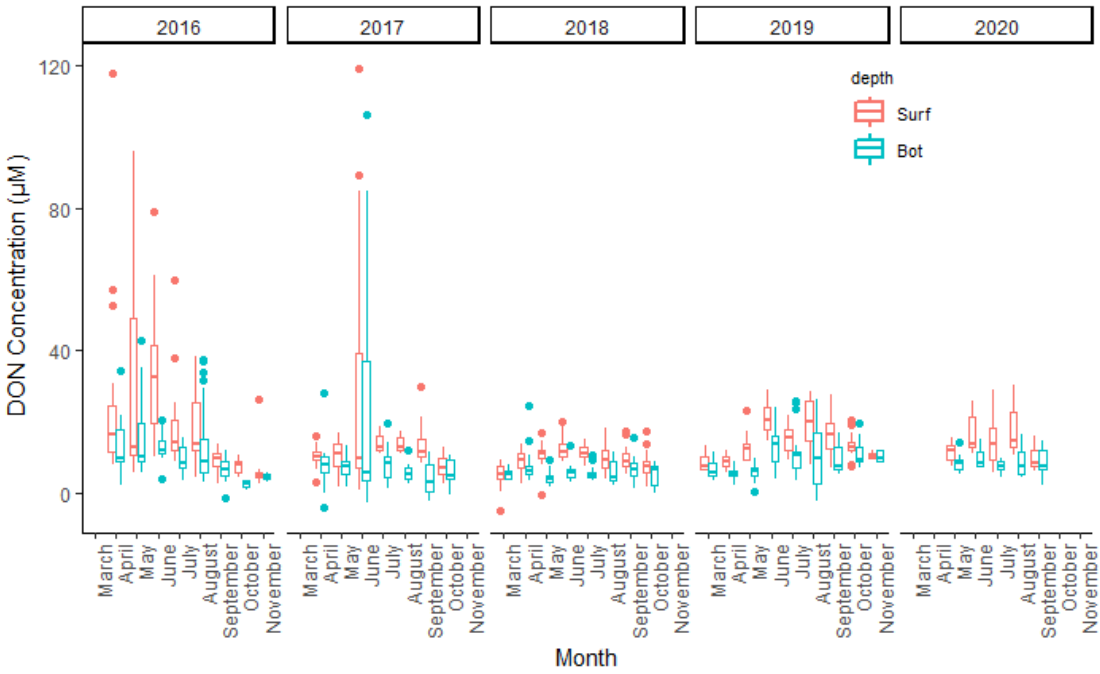

Figure 2.7 Dissolved organic nitrogen concentration across all sampling months and years.

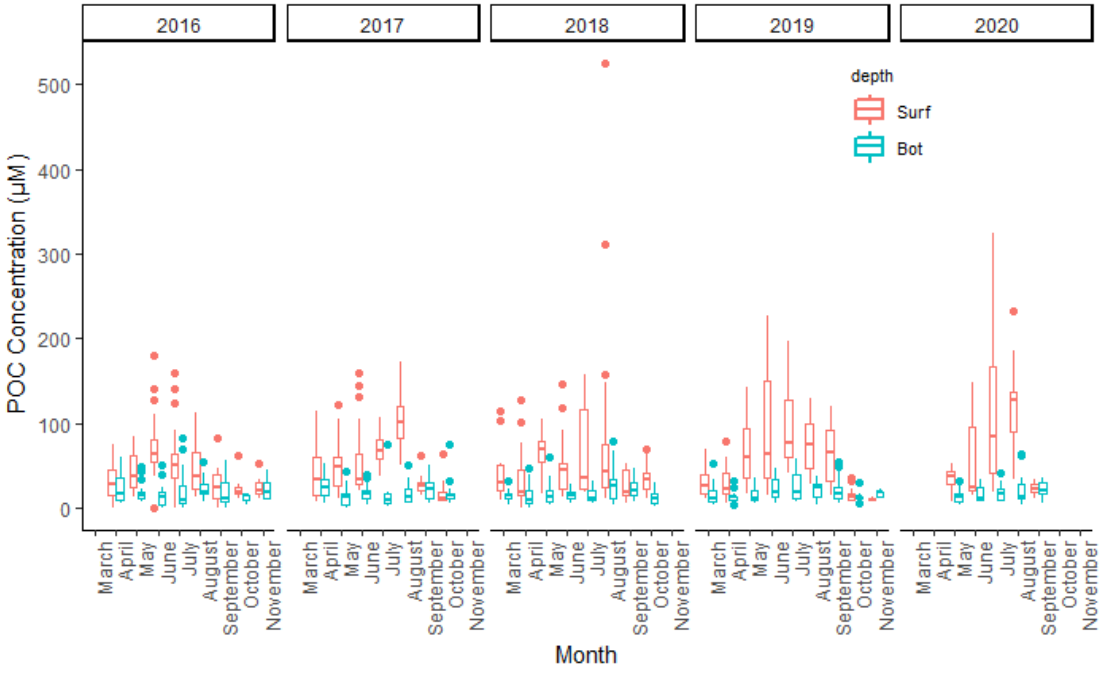

Figure 2.8 Particulate organic carbon concentration across all sampling months and years.

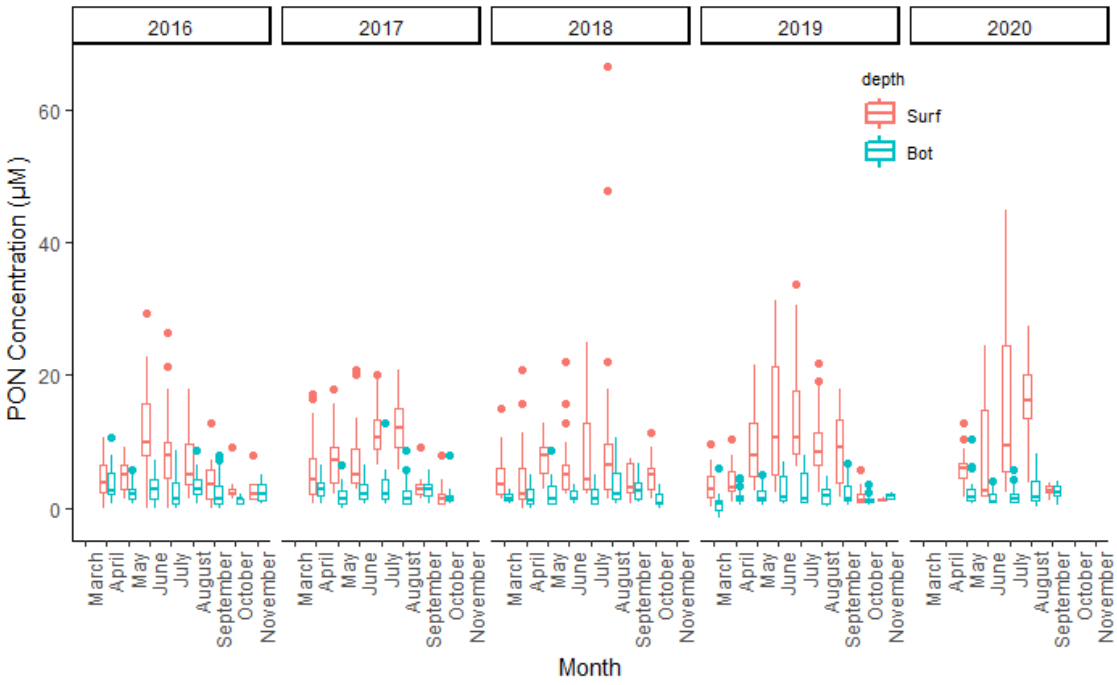

Figure 2.9 Particulate organic nitrogen concentration across all sampling months and years.

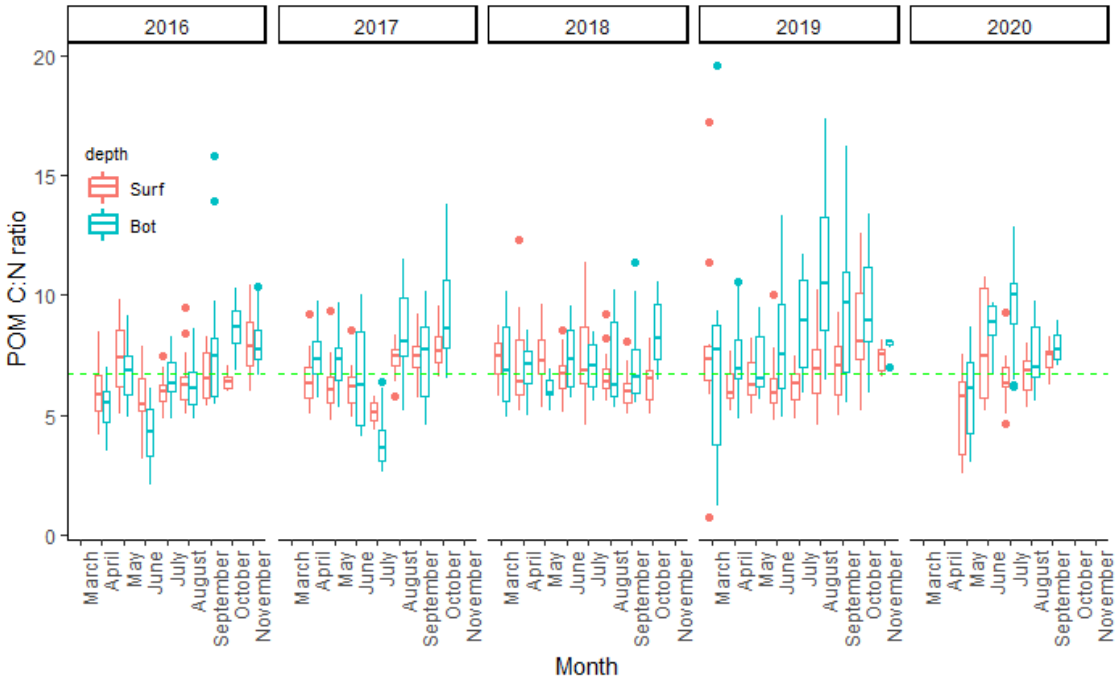

Figure 2.10 C:N by depth across all sampling months in all sampling years. Green dashed line indicates a C:N ratio of 6.7, the Redfield ratio.

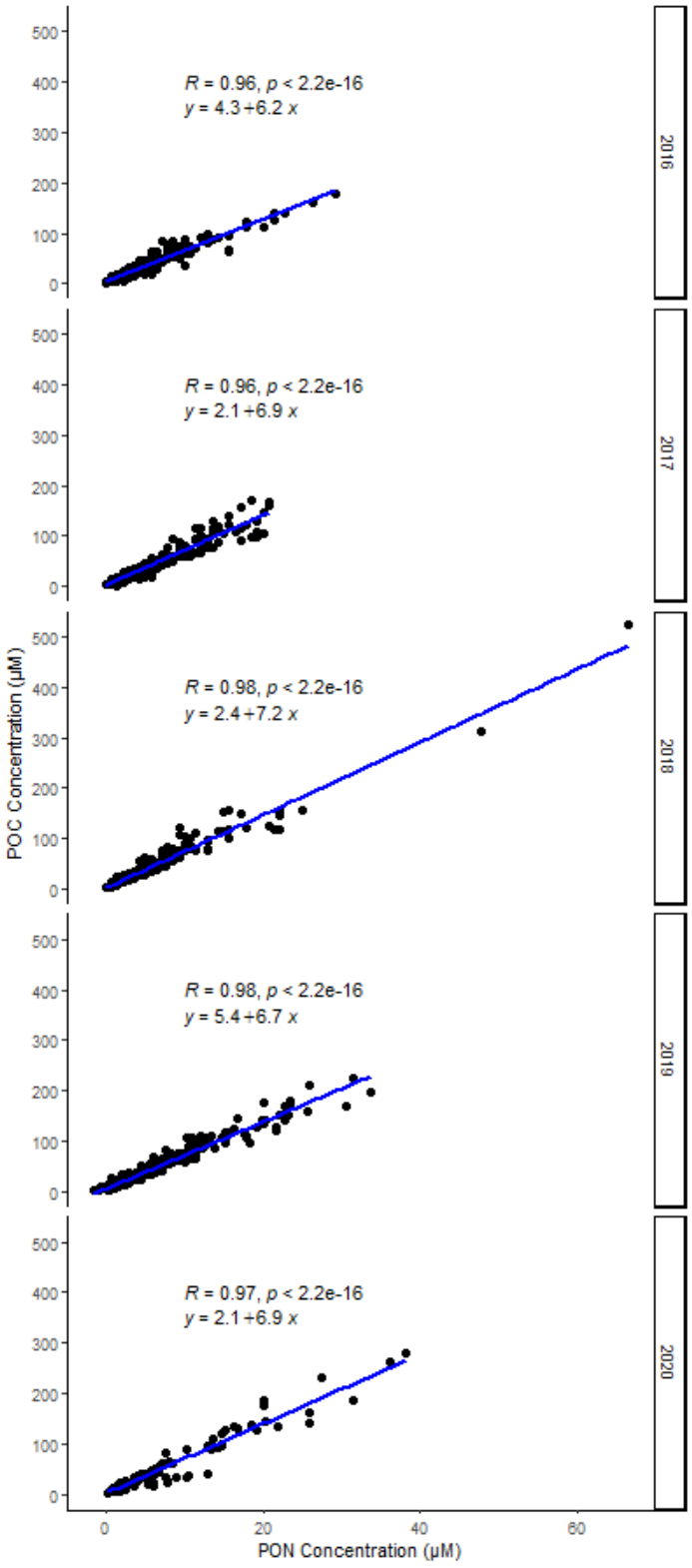

Figure 2.11 Particulate organic matter carbon vs. nitrogen over all 5 years. The slope of all years is near the Redfield ratio (6.7).

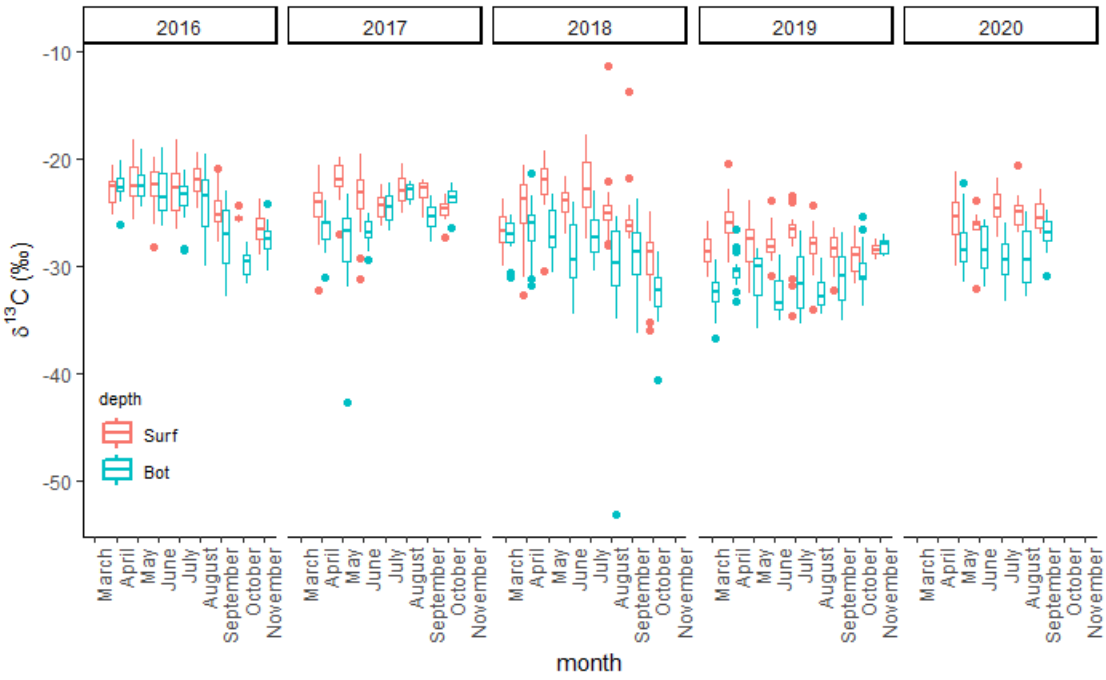

Figure 2.12 $\delta^{13}C$ by depth across all sampling months in all sampling years.

Figure 2.13 $\delta^{13}C$ by depth across all sampling months in all sampling years.

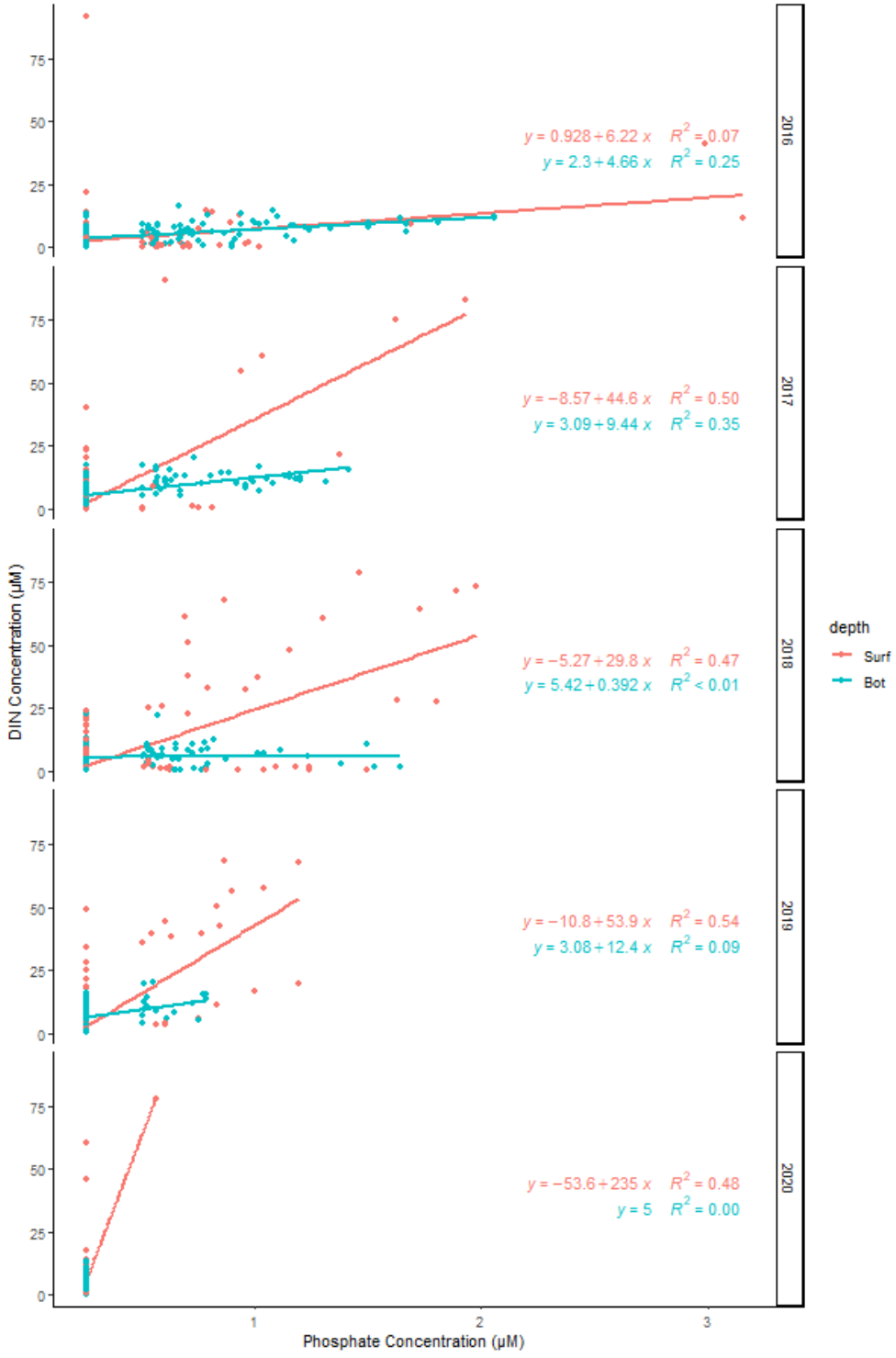

Figure 2.14 DIN versus PO_4 concentrations across all 5 years by surface and bottom water sampling. For all years combined, surface water Pearson correlation r = 0.46 and bottom water r =0.16.

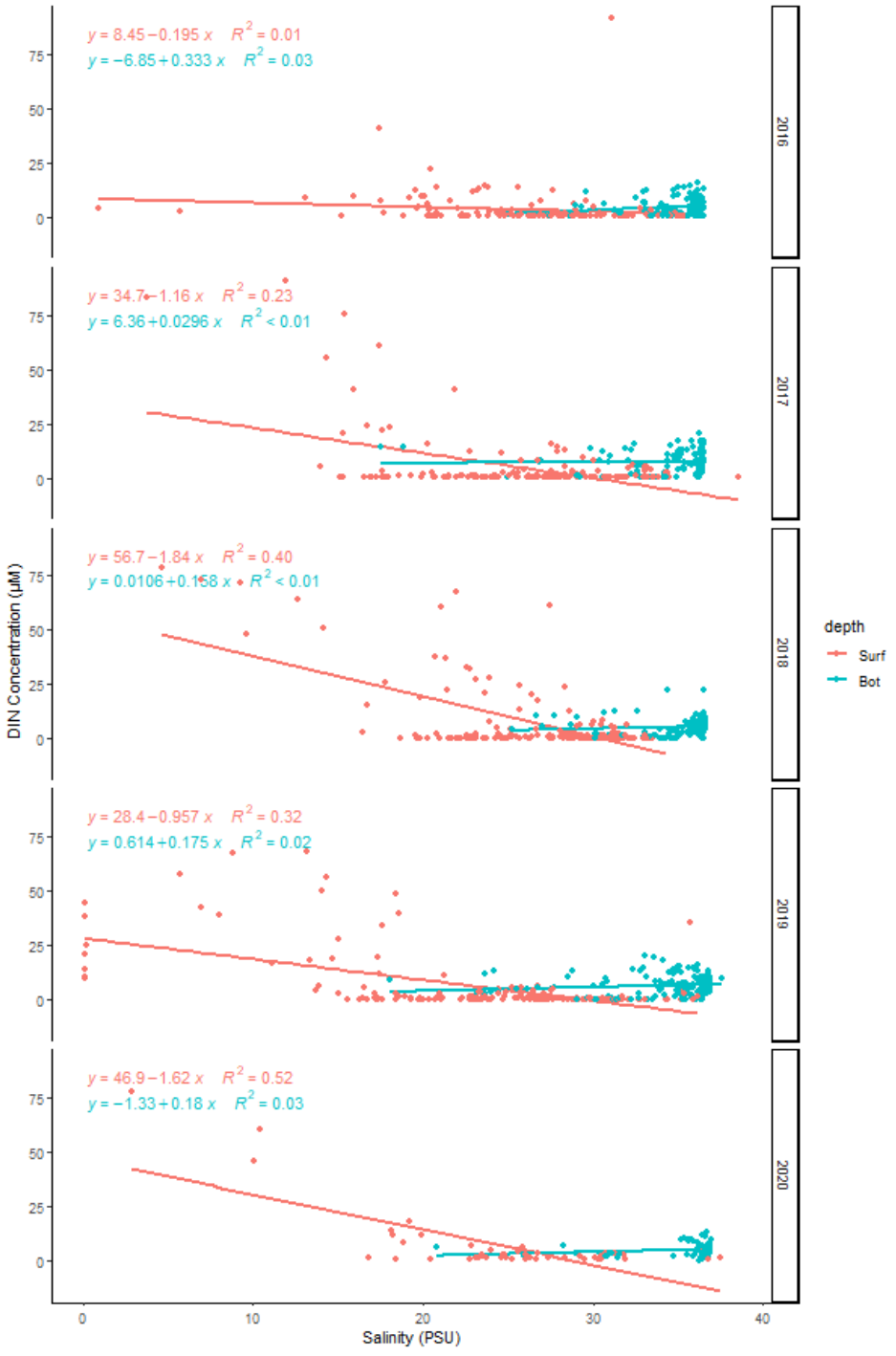

Figure 2.15 Salinity versus DIN concentrations across all 5 years by surface and bottom water sampling. For all years combined, surface water Pearson correlation r = -0.45 and bottom water r = 0.13.

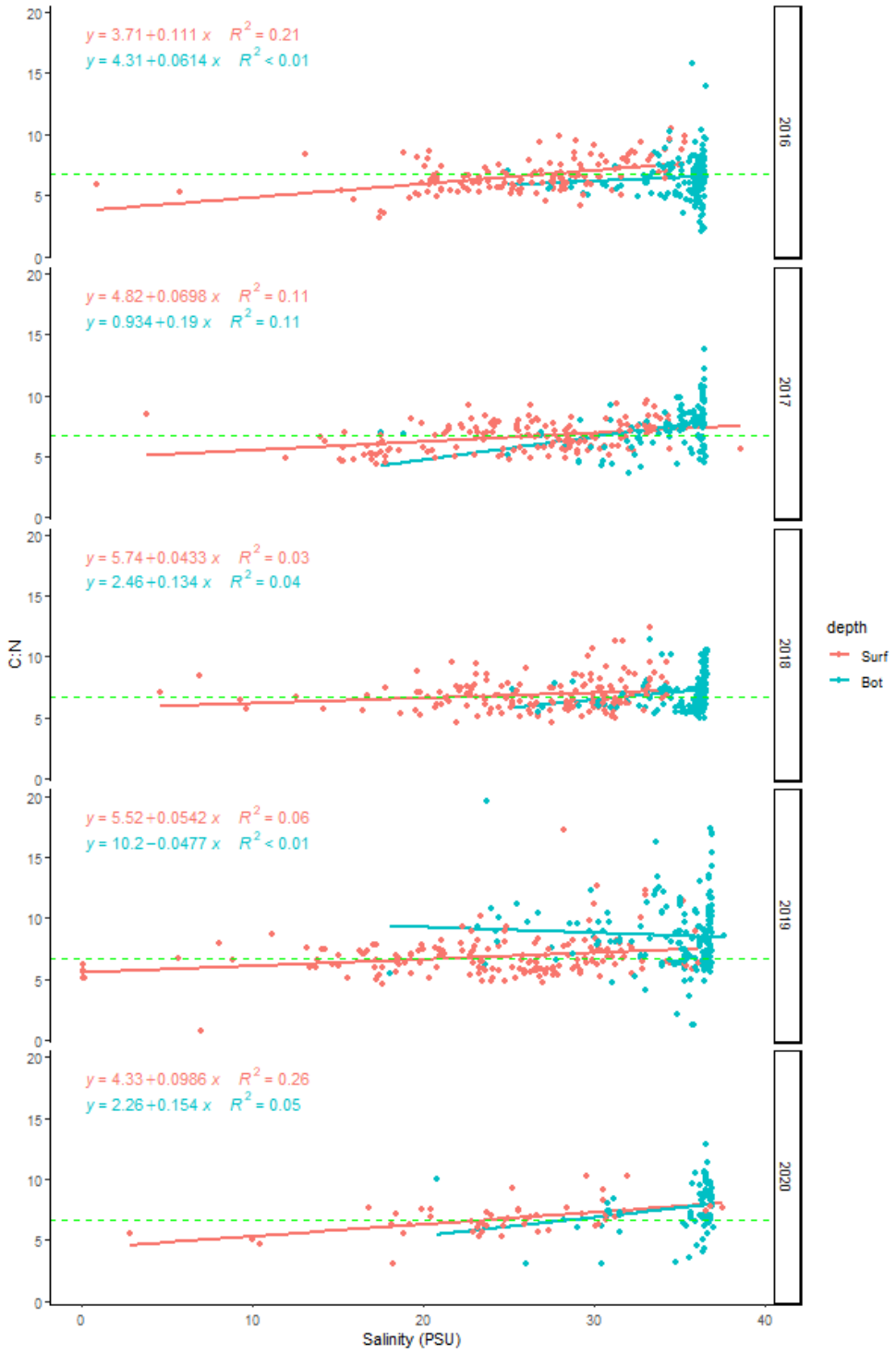

Figure 2.16 Salinity versus POM C:N across all 5 years by surface and bottom water sampling. For all years combined, surface water Pearson correlation r = 0.30 and bottom water r = 0.06. Green dashed line indicates the C:N Redfield ratio of 6.7.

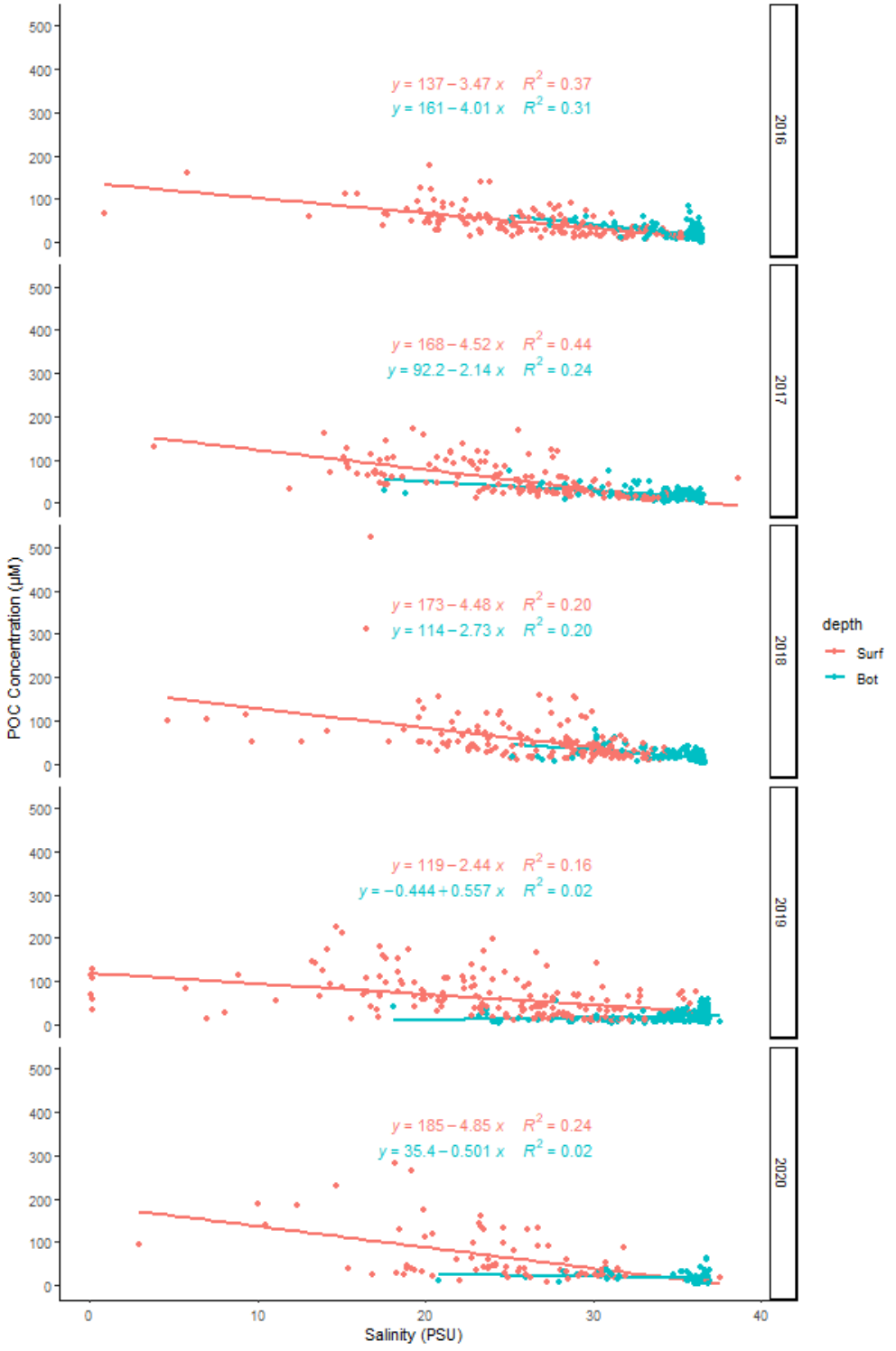

Figure 2.17 Salinity versus POC concentration across all 5 years by surface and bottom water sampling. For all years combined, surface water Pearson correlation r = -0.47 and bottom water r = -0.23.

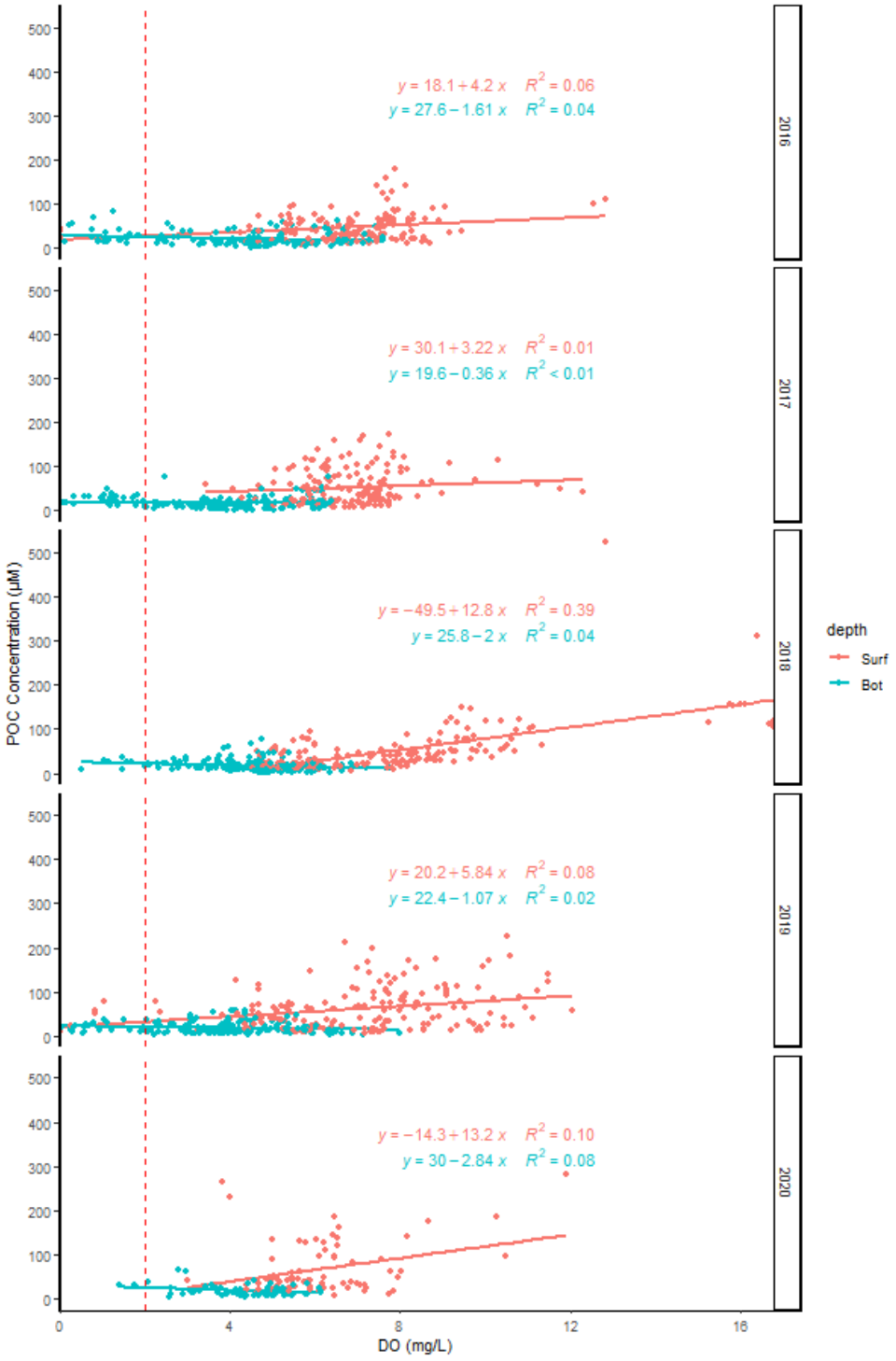

Figure 2.18 POC versus DO across all 5 years by surface and bottom water sampling. For all years combined, surface water Pearson correlation r = 0.43 and bottom water r = 0.06. Red short dashed line indicates threshold for hypoxic conditions., black line indicates anoxic conditions (1).

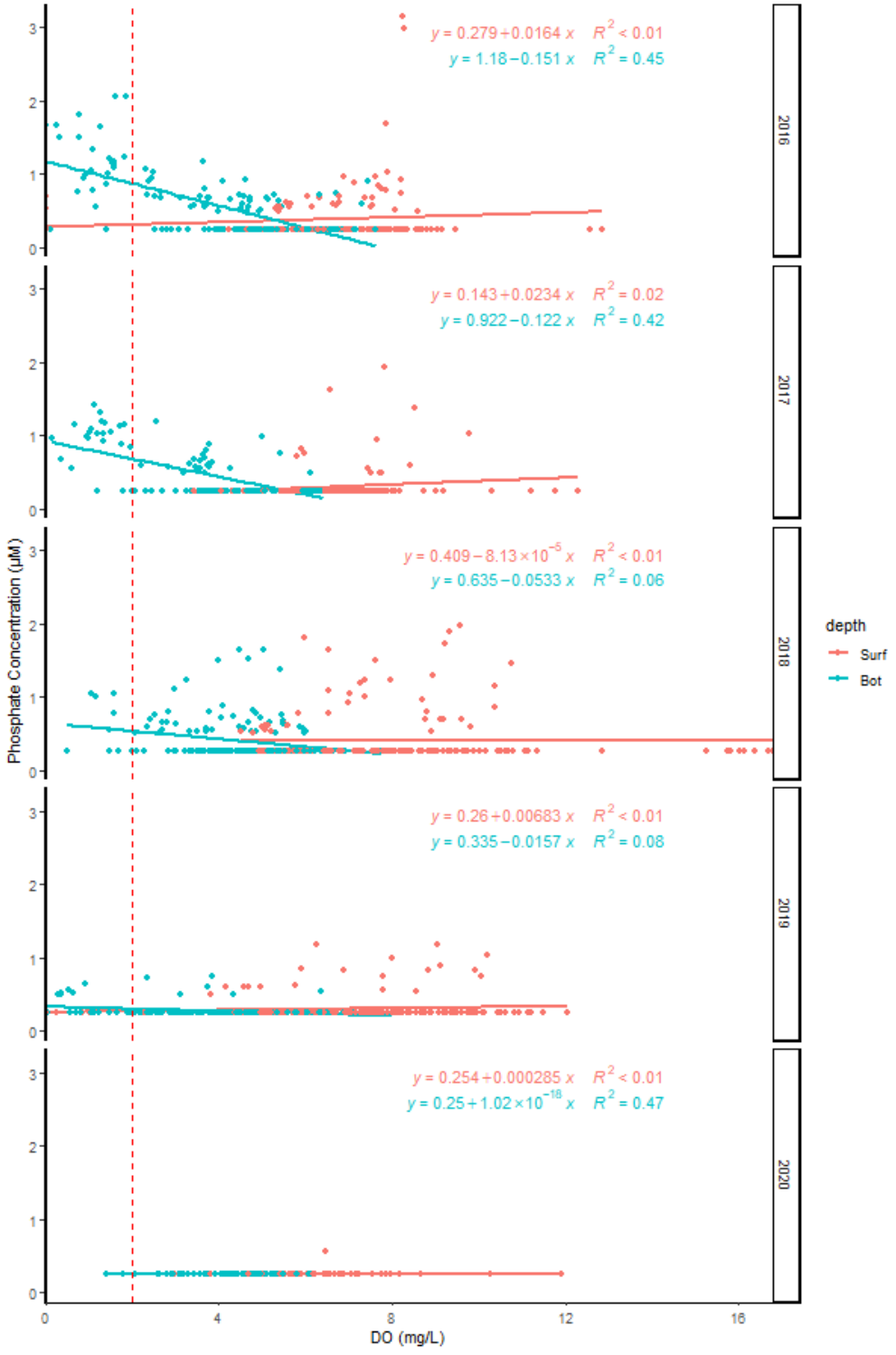

Figure 2.19 PO_4 versus DO across all 5 years by surface and bottom water sampling. For all years combined, surface water Pearson correlation r = 0.03 and bottom water r = -0.38. Red dashed line indicates threshold for hypoxic conditions.

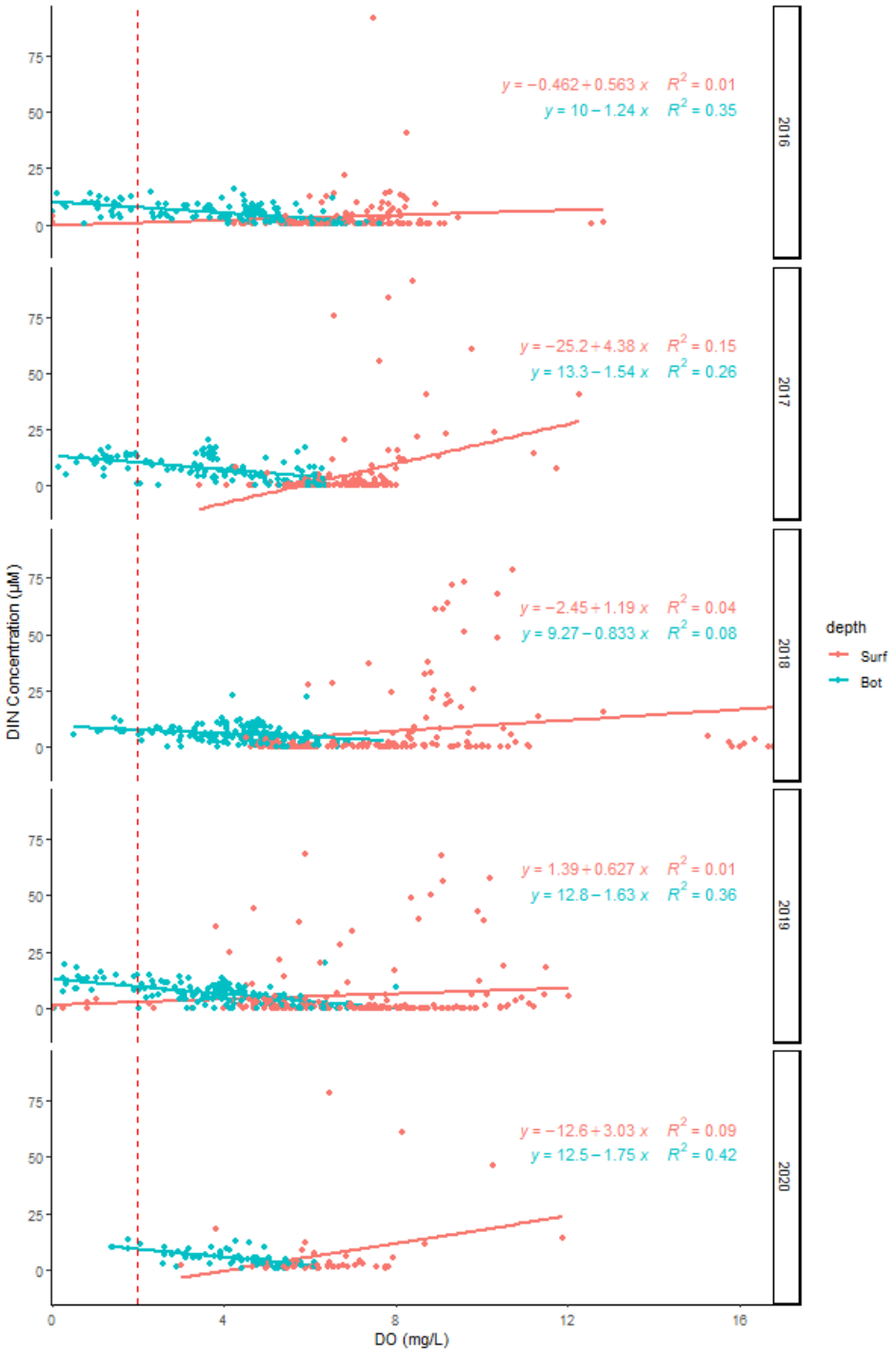

Figure 2.20 DIN versus dissolved oxygen across all 5 years by surface and bottom water sampling. For all years combined, surface water Pearson correlation r = 0.15 and bottom water r = -0.58. Red dashed line indicates hypoxic conditions (1).

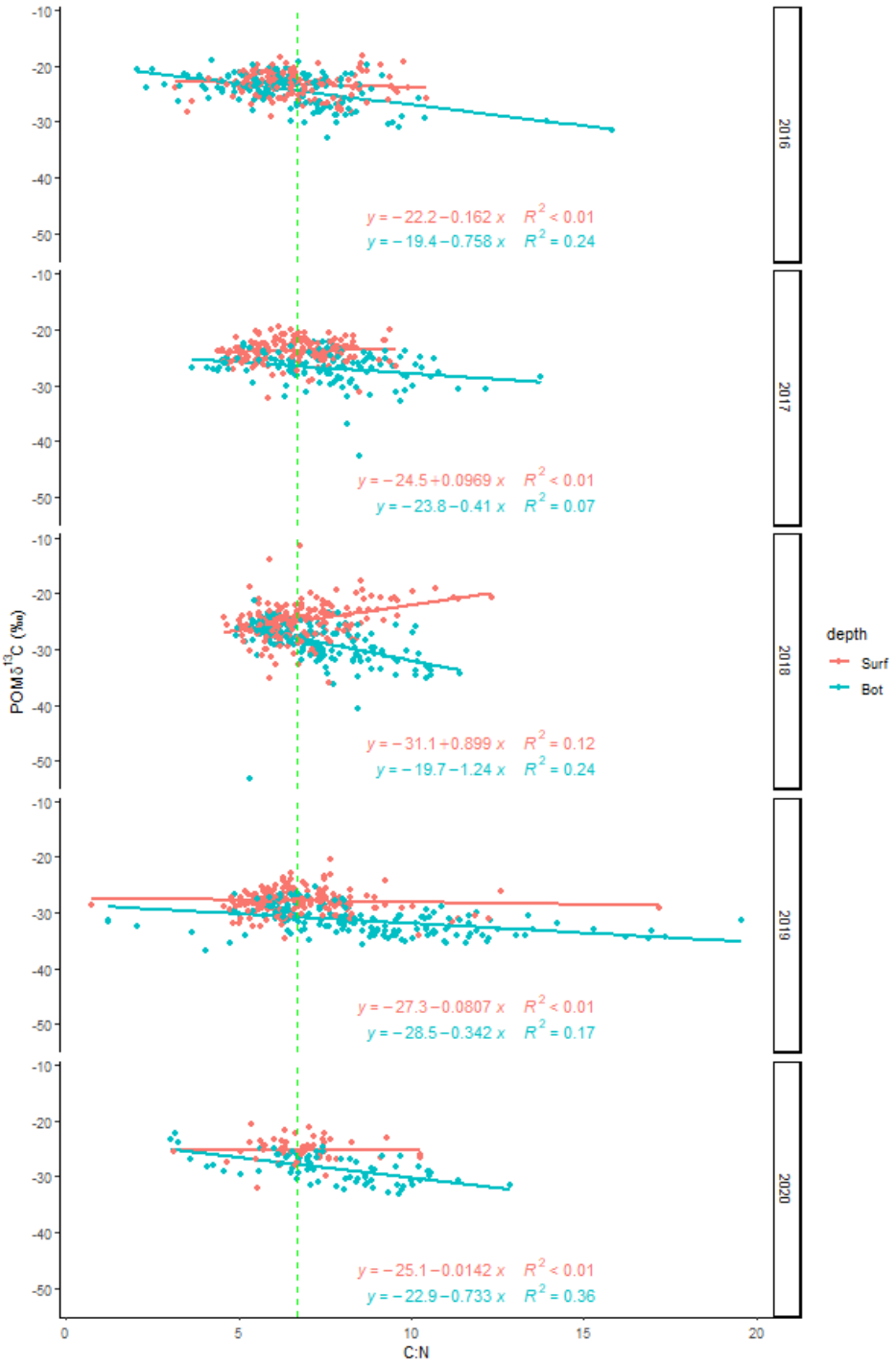

Figure 2.21 POM δ13C versus POM C:N across all 5 years by surface and bottom water sampling. For all years combined, surface water Pearson correlation r = 0.13 and bottom water r = -0.57. Green dashed line indicates the C:N Redfield ratio of 6.7.

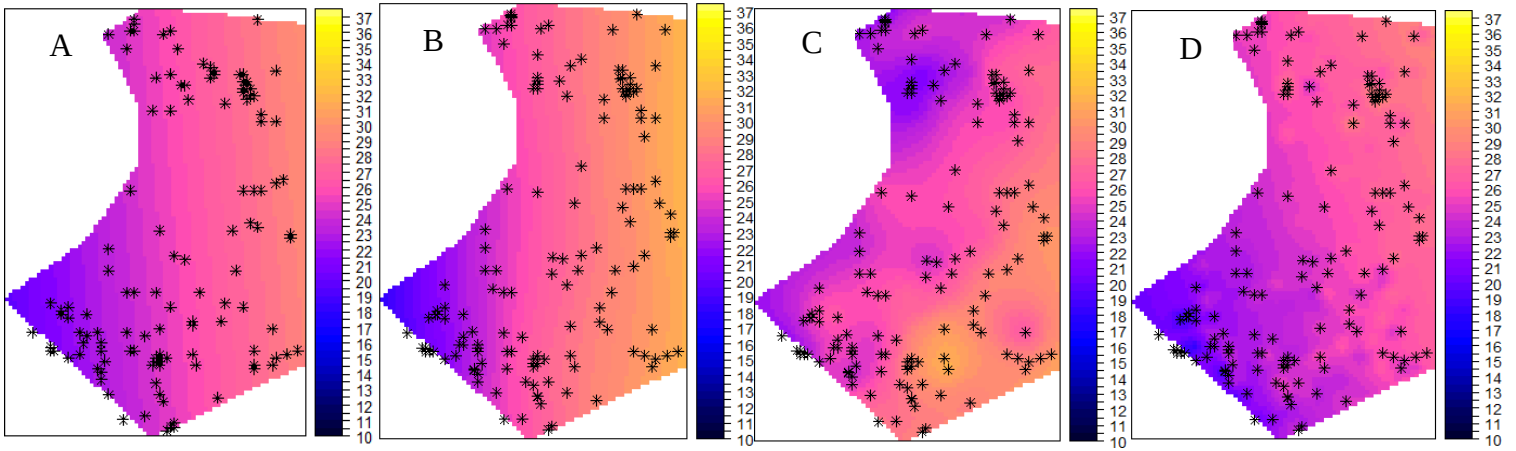

Figure 2.22 Mean salinity values over entire study (A), and under low (B), mid (C), and high (D) freshwater outflow regimes of surface water.

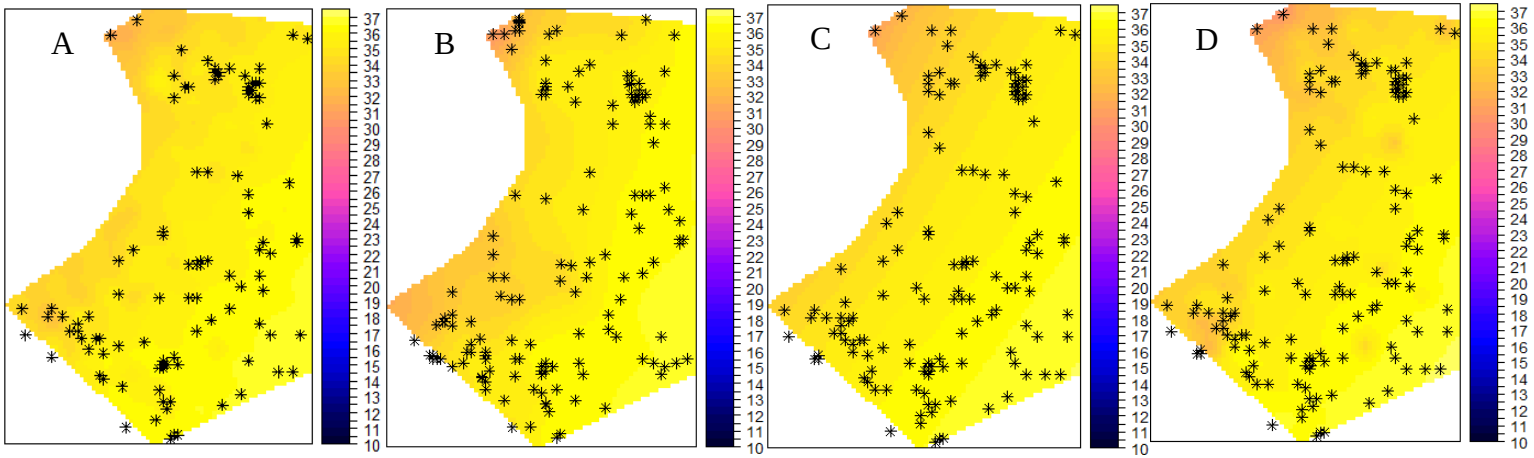

Figure 2.23 Mean salinity values of entire study (A), and under low (B), mid (C), and high (D) freshwater outflow regimes of bottom water.

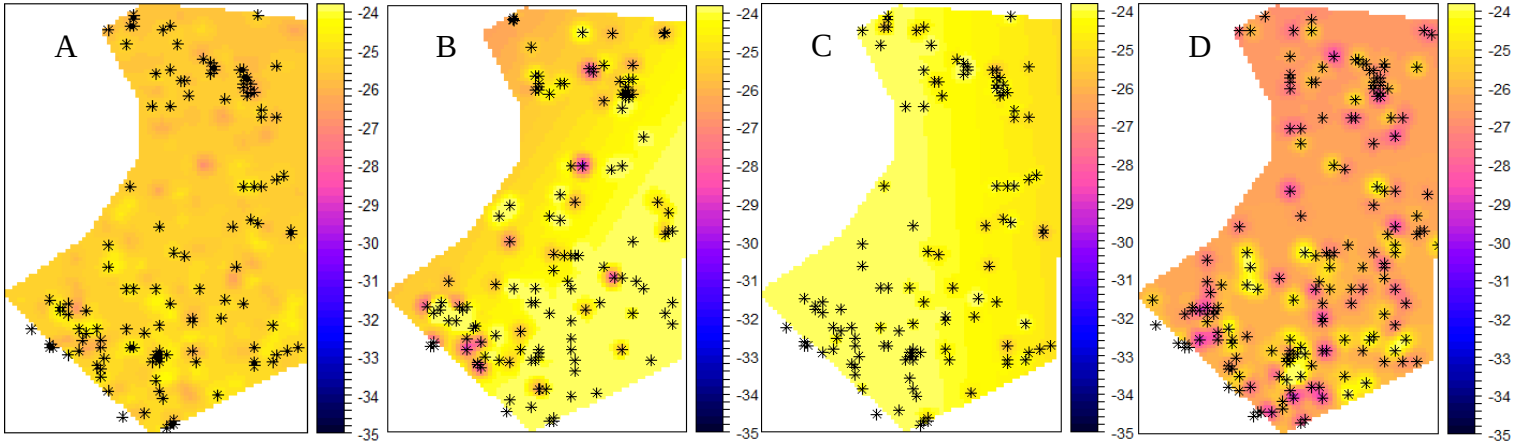

Figure 2.24 Mean $\delta^{13}C$ values of POM of entire study (A), and under low (B), mid (C), and high (D) freshwater outflow regimes of surface water.

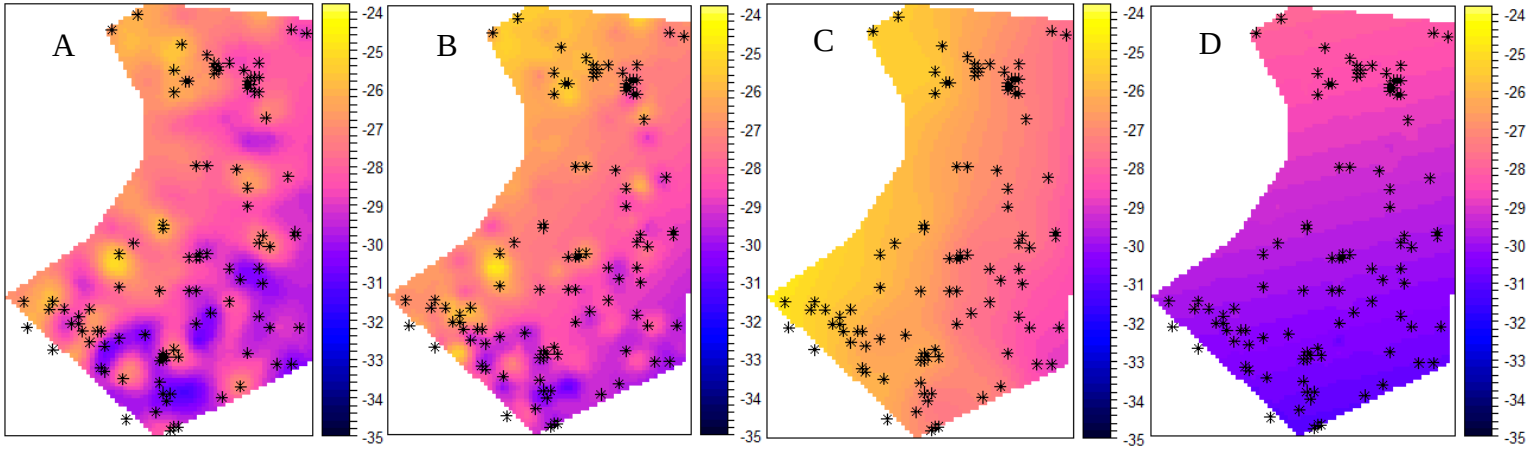

Figure 2.25 Mean $\delta^{13}C$ values of POM of entire study (A), and under low (B), mid (C), and high (D) freshwater outflow regimes of bottom water.

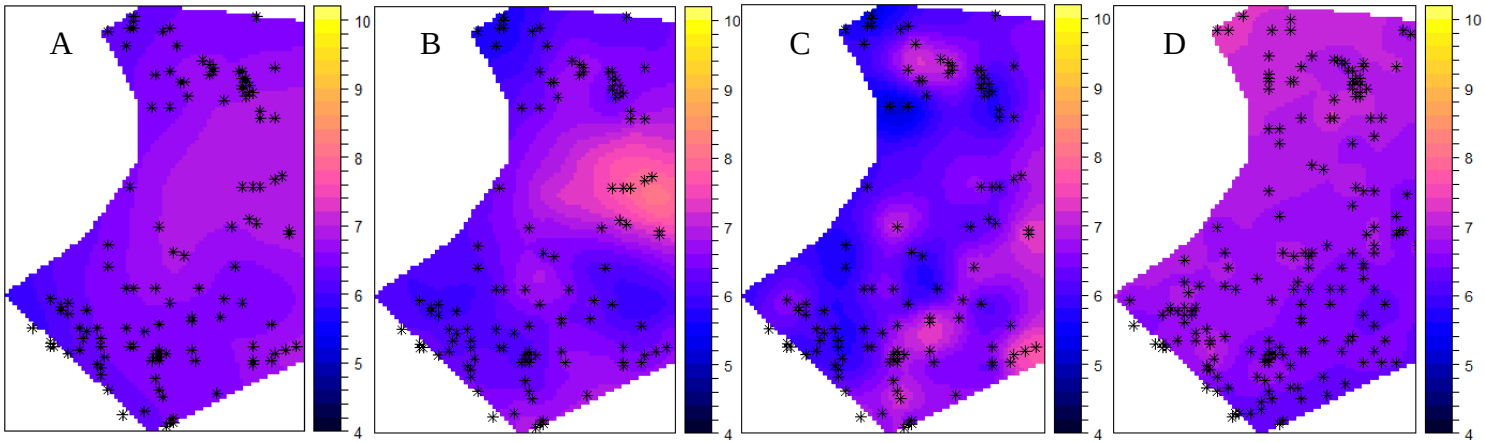

Figure 2.26 Mean C:N values of POM of entire study (A), and under low (B), mid (C), and high (D) freshwater outflow regimes of surface water.

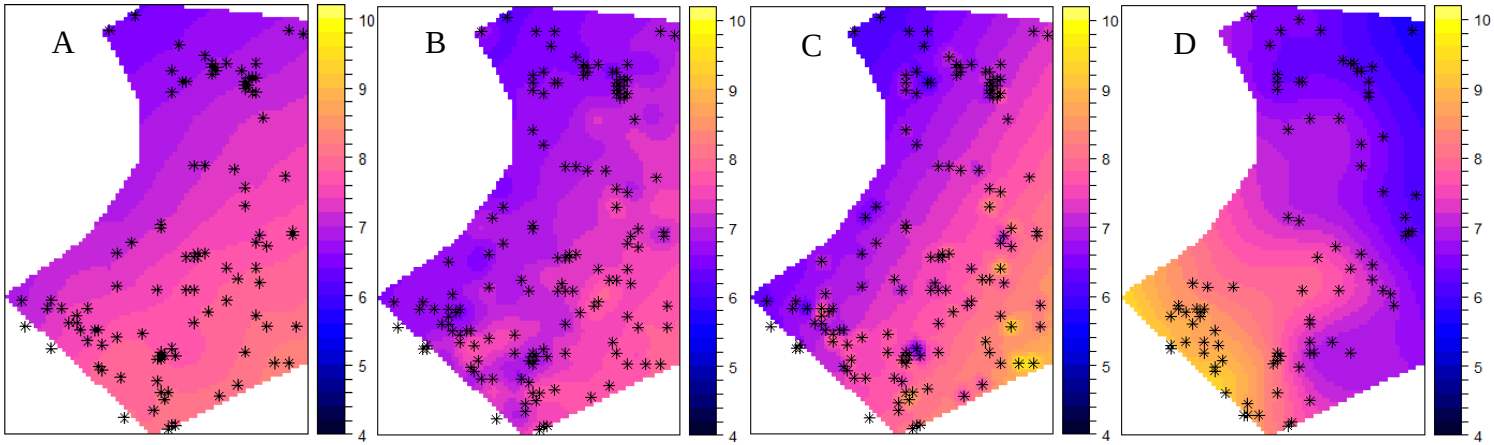

Figure 2.27 Mean C:N values of POM of entire study (A), and under low (B), mid (C), and high (D) freshwater outflow regimes of bottom water.

CHAPTER III – RIVERINE INFLUENCE ON RED SNAPPER DIET AND CONDITION IN THE NORTHERN GULF OF MEXICO

3.1 Abstract

In the Northern Gulf of Mexico Red Snapper have long been characterized as general, benthically oriented predators. However, riverine impacts to the region significantly control salinity, nutrients, and particulate organic matter present in the system, which in turn impact the Red Snapper prey assemblage. Results of stomach content alone can artificially skew results towards less digestible material such as bone and carapace while softer, more digestible food items such as fish eggs may be underestimated. Sampling the prey field directly is difficult due to the wide range of potential diet options available in a variety of depths and habitats. In this study, using bulk stable isotope analysis of prey collected directly from Red Snapper stomachs, we use Bayesian mixing models to determine contributions to Red Snapper diet under different river outflow regimes caused by the Mississippi, Pearl, Pascagoula, and Mobile Rivers and compare these to results from traditional stomach content analysis. Low outflow regimes had the highest prey diversity of the three hydrological regimes examined. Red Snapper diet was shown to be the least diverse under high flow, and condition of Red Snapper tended to decrease with increasing outflow. These results have the potential to allow managers to better predict Red Snapper diet according to river outflow, and thus the likely body conditions of the fish. They also suggest that increasing rainfall in the Mississippi River basin predicted under future climate change scenarios will lead to a decline in Red Snapper condition.

3.2 Introduction

The stable isotope value of carbon ($\delta^{13}C$) values of consumers are indicative of primary carbon sources that form the base of the food web since carbon exhibits little isotope fractionation (<1 ‰) with trophic transfer while nitrogen in consumer tissues becomes enriched in ^{15}N in a predictable manner by 2.2 to 3.4‰ with each trophic step. By plotting an organism's isotope values in two-dimensional isotope space ($\delta^{13}C$ vs $\delta^{15}N$) one can determine isotopic niche areas of organisms, a descriptive framework that enables direct comparison of isotopic niche space within or among species. This isotopic niche space contains ecological information based on isotope values of primary producers and how stable isotopes mix and fractionate through the food web, and therefore closely aligns with a subset of the *n*-dimensional Hutchinsonian niche space. The Hutchinsonian niche space incorporates a suite of environmental parameters a species relies upon plotted in a multiple dimension coordinate system to describe resource use and required habitat parameters for a species (Hutchinson 1957; Layman et al. 2012; Syväranta et al. 2013). The stable isotope values of carbon and nitrogen in fish muscle tissue integrate this dietary information over weeks to months for many fish species and can be as long as a year for large offshore pelagics such as Bluefin Tuna (Madigan et al. 2012), though this time period is much shorter in smaller fish (~170 days in small cyprinids) (Busst and Britton 2017). The time required for muscle tissue to reflect dietary changes is dependent on the time it takes for tissues to be replaced. The integration period of new isotopic ratios varies between tissue types and organism size. For example, a larger fish will take longer to incorporate the isotopic values of their diet than a smaller fish, and tissues such as plasma and liver have faster tissue turnover rates and will reflect isotope changes faster

than muscle tissue. Isotopic incorporation of fish muscle tissue has been shown to be allometrically correlated, slowing predictably with increased body size (Vander Zanden et al. 2015). Because of this relationship, dietary changes can be assessed as individuals move spatially, or as they move to higher trophic positions as they grow and consume larger prey which usually feed at higher trophic levels.

With the evolution of fisheries management strategies, more focus has been placed on ecosystem-based fisheries management (EBFM), which requires an in depth understanding of how a target species interacts with its habitats and other members of the food web. Different Red Snapper diets studies have shown differences in how Red Snapper utilize their habitats to feed, agreeing only that Red Snapper are generalist predators (Gallaway et al. 2009)(Table 2.1). Szedlmayer & Lee (2004) used SCUBA visual surveys and volumetric measurement of prey in gut contents to study Red Snapper diets in Alabama biweekly and showed that Red Snapper diet shifted from pelagic prey as juveniles to reef associated prey as adults once they settled on complex structure. Wells et al. (2008) used stable isotope analyses of Red Snapper muscle tissue and potential prey resources as well as stomach content analyses to study Alabama Red Snapper diets seasonally and found they consumed both pelagic and benthic prey such as squid, fish, mantis shrimp, penaeid shrimp, and crabs from benthic habitats adjacent to reefs throughout their life. McCawley et al. (2006) collected Red Snapper in Alabama at 2 hour time intervals and found that Red Snapper were opportunistic feeders during the daytime but fed on benthic invertebrates from sandy bottoms surrounding reef structure at night. Tarnecki & Patterson (2015) examined Red Snapper diets in Alabama and Florida waters before and after the Deep Water Horizon oil spill and found that Red Snapper diet was

dependent on the relative abundances of potential prey resources, which shifted post oil spill, resulting in Red Snapper feeding at a slightly higher trophic level. Szedlmayer & Brewton (2019) used DNA barcoding to identify digested remains of prey from gut content in Alabama state waters and determined that Red Snapper fed on prey from both open water and reef habits across many taxonomic groups and at various trophic levels. Later, Brewton et al. (2020) studied the muscle tissue stable isotopes and stomach contents of adult Red Snapper across a variety of habitats in the northwestern GOM off Port Aransas, TX, and found that diets were "complex and inconsistent" across habitat, size class, and year of sampling.

These various studies have determined that Red Snapper diets varies spatially and temporally in the NGOM, however the inherent variability in the prey field across the region limits broad conclusions on Red Snapper diet beyond describing them as generalist predators. Some studies focused on the Alabama artificial reef area (Szedlmayer and Brewton 2019; Szedlmayer and Lee 2004; McCawley et al. 2006; Wells et al. 2008) or the Texas continental shelf (Brewton et al. 2020) and occurred over relatively short time periods. Such limitations on study designs are common and justified but do prevent incorporating long term variability in regional hydrological regimes (i.e. amount of freshwater inflow) as informative parameters of study. Furthermore, some studies use stomach content analysis to determine diet, which only gives a snapshot of diet. This technique can skew results towards less digestible material such as carapace and bone and away from soft prey items such as gelatinous organisms and fish eggs that are quickly digested. The Wells et al. (2008) study did look at seasonal changes impact on diet but used stable isotope values of potential prey resources collected independently

rather than stomach content analysis. Despite potentially missing important prey items for inclusion in stable isotope analysis, they found that habitat type had a significant effect on prey source contribution, despite similar prey community assemblages. The Tarnecki and Patterson (2015) and Wells et al. (2008) studies suggests that any significant alteration to the prey assemblage may alter the diet of Red Snapper in a predictable way if the effect of the perturbation on the prey is known.

Variability in freshwater outflow in coastal ecosystems from regional rivers as well as periodic openings of water diversions such as the Bonne Carré Spillway for flood control alter the hydrological regimes of the study region (Whitfield 1996). Increased output for these sources significantly alters the salinity, nutrient regimes, and particulate organic matter distribution in the water column from the Mississippi Bight to the Mississippi Delta. Such changes to the physical and biogeochemical environment have the capacity to strongly affect the prey assemblage of the region. For example, decreased salinity in the study region may cause a decrease in abundance of certain prey species. Szedlmayer and Lee's 2004 study found that adult Red Snapper diet in Alabama was primarily composed of squid, and reef fish such as wrasse and blennies. *Lolliguncula brevis*, the bay squid is common across the Gulf of Mexico has a wide salinity tolerance range that allows it to inhabit inshore bays (Jackson et al. 1997). However, the lowest salinity it can tolerate under laboratory conditions is ~17.5 psu (Hendrix et al. 1981) and in this study, salinity regularly reached below 20 psu. Blennies are also common in the NGOM on artificial reefs. A study in Alabama which was occasionally impacted by freshwater outflow from Mobile Bay found a significant negative relationship between blenny abundance and salinity (Topolski and Szedlmayer 2004). Inversely, increased

nutrients in a region may increase abundance of certain species. An overview of the relationship between nutrients and fisheries production by Breitburg et al. (2009) states that increases in nutrients increases total fishery biomass despite hypoxia caused by eutrophication. In fact, the nutrients delivered by rivers is one of the attributes of this study region that earned it the moniker "the Fertile Fisheries Crescent" (Gunter 1963). Thus, although Red Snapper may be generalist predators, their diets may be more predictable than previously assumed based on environmental drivers of the prey assemblage.

In this study, we have attempted to determine if Red Snapper diet is more predictable than previously indicated by analyzing diet during different outflow regimes over 5 years with two different methods. Stomach content and stable isotope analyses were performed on collected Red Snapper. Then stable isotope analysis was performed on prey items collected as part of the stomach content analysis for use in stable isotope mixing models. We hypothesize results of stomach content analysis and isotope mixing models will vary under different hydrological regimes across the study area. Incorporating stable isotope analysis of true prey items provides a more temporally and spatially integrated insight into trophic relationships of organisms relative to stomach content analysis alone which only provide a snapshot of diet at the time of capture. We also analyzed Red Snapper body condition using Fulton's K to determine if the changes in hydrological regimes and Red Snapper diet caused any notable change to their condition. In this study, we grouped individuals by time collected, with groupings determined by river outflow rates as the most significant change to the environment.

3.3 Methods

3.3.1 Sample collection

Red Snapper were collected from bare bottom control sites and reef fish habitats (artificial reefs and oil/gas rigs) in the study region over 5 years (2016 through 2020) from March through October using SEAMAP Vertical Line Survey Protocol, Version 1.7 (Rester 2015). At each sampling site, three bandit reel lines were dropped to the bottom for 5 minute soaks. Each line was baited with Atlantic Mackeral with 10 hooks of either 8/0, 11/0, or 15/0 to target a wide size range. After the lines were retrieved, captured fish were immediately placed on ice. Within 24 hours, total, standard, and fork length and weight were measured, a muscle tissue sample was taken from the left dorsal quadrant of the fish for stable isotope analysis the stomach and upper intestines were removed, and otoliths were extracted. All tissue samples were placed on ice until return to the lab where they were frozen at -20°C until analysis.

Stomach contents were thawed and rinsed over a 500µm sieve, then morphologically identified to the lowest possible taxonomic level using published scientific literature and identification guides (Fahay 1983; McEachran and Fechhelm 2006; Carpenter 2002a; Carpenter 2002b; Richards 2005; Mceachran and Fechhelm 1998). Prey samples too digested or damaged to be identified with sufficient tissue (~1 cm^3) were refrozen until processed for DNA barcoding (Handy et al. 2011). Samples for barcoding were placed on a clean petri dish and cored (2-3 mm^3) with flame sterilized forceps and scalpels to remove tissue that may have been contaminated by the Red Snapper's stomach lining and/or gastric fluids. DNA from each sample was extracted using a commercial kit (DNeasy Blood and Tissue kit, Qiagen). The ~650bp barcode

region of cytochrome C oxidase Subunit I (COI) was amplified then visualized on a 2% agarose gel and positive reactions were sent to Eurofins for PCR clean-up and single-read sequencing. Sequences were trimmed using CLC Main Workbench to remove ambiguous and/or low-quality sequence, and primer sequence. DNA barcode sequences were analyzed using the Barcode of Life Data System (BOLD) and/or NCBI BLAST to identify the closest match(es) to known COI sequences. The closest match was identified based on a sequence similarity of at least 99% and >500 bp for species, 95-99% and >500 bp for genus, <95% and >500 bp OR >95% and 300-500 bp for family. Any prey material identified visually or that remained after the DNA barcoding procedure was refrozen until prepared for SIA.

Dorsal muscle tissue of collected fish and prey samples were freeze dried and ground to a fine powder with a mortar and pestle. A subset of ground tissue was packed into tin capsules and analyzed for $\delta^{13}C$ and $\delta^{15}N$ with a Thermo Delta V Advantage stable isotope ratio mass spectrometer coupled to a Costech elemental analyzer via a Conflo IV interface. A NIST certified standard along with a secondary lab standard was used as reference to ensure accurate results.

Plankton samples were collected and analyzed to determine position in the Red Snapper food chain relative to particulate organic matter and prey items in the system during 2019. Plankton samples were taken by towing a 553-µm mesh bongo net obliquely to within 1-m above the bottom. Separate mechanical flow meters (General Oceanic, Inc. 2030R) were used to determine how much water was filtered by each net. Plankton from one net were preserved in ethanol for identification and enumeration while the plankton in the second net was frozen for bulk stable isotope analysis. Plankton used

for identification were IDed under Nikon SMZ1000 Dissection Scope to the class level. Plankton collected for isotope analysis were separated into size fractions of <63µm, <333µm, and <553µm prior to freezing and then processed as described above. Plankton were counted and an average abundance (number per m^3 was calculated).

3.3.2 Data analysis

Shannon Weiner diversity index calculated to determine prey diversity between the different outflow regimes and years using the diversity function in the BiodiversityR package in R. Red Snapper body condition was analyzed using Fulton's K (equation 2) (Ricker 1978; Nash et al. 2006).

Equation 2.

$$K = \frac{weight}{lenght^3}$$

Body condition was then compared across years and outflow regimes using one way ANOVA to determine if changes in hydrological regimes or diet affect the condition of Red Snapper. Stomach content analysis is presented using frequency of occurrence (%FO) (eq. 3) and index of relative importance (%IRI) (eq. 4) which were calculated as below:

Equation 3.

$$\%FO = (frequency/number)*100$$

Equation 4.

$$\%\ IRI = frequency*(numeric\ \% + weight\ \%)$$

Isotope values of Red Snapper and their prey were input into SIMMR to determine relative proportions each prey item that contributed to Red Snapper diets under different outflow regimes (Parnell 2019). Outflow regimes were assigned by the amount of outflow from the Mississippi River, Pearl plus Pascagoula Rivers, and Mobile River as described in Chapter 1. These freshwater sources were combined for a total outflow and the high outflow condition was assigned to periods with over 28,317 m^3/s, mid outflow condition assinged to 16,990 – 28,317 m^3/s, and the low outflow condition assinged to less than 16,990 m^3/s. Any prey items from Red Snapper stomachs with less than 5 occurances during an outflow regime were removed from the analysis. Trophic enrichment factors for $\delta^{13}C$ and $\delta^{15}N$ were assigned as $1.0 \pm 0.5‰$, and $3.4 \pm 0.7‰$, respectively (Post 2002; France and Peters 1997). The SIMMR models included informative priors based on %FO during that outflow period.

3.4 Results

3.4.1 Red Snapper

Of the total 2105 Red Snapper collected, 644 (30.6%) had empty stomachs, 115 in 2016 (24.6%), 82 in 2017 (19.5%), 208 in 2018 (36.9%), 179 in 2019 (41.8%) and 60 in 2020 (26.7%). Sample numbers per year ranged from 416 – 556 except for 2020 when which had a reduced sampling effort due to COVID restrictions (Table 2.2 468 fish were collected in 2016, 421 in 2017, 563 in 2018, 428 in 2019, and 225 in 2020). Fish total length and weight ranged from 180 to 853 mm and 0.08 to 8.5 kg, respectively. Red Snapper with total length between 300 and 400 mm and weights between 0.5 to 1kg were the most common collected (Table 2.2 & 2.3). Body condition of Red Snapper was

significantly different across the 5 years (Two way ANOVA, df=4, F=3.51, p=0.02) but not by outflow regime (Two way ANOVA, df=2, F=0.86, p=0.44) (Table 2.4). This was likely due to very high variability in body condition of fish in 2016 which were found to have a significantly higher Fulton's condition factor compared to fish from other years (Tukey Post Hoc p<0.00 for 2016 vs all years which were not different from each other) (Fig. 2.1).

Red Snapper stable isotope values were generally similar across the five years and three outflow regimes, with $\delta^{13}C$ ranging from -24.09‰ to -15.77‰ and $\delta^{15}N$ from 11.29‰ to 16.68‰ (Figs 2.2-2.6). In 2016, the range of isotope values were small from -18.16‰ to -15.93‰ for $\delta^{13}C$, and 12.99‰ to 15.79‰ for $\delta^{15}N$. In 2017 the $\delta^{13}C$ range was larger with some lower values, (-24.09‰ to -16.10‰). The $\delta^{15}N$ range was also slightly larger extending from 11.71‰ to 15.54‰, with two outliers below 13‰ extending the lower range. Though smaller than in 2017, the range of isotope values in 2018 were also larger than in 2016 with $\delta^{13}C$ ranging from -22.14‰ to -16.31‰, and $\delta^{15}N$ extending higher than in other years (12.84‰ to 16.41‰). In 2019 the $\delta^{13}C$ and $\delta^{15}N$ ranges narrowed again with carbon ranging from -21.92‰ to -16.40‰ with one outlier below -20‰, and the $\delta^{15}N$ ranging from 11.29‰ to 16.16‰. Lastly in 2020, the $\delta^{13}C$ was again low, ranging from -19.61‰ to -15.77‰ with two outliers below -18. The $\delta^{15}N$ values in 2020 exhibited the smallest range of all five years from 15.55‰ to 16.68‰, reaching the highest values measured since 2016. There was a significant increase in average $\delta^{15}N$ values over the 5 years (Two way ANOVA df=4, F=565.18, p<2E-16), with only 2016 and 2017 being comparable (Tukey Post Hoc p<0.00 for all comparisons except between 2016 and 2017). Red Snapper $\delta^{15}N$ was also significantly

lower during the low outflow regime than in the mid or high outflow regimes (Two way ANOVA df=2, F=24.43, p=3.24E-11; Tukey Post Hoc p<0.00 between mid and low and high and low outflow regimes) (Fig. 2.5). Values of $\delta^{13}C$ was significantly different across the 5 years and three outflow regimes (Two way ANOVA, year: df=4, F=141.18, p < 2E-16; outflow: df=2, F=32.64, p = 1.1E-14) (Fig. 2.6). Mean $\delta^{13}C$ in 2016 and 2020 were not different and were higher than in the other years which were not different from each other (Fig. 2.4).

3.4.2 Red Snapper Stomach Content Analysis

A total of 10,731 prey items were collected from Red Snapper stomach content, and 855 (8.0%) of those prey items had enough tissue available after genetic barcoding identification for stable isotope analysis. Prey as they were visually identified by CFRD's Dyan Gibson or DNA barcoded are presented in table 2.6. Of prey that were identified, 57.9% were DNA barcoded. Over the 5 years of the study prey diversity did not significantly change and was not significantly different across the three outflow regimes (One way ANOVA years: df=4, F-0.57, p=0.69; outflow: df=2, F=0.708, p=0.512) (Table 2.5). However prey diversity declined with increasing outflow which was reflected across years in the Shannon Weiner index. All prey % FO and % IRI are presented in Table 2.6. Portunidae crabs were the most common Red Snapper diet item followed by Stomatopoda, Malacostraca crabs, Squillidae Stomatopoda, Actinopterygii, Sergestidae shrimp, and lastly Pteropods. All other prey items made up less than 5% of the diet. Sergestidae shrimp were the most important diet species determined by the IRI calculation, followed by Portunidae crabs, Stomatopoda, and Stomatopoda Squillidae. All other prey groups had an IRI percentage of under 5%.

Prey from Red Snapper stomachs were categorized into fish, cephalopods, crabs, lobsters, shrimp, stomatopods, and 'other' for analysis to be compared to stable isotope results and % FO of these categories are presented here. Fish was the most common prey category representing 33.8% of all prey consumed, with the most common identified as Actinopterygii (77.6%), followed by Lutjanidae (3.6%), then Ophichthidae (3.1%), and Sciaenid (2.7%). Twenty-four other fish taxa were found in Red Snapper stomach contents, but each made up less than 2% of the diet. Crabs were the next most common prey category (24.3%) with Portunidae crabs (74.3% of total crabs) being identified most often. These were followed by Pseudorhombillidae (7.8%), Calappidae (5.5%), Albunidae (3.2%), Parthenopidae (2.1%), and Raninidae (2.0%). Nine other crab taxa were consumed that were under 2% of the crab prey items. The third most common prey type was stomatopods which were not subdivided into lower taxonomic resolution made up 17.1% of the diet. The 'other' category was the fourth most common diet type making up 13.4%. Members of the 'other' category were diverse, encompassing mostly benthic and pelagic invertebrates. The most common prey item of the other group was gastropods which made up 3.5% of the category followed by amphipods (2.4%), teuthids (7.6%), mysids (6.8%), bivalves (6.1%), salps (4.5%), ostracods (3.4%), and polychaetas (2.4%). Thirteen other taxa made up less than 2% of the 'other' diet category. Shrimps were the fifth most common diet type making up 10.7% of Red Snapper diet with the most common being Sergestidae which made up 46.9% of the shrimp prey type followed by Penaeidae (43.6% of shrimp taxa), and Alpheidae (4.6% of shrimp taxa). Five other shrimp taxa made up less than 2% of the shrimp category. Lobsters and Cephalopods each made up less than 1% of the Red Snapper diet.

Under the high outflow regime, Red Snapper primarily consumed fish which made up 37.6% of the diet, followed by crabs (22.1%), shrimp (14.9%), and 'other' (13.7%). Stomatopods and lobsters each made up less than 10% of the diet. The most common diet item consumed by Red Snapper under the high outflow regime were Actinopterygii fishes which made up 30.6% of the diet and 81.5% of fish found in SCA, followed by Portunidae crabs (17.3%) which made up 78.3% of crabs consumed, Stomatopoda (10.4%) which were not further divided, Sergestidae shrimp (8%) which made up 53.3% of shrimp consumed, gastropods (6.8%) which made up 49.2% of the 'other' group, and Penaeidae shrimp (6.3%) which made up 42.4% of shrimp. All other prey items contributed less than 5% to the diet of Red Snapper. Under the mid outflow regime, Red Snapper again most commonly consumed fish (35.8%), followed by crabs (24.7%), stomatopods (14.5%), 'other' (13.1%), and shrimp (11.5%). Lobsters and cephalopods made up less than 1% of the Red Snapper diet. Under this regime the most common specific diet items was again Actinopterygii fishes (26.4%, 73.6% of fish), followed by Portunidae crabs (19.6%, 70.4% of crabs), stomatopods (14.5%), and Sergestidae (6.5%, 56.7% of shrimp). All other prey types contributed less than 5% of the diet. Under the low outflow regime, the most common diet item was fish (28.8%), followed by crabs (25.7%), then stomatopods (25%), other (13.3%), and shrimp (6.4%). Again, Cephalopods and lobsters collected under this regime contributed least, 3.7% for both. Under this regime, the most common diet item in gut content was stomatopods which made up 25.0% of the diet, followed by Actinopterygii (22.3%, 77.1% of fish), and Portunidae (17.3%, 67.4% of crabs). All other prey items contributed less than 5% to the Red Snapper diet under the low outflow regime.

3.4.3 Prey Stable Isotope Analysis

Prey isotopes across all five years were broadly grouped into fish, cephalopods, crabs, Stomatopods, shrimp, and 'other' (Fig 2.7). The most common prey group analyzed for stable isotopes was crabs which had a large $\delta^{13}C$ range of -25.00‰ to -11.03‰, and a $\delta^{15}N$ range of 2.42‰ to 14.79‰. The crab category was comprised of 11 families with the most common being Portunidae crabs, making up 86.4% of the crabs consumed. The fish category was the second most common prey group analyzed for isotope values and had a $\delta^{13}C$ range from -27.33‰ to -12.63‰ and a $\delta^{15}N$ range from 4.44‰ to 15.25‰. This group had the largest variety with 21 different families present in Red Snapper diets across the five years, with Lutjanidae and Ophichthidae being the most common. The third most common diet items analyzed for isotopes were Stomatopods, all from the family Squillidae. which had a $\delta^{13}C$ range from -21.55‰ to -14.93‰ and a $\delta^{15}N$ range from 1.58‰ to 14.40‰. Shrimp were the fourth most common group analyzed for stable isotopes ranging in $\delta^{13}C$ from -23.48‰ to -16.94‰ and $\delta^{15}N$ from 6.32‰ to 14.48‰. The shrimp group consisted of three families with the most common being Penaeidae. The 'other' category consisted of a variety of uncommon diet items, including Pyrosomatidae, Thecosomata, Amphipoda, Ceriantharia, Bivalvia, Cerripedia, Naticidae, and Salpidae with $\delta^{13}C$ that ranged from -21.87‰ to -13.47‰ and $\delta^{15}N$ ranged from 4.28‰ to 14.31‰. Cephalopods made up the smallest category analyzed for isotopes, with $\delta^{13}C$ that ranged from -19.20‰ to -16.94‰ and $\delta^{15}N$ that ranged from 10.41‰ to 13.85‰. This category was primarily composed of Loliginidae squids with one occurrence of Octopodidae. Lutjanidae prey items were in fact genetically identifided in this study to be *Lutjanus campechanus* (Red Snapper), which suggests

some canibalism is occuring under this outflow regime although only 31 of the total 2105 (1.5%) individuals were found to have cannibalized other Red Snapper. It was a slightly more frequent occurance in males (20 males vs 12 females), in 2016 (20 occurances in 2016, 3 in 2017, 5 in 2018, 1 in 2019, and 3 in 2020), and on platforms (23 vs 9 on artificial reefs), but Lutjanidae prey items were evenly distributed amongst age and size classes and were not unique to any area of the sampling region.

Red Snapper and their prey were plotted in isotope space by outflow regime (Fig. 2.8). Here there is a visible shift from stomatopods dominating the lower trophic levels of the prey structure under the low outflow, to a mix of stomatopods and crabs in the mid outflow, to primarily crabs under the high outflow. Fish and shrimp appear to remain consistent in isotope space position. When particulate organic matter (POM) and simultaneous collection of zooplankton in 2019 were included and the plots also split out by year, consistent linear change in isotope space reminiscent of a food chain structure from POM to zooplankton, to prey, to Red Snapper predators appears (Fig 2.9). However, POM consistently has lower isotope values than zooplankton or Red Snapper prey. POM isotope ranges become wider under higher outflow rates in later years and distinctly shifted to lower isotope values.

3.4.4 Plankton

A total of 31 tows were completed across the entire study (Table 2.7). On average, 382 ± 512 holoplankton per cubic meter and 19 ± 20 meroplankton per cubic meter were collected in each tow. Of the holoplankton collected, Calanoid copepods were most common on average (62.52% of total average occurrence), followed by Cladocerans (17.53%) and Chaetognaths (5.65%). Of the meroplankton collected,

barnacle nauplii were most commonly collected on average (23.83%) followed by fish eggs (15.05%) and crab zoea (11.91%) (Fig. 2.10). Month and depth strata tended to impact the abundance of total zooplankton collected though not significantly (Two way ANOVA month: df=7, F=11.095, p=0.851; depth strata: df=2, F=10.931, p=0.838). Copepod abundance however, was significantly positively correlated with depth strata, increasing with increasing depth (Pearson correlation, r = 0.46, p = 0.03). Copepods were the most commonly collected zooplankton overall, with the most common copepod collected being calanoid copepods (99.7% of all copepods collected). Abundance of total zooplankton and copepods were not affected by outflow regime (ANOVA total: df=2, F=2.671, p=0.093; copepods: df=2, F=1.924, p=0.171), nor were $\delta^{13}C$ values across any size fraction (Two way ANOVA outflow: df=2, F=1.489, p=2.34; size fraction: df=2, F=0.518, p=0.598). Nitrogen isotope values, however, were significantly impacted by outflow, but not by size fraction (Two way ANOVA outflow: df=2, F=5.910, p=0.005, size fraction: df=2, F-1.814, p=0.172). There was no difference in $\delta^{15}N$ between the mid and low outflow regimes, but plankton $\delta^{15}N$ during high outflow was significantly lower than those from the mid (Tukey HSD p=0.025) and the low flow conditions (Tukey HSD p=0.019)(Fig. 2.11).

3.4.5 SIMMR Models

Under the high outflow regime 8 prey groups were identified with 704 total Red Snapper (Fig. 2.12). The most common dietary item found in stomach content was Portunidae with 91 individual occurrences. Pseudohombillidae were the only other crab family present in mixing model results. Three families of fish were present as well as two families of shrimp and stomatopods (which included *Squillidae squilla* and *S.*

empusa). Mixing model results showed dominate prey items that contributed to the estimated Red Snapper diet proportions under the high outflow conditon were, Cynoglossidae fish, Portunidae crabs, and Pseudorhombillidae crabs (Fig. 2.13). At the 50% confidence interval, Cynoglossids made up 54.5% of the diet, Portunidae crabs made up 27.6%, and Pseudorhombillidae crabs made up 11.2%. All other prey items contirbuted up less than 10% of the diet at this confidence interval.

Under the mid outflow regime 575 Red Snapper and six prey types were used for the SIMMR analysis (Fig. 2.14) with Portunid crabs and Stomatopod being most common available for stable isotope analysis. Other than these, there was one other crab family, two fish families, and one shrimp family. Middle ouflow regime Red Snapper diets were dominated by Albunidae crabs (50.5%) and Ophichthid eels (31.8%) at the 50% confidence interval (Fig 2.15) while Portunidae crabs only made up 9% of the estimated diet item proportions. Penaeid shrimp and Lutjanid fish also had small contributions to the diet, making up 3.4% and 4.3% respctively at the 50% confidence interval. Stomatopods did not significantly contribute to the diet under this outflow regime, making up less than 1%.

In the low outflow condition 674 Red Snapper were included in the SIMMR analysis with six prey types (Fig. 2.16). In this outflow regime, the most common diet items analyzed for stable isotopes were Portunidae crabs and Stomatopods by far with one shrimp family and three fish families making up the remainder of the diet items included. The Red Snapper dietary proportions in the low outflow condition had the most contribtors (Fig 2.17). At the 50% confidence interval, Portunidae crabs made up the majority of the diet (37.8%), followed by Lutjanidae fish (34.0%), and Ophichthidae

eels (25.8%). Smaller contributors included Stomatopods (1.3%), Penaeidae shrimp (1.4%) and Sciaenidae fish (1.1%).

3.5 Discussion

Increased unseasonal river outflow into the NGOM by the Mississippi and smaller regional rivers is a significant driver to the ecology of the region (Chapter 1). During 2016, high precipitation in the Great Plains resulted in very high water levels in the Mississippi River, causing the Bonnet Carré spillway to be opened throughout most of January (Fig. 0.1). This was followed by a dry year in 2017, which had lower outflow than usual in all rivers except the Pascagoula River which exhibited a typical spring and fall high discharges. In 2018 there was again high peak flow early in the year causing a near month long opening of the spillway in March although there was no fall peak. Unusually high outflow in 2019 with both spring and fall peaks from all rivers, resulted in the longest opening in the Bonnet Carré Spillway's history being opened twice for 44 days from February 27th to April 11th, and then for 79 days from May 10th to July 27th. Then in 2020 there was again an early peak year with no fall peak, resulting in the spillway being opened for nearly the whole month of April. This clearly shows the inconsistent outflows from the rivers of the region.

Lower $\delta^{13}C$ in POM relative to zooplankton or other organisms is typical, but the decrease in $\delta^{13}C$ values in later wetter years without a $\delta^{13}C$ shift in the Red Snapper or prey suggests that a more isotopically enriched basal resource relative to POM is also contributing to this food web, and to higher $\delta^{15}N$ values (Peterson and Fry 1987). In 2016 and 2017, POM $\delta^{13}C$ are closer in isotope space to prey but shifted lower as years went

on. As these were years with low river outflow, POM during this period is likely more indicitive of phytoplankton while in later wetter years, the lower POM $\delta^{13}C$ values indicate more riverine influence (Chapter 1).

Though rivers deliver large amount of inorganic nutrients to coastal regions, these nutrients are quickly taken up by marsh macrophytes along the coast and phytoplankton in the water column. Increased assimilation and possible benthic denitrifiation of nitrate in the Mississippi River has been shown to increase nitrate $\delta^{15}N$ downstream (Battaglin et al. 2001) and zooplankton have been shown to primarly utilize more labile carbon from phytoplankton production rather than refractory POM delivered by river discharge (Schlacher et al. 2009). The enrichment of $\delta^{15}N$ under low outflow regimes may be due to water released by rivers being filtered by marshes to some degree, which causes biological processing, nitrificaion, and denitrification which can result in an increase in nitrate $\delta^{15}N$ (Battaglin et al. 2001). However, under high outflow conditions, these nutrients may be pulsed quickly through marshes to estuaries with less biological processing (Bianchi et al. 2011). Collected zooplankton samples from 2019 were dominated by calanoid copepods which are phytoplankton grazers and thus would reflect isotopic changes in phytoplankton caused by isotopic changes in the nitrogen sources. The decline in zooplankton $\delta^{15}N$ coincides with the increase in outflow from the rivers in the region which delivers higher nutrient loads to the area, presumably increasing phytoplankton production. These blooms are then utilized by zooplankton, causing shifts in their $\delta^{15}N$. Inorganic nitrogen sources appear to be almost entirely sourced from the riverine nutrients delivered to the region under high outflow conditions. The shift in basal resources can be seen in figure 2.9. Under the higher discharge rates in later years,

the food web appears to shift away from POM in isotope space and the isotopic ranges of POM become wider. Though phytoplankton stable isotopes could not be measured in this study, we assume that phytoplankton blooms are the primary base of the food web under these higher outflow conditions.

Previous diet studies largely agree with the SCA results from this study, identifying Actinopterigii fishes as the most common dietary items, with crabs, shrimp, and stomatopods making up the majority of the rest of the diet. Szedlmayer and Lee (2004) using stomach content analysis off the Alabama coast found that Red Snapper diet was dominate by Osteichthyes (bony) fishes, Cephalopods, and shrimp in which they included stomatopods. Wells et al. (2008) also identified fish, squid, and crabs as primary diet contributors. On the Louisiana shelf, Simonsen et al. (2015) used stomach content analysis and found that Red Snapper diet was dominated by teleost fishes and crustaceans across standing, toppled, and natural reefs, but greater amounts of crustaceans were consumed on toppled platforms, and diet was most varied on natural reefs. McCawley et al (2006) found that Red Snapper fed primarily on pelagic fishes during the day and benthic crustaceans at night. A seasonal analysis of Red Snapper diet by McCawley and Cowen (2007) found that demersal crustaceans, fishes, and pelagic zooplankton made up the bulk Red Snapper prey, with *Squilla empusa* having the highest % IRI and dominated diet in summer and winter. Crabs were the largest category in the fall and pelagic zooplankton in spring. Consistently throughout these studies, crabs, bony fishes, and stomatopods are determined to be the most common prey items in Red Snapper stomach contents, which agrees with the results from this study.

Stable isotope analysis of Red Snapper muscle tissue by several diet studies also agree with observations by this study. Simonsen et al. (2015) used stable isotope analysis of Red Snapper muscle tissue and found standing platforms were most enriched in $\delta^{15}N$ which was attributed to feeding at a higher trophic level. Similarly, Tarnecki and Patterson (2015) found Red Snapper $\delta^{15}N$ increased after the Deep Water Horizon oil spill and attributed the change to feeding at a higher trophic level. $\delta^{15}N$ in our study also increased over the 5 years, which may be due to feeding at a higher trophic level but can be linked to increased fresh water outflow from the region's rivers in later years. $\delta^{13}C$ in our study also changed by year with higher values under the high outflow regime and in periods directly following years with heave precipitation. Wells et al. (2008) also found that $\delta^{13}C$ of Red Snapper significantly changed seasonally, with the lowest values in the winter and spring, and the highest values during summer and fall, increasing during periods of higher precipitation and river outflow.

Prey of Red Snapper accordingly shifted with river outflow regimes. Prey diversity was higher under the low outflow regimes in 2016 and 2017, when the area had been recently impacted by river borne nutrients in early 2016 but were not inundated with fresh water over the rest of the year or in 2017. Under the low outflow regimes, Red Snapper SCA and stable isotopes both determined crustaceans were the dominate prey itmes, stomatopods by SCA and Portunid crabs by stable isotopes. Various fishes were then found to make up the next highest proportions. Under the mid outflow regime there was less agreement between the two analyses. SCA determined fish to make up the highest proportion of the diet, then crustaceans, while the stable isotope mixing model determined benthic crabs and eels made up the highest proportions. Under the high

outflow regime stomach content analysis and stable isotope analysis most closely agreed with both finding first fish be make up the highest dietary proportion, then protunidae crabs.

While both stomach content and stable isotope analyses found common primary diet items, items that were determined to contribute less to the diet usually did not agree. Under the mid outflow regime specificially, there was a distinct difference between the restults from the SCA and the mixing model. Both analyses picked out the importance of Actinopterygii fish and Portunidae crabs, but SCA tended to over emphasize the stomatopods and the stable isotope mixing model tended to over emphasize cannaibalized Lutjanidae as well as other fishes more often. Stomach content analysis has the distinct disadvantage of over emphasizing less digestable material which potentially skews results towards these diet items. This is likely why stomatopods are so commonly considered significant in SCA results, but were never considered primary diet items in the stable isotope mixing models. This is also likely why Ophichthid eels were never a dominate diet item according to SCAbut did contribute higher dietary proportions in the mixing models. The position difference in isotope space of prey Lutjanidae and their predators (the equivalent of 1 trophic erichment factor for both $\delta^{13}C$ and $\delta^{15}N$) lend to Lutjanidae prey being a higher perportion of diet in the mixing model, overemphasizing cannibalism. When resolving the different possible contributions, prey with this isotopic difference from predator isotope values are treated as a near “perfect fit”. Along these same lines, stomatopods, despit having high % IRI and being common diet items in the literature, were never determined to contribute much to Red Snapper diets in stable isotope mixing models. This is likey due to the large $\delta^{15}N$ range of stomatopods, which makes it

difficult for the model to fit them into the dietary proportions without large errors. Despite the disagreements between the two analyses, under the high outflow regimes, Actinopterygii fishes and Portunidae crabs both were found to be make up a large proportion of the Red Snapper diet. However under the high outflow regime, there is also a decrease in prey diversity which may best explain why these two methods would agree.

Two major conclusions can be drawn from these results. First, the diet of Red Snapper varied subtly though not signifiantly under different outflow regimes. Second, this variation was reflected in the isotopes of Red Snapper. Though this study cannot determine if this was due to changes in Red Snapper feeding at a higher trophic level, changes to prey assemblage, or shifts in the baseline $\delta^{15}N$ value, the change can be linked to river outflow. Chapter 1 showed changes to POM carbon and nitrogen concentrations and $\delta^{13}C$ in the study region under different outflow regimes, which resulted in POM $\delta^{13}C$ shifting lower with increasing river outflow. Zooplankton collections also showed increases of $\delta^{15}N$ with increasing outflow.

Stomach content analysis did not capture the changes to the Red Snapper diet under the different outflow regimes that were captured by the stable isotope mixing models, but stomach content was an integral part of the study. Stable isotope analysis of the stomach contents allowed us access to prey items such as the burrowing crabs and eels identified in the mid outflow, and the various fish types and invertebrates that would have been nearly impossible to collect due to the wide variety of gear types that woud be required, The sampling effort necessary to collect the broad span of prey items found in SCA over the different years, seasons, and over the entire sampling region were impracticle given the sampling design of this study.

3.6 Conclusions

The measured changes of POM stable isotope values which represent the base of the food web did not appear to alter Red Snapper diet significantly, but there were trends that were visible. The increase in abundance of zooplankton grazing on phytoplankton subsequently reflect more terrestrial isotope values and shift the isotope values of Red Snapper and their prey. Red Snapper stable isotope values reflect some of this change. Fulton K factor estimates suggest changes at the base of the food web with increasing outflow caused an increase in Red Snapper condition. Though not a significant change, Red Snapper condition did decline with increasing outflow, suggesting that the more dynamic, moderate to low outflow regimes produce higher Red Snapper condition. However, increased river flow predicted under various climate change scenarios due to increased precipitation in the upper Mississippi and Ohio river basins (Jha et al. 2006), as well as more frequent and longer openings of river diversions for flood control and new construction of sediment diversions currently underway, suggest that higher outflow is much more likely to be the new normal in the future (Driessen and van Ledden 2013). Understanding how this will impact base of the food web, and thus the condition of Red Sapper is imperitive to better managing the speices in the future.

Table 3.1 Studies analyzing Red Snapper diet in the Northern Gulf of Mexico.

Study	Method	Location	Habitat	Time	Diet
Gallaway et al. (2009)	Review of previous studies focused on Red Snapper populations	Northern Gulf of Mexico	Offshore petroleum platforms and artificial reefs	various	Opportunistic day and night feeders
Szedlmayer & Lee (2004)	SCUBA visual surveys Stomach content analysis	South of Mobil Bay, Alabama	Open flat substrate and artificial reefs	Every 2 weeks from June to December of 1994	Shift from pelagic prey as juveniles to reef associated prey as adults
Wells et al. (2008)	Bulk stable isotope analyses of Red Snapper and potential prey muscle tissue Stomach content analysis	NGOM continental shelf in Alabama state waters	Sandy bottom, low relief shell-rubble, high relief shell-rubble, and natural reefs	Seasonally in 2004 and 2005	Benthic and pelagic prey from sandy/muddy habitats adjacent to structure
McCawley et al. (2006)	2 hour time interval gut content analysis	Hugh Swingle General Permit Area, NGOM in Alabama state waters	Artificial reefs	July and August of 2000	Opportunistic daytime feeders. Night time benthic invertebrate feeders from sandy bottoms
Tarnecki & Patterson (2005)	Bulk stable isotope analysis of Red Snapper muscle tissue Stomach content analysis	South of Dauphin Island Alabama to southeast of Destin, FL	Natural and artificial reef sites	Before and after the Deep Water Horizon oil spill (2009-2010 and 2010-2011	Dependent on relative abundances of potential prey resources
Szedlmayer & Brewton (2019)	DNA barcoding of gut content	Alabama state waters	Artificial reefs	September 2012 to November 2015	both open water and reef habitats across many taxonomic groups at various trophic levels
Brewton et al. (2020)	Bulk stable isotope analysis of Red Snapper muscle tissue Stomach content analysis	Northwestern GOM, offshore of Texas	Natural reefs, reefed platforms, and standing oil and gas platforms	May through September 2013-2015	"Complex and inconsistent"

Table 3.2 Number of Red Snapper collected by year and total length (mm)

	2016	2017	2018	2019	2020	total
<300	32	43	50	34	23	182
300-400	178	217	254	187	87	923
400-500	122	98	152	156	86	614
500-600	71	36	62	40	35	244
600-700	23	20	33	8	9	93
700-800	10	6	12	3	0	31
800-900	1	1	0	0	0	2
total	437*	421	563	428	225	

*31 fish sampled in April in 2019 were not measured for total length

Table 3.3 Number of Red Snapper collected by year and weight (kg)

	2016	2017	2018	2019	2020	total
<0.5	79	99	108	74	15	375
0.5-1	169	184	247	192	111	903
1-1.5	88	56	92	89	36	361
1.5-2	52	32	30	41	33	188
2-2.5	34	15	28	17	10	104
2.5-3	13	10	15	5	10	53
3-3.5	6	9	8	3	2	28
>3.5	27	16	35	7	8	93
total	468	421	563	428	225	

Table 3.4 Fulton's K condition for Red Snapper in each year under each outflow regime.

	All years	2016	2017	2018	2019	2020
Low	1.45E-08	1.58E-08	1.38E-08	1.39E-08	1.39E-08	1.36E-08
Mid	1.40E-08	1.43E-08	1.39E-08	1.38E-08	1.43E-08	-
High	1.37E-08	-	1.42E-08	1.33E-08	1.36E-08	1.38E-08
All outflows		1.52E-08	1.40E-08	1.36E-08	1.38E-08	1.37E-08

Table 3.5 Shannon Weiner index values of prey assemblage based on visual identification of stomach content.

	2016	2017	2018	2019	2020	overall
Low	2.295	2.001	1.652	0.637	0.924	4.52 ± 0.704
Mid	2.709	1.944	1.342	0.562	-	4.24 ± 0.910
High	-	2.262	1.592	2.317	2.310	4.20 ± 0.996
Overall	3.73 ± 0.293	4.10 ± 0.170	3.90 ± 0.164	3.74 ± 0.993	3.66 ± 1.163	

Table 3.6 Occurrence of prey in stomach content following visual identification by CFRD's Dyan Gibson and DNA barcoding.

Phylum	Class	Order	Family	%Numerical	%Frequency	%Weight	%IRI
Porifera				0.0093	0.0721	0.0001	0.0001
Cnidaria				0.0280	0.2163	0.0004	0.0005
	Hydrozoa	Hydrozoa	Hydrozoa	0.0093	0.0721	0.0001	0.0001
	Anthozoa	Penicillaria	Arachnactidae	0.0093	0.0721	0.0385	0.0003
Annelida	Polychaeta			0.0839	0.5768	0.0086	0.0046
	Nematoda		Nematoda	0.0373	0.2163	0.0005	0.0007
Echinodermata	Asteroidea	Forcipulatacea	Asteriidae	0.0093	0.0721	0.0015	0.0001
Mollusca			Mollusca	0.0559	0.4326	0.0023	0.0022
	Gastropoda	Gastropoda	Gastropoda	0.4939	2.6676	0.0172	0.1184
		Gymnosomata	Gymnosomata	0.0652	0.2163	0.0005	0.0012
		Neogastropoda	Fasciolariidae	0.0093	0.0721	0.0001	0.0001
		Neotaenioglossa	Carinariidae	0.0093	0.0721	0.0012	0.0001
			Naticidae	0.0466	0.1442	0.1062	0.0019
		Pteropoda	Pteropoda	9.1045	5.8399	0.3545	4.7968
	Bivalvia	Bivalvia	Bivalvia	0.0839	0.6489	0.0123	0.0054
		Veneroida	Tellinidae	0.0093	0.0721	0.0010	0.0001
			Veneridae	0.0093	0.0721	0.0077	0.0001
	Cephalopoda	Octopoda	Octopodidae	0.0093	0.0721	0.1951	0.0013
		Teuthida	Ommastrephidae	0.0373	0.2884	1.1357	0.0294
			Teuthida	0.2516	1.5141	0.9973	0.1642
Arthropoda			Unid. Crustacean	0.0280	0.2163	0.0004	0.0005
	Thecostraca	Copepoda	Copepoda	0.0466	0.2163	0.0001	0.0009
		Siphonostomatoida	Caligidae	0.0186	0.1442	0.0001	0.0002
	Ostracoda	Ostracoda	Ostracoda	0.1398	0.9373	0.0024	0.0116

Table 3.6. continued

Phylum	Class	Order	Family	%Numerical	%Frequency	%Weight	%IRI
	Malacostraca		Malacostraca	6.1970	8.2192	0.3816	4.6953
		Stomatopoda	Stomatopoda	12.5897	14.3475	1.6991	17.8022
			Gonodactylidae	0.0932	0.0721	0.0215	0.0007
			Squillidae	1.3885	8.0750	11.8255	9.2657
		Decapoda	Decapoda	0.0186	0.1442	0.0153	0.0004
			Aethridae	0.0746	0.4326	0.6210	0.0261
			Albuneidae	0.2516	0.9373	0.2836	0.0436
			Alpheidae	0.1491	1.0094	0.0242	0.0152
			Calappidae	1.5562	2.5955	0.1056	0.3746
			Caridea	0.0093	0.0721	0.0007	0.0001
			Chirostylidae	0.0932	0.0721	0.0079	0.0006
			Hippoidea	0.0280	0.1442	0.1143	0.0018
			Inachoididae	0.0280	0.1442	0.1014	0.0016
			Leucosiidae	0.0280	0.2163	0.0959	0.0023
			Luciferidae	0.0373	0.2884	0.0002	0.0009
			Menippidae	0.0466	0.2884	0.0698	0.0029
			Ocypodoidea	0.1771	0.0721	0.0032	0.0011
			Paguridae	0.0093	0.0721	0.0954	0.0007
			Paguroidea megalopae	0.0559	0.3605	0.0041	0.0019
			Palaemonidae	0.0652	0.2884	0.0016	0.0017
			Parthenopidae	0.1211	0.7210	0.1559	0.0173
			Penaeoidea	1.0344	2.7397	1.2200	0.5363
			Penaeidae	0.5684	3.3886	7.3526	2.3308
			Pilumnidae	0.0093	0.0721	0.0081	0.0001

Table 3.6. continued

Phylum	Class	Order	Family	%Numerical	%Frequency	%Weight	%IRI
			Portunidae	3.5132	14.4917	14.9948	23.2906
			Processidae	0.0186	0.1442	0.0013	0.0002
			Pseudorhombilidae	0.3541	2.3071	0.4851	0.1681
			Raninidae	0.1584	0.5047	0.4664	0.0274
			Scyllaridae	0.0093	0.0721	0.0004	0.0001
			Sergestoidea	0.0466	0.2163	0.0002	0.0009
			Sergestidae	50.3960	6.5609	2.0176	29.8615
			Sicyoniidae	0.0280	0.2163	0.3043	0.0062
			Solenoceridae	0.2050	0.9373	0.4346	0.0521
			Stenopodidae	0.0093	0.0721	0.0002	0.0001
			Xanthoidea	0.0093	0.0721	0.0239	0.0002
			Xanthidae	0.0559	0.4326	0.0353	0.0034
	Isopoda	Isopoda	Isopoda	0.0559	0.2884	0.0001	0.0014
		Mysida	Mysida	2.3111	1.4420	0.0534	0.2961
			Mysidae	0.0466	0.3605	0.0002	0.0015
		Amphipoda	Amphipoda	1.0996	2.7397	0.0236	0.2672
			Brachyscelidae	0.6244	1.5141	0.0135	0.0839
			Gammaridea	0.0093	0.0721	0.0001	0.0001
			Hyperiidea	0.1118	0.3605	0.0017	0.0036
			Phronimidae	0.0746	0.5047	0.0019	0.0034
			Phrosinidae	0.1677	0.5047	0.0034	0.0075
			Platyscelidae	0.1398	0.6489	0.0014	0.0080
Chordata			Tunicata	0.1211	0.1442	0.1257	0.0031
	Thaliacea	Pyrosomatida	Pyrosomatidae	0.1025	0.2884	0.8557	0.0240
		Salpida	Salpidae	0.1771	0.8652	0.0048	0.0137

Table 3.6. continued

Phylum	Class	Order	Family	%Numerical	%Frequency	%Weight	%IRI
	Actinopterygii		Actinopterygii	1.9756	8.0750	2.5749	3.1908
		Anguilliformes	Anguilliformes	0.0466	0.3605	0.1139	0.0050
			Congridae	0.0373	0.2884	1.3445	0.0346
			Moringuidae	0.0093	0.0721	0.0204	0.0002
			Ophichthidae	0.2516	1.6583	2.1151	0.3408
		Batrachoidiformes	Batrachoididae	0.0093	0.0721	0.0034	0.0001
		Clupeiformes	Clupeidae	0.1211	0.6489	5.1287	0.2958
			Engraulidae	0.0839	0.6489	0.6381	0.0407
		Gadiformes	Bregmacerotidae	1.2860	0.6489	0.9010	0.1232
			Gadidae	0.0093	0.0721	0.0831	0.0006
		Gasterosteiformes	Syngnathidae	0.0652	0.2163	0.0038	0.0013
			Synodontidae	0.0186	0.1442	0.0610	0.0010
		Lophiiformes	Lophiiformes	0.0093	0.0721	0.0689	0.0005
		Mugiliformes	Mugilidae	0.0093	0.0721	0.1347	0.0009
		Ophidiiformes	Ophidiidae	0.0839	0.6489	0.8533	0.0528
		Perciformes	Blenniidae	0.0093	0.0721	0.0139	0.0001
			Carangidae	0.0839	0.6489	0.4295	0.0289
			Gobiidae	0.0093	0.0721	0.0195	0.0002
			Lutjanidae	0.0839	0.6489	2.5934	0.1509
			Pomatomidae	0.0093	0.0721	2.0853	0.0131
			Sciaenidae	0.2143	1.5141	8.3780	1.1297
			Serranidae	0.0373	0.2884	0.2603	0.0075
			Stromateidae	0.0186	0.1442	0.3385	0.0045
		Scombriformes	Scombridae	0.1398	0.1442	0.0664	0.0026
			Trichiuridae	0.0466	0.2884	0.6416	0.0172
		Pleuronectiformes	Cynoglossidae	0.1118	0.8652	0.7529	0.0650

Table 3.6. continued

Phylum	Class	Order	Family	%Numerical	%Frequency	%Weight	%IRI
			Paralichthyidae	0.0652	0.4326	0.8525	0.0345
		Scorpaeniformes	Scorpaeniformes	0.0093	0.0721	0.0010	0.0001
			Triglidae	0.0932	0.7210	1.0145	0.0694
		Tetraodontiformes	Tetraodontidae	0.0093	0.0721	0.0009	0.0001
			Tetraodontiformes	0.0093	0.0721	0.0050	0.0001

Table 3.7 Count of plankton per m3 corrected for aliquot volume.

Class	Order	average count	standard deviation	average % Frequency of Occurrence
Arthropoda	Calanoid copepod	233.01	361.76	58.89
	Cyclopoid copepod	1.55	3.61	0.39
	Harpacticoid copepod	0.14	0.38	0.04
	Poecilostomatoid copepod	7.77	13.18	1.96
	Parasitic copepod	0.14	0.27	0.04
	Copepod nauplius	0.56	1.03	0.14
	Ostracod	7.08	9.95	1.79
	Mysid Shrimp	1.84	3.96	0.47
	Cladoceran	72.65	276.74	18.36
	Amphipod	1.07	1.46	0.27
	Isopod	0.08	0.26	0.02
Chaetognatha	Chaetognath	20.43	24.39	5.16
Cnidaria	Hydromedusae	2.54	4.70	0.64
	Siphonophore (pneumatophore)	0.57	2.01	0.14
	Siphonophore (nectophore)	4.75	6.72	1.20
Ctenophora	Chtenophore (larval)	0.40	0.99	0.10
Annelida	Polychaete	3.05	7.64	0.77
	Polychaete Larvae	0.75	1.41	0.19
Mollusca	Pteropod	0.46	0.86	0.12
	Heteropod	0.46	0.94	0.12
Cephalopoda	Cephalopod	0.02	0.12	0.01
Chordata	Salp	0.83	1.82	0.21
	Doliolid	4.63	7.18	1.17
	Larvacean	11.32	33.24	2.86
Mollusca	Gastropod larvae	0.88	1.28	0.22
	Bivalve larvae	0.23	0.58	0.06
Lophophores	Brachiopoda (lingula larva)	0.99	2.65	0.25
	Ectoprocta (Bryozoa larvae)	0.01	0.05	0.00
Echinodermata	Echinoderm	0.13	0.48	0.03
Arthropoda	Barnacle nauplii	5.08	11.42	1.28
	Barnacle cypprid	0.02	0.09	0.00
	Stomatopod	0.51	0.80	0.13
Decapod	Crab zoea	2.06	2.79	0.52
	Crab megalopa	0.15	0.39	0.04
	Other decapod	5.34	4.55	1.35
	Lobster Larvae	0.09	0.22	0.02
Other	Cumacean	0.03	0.17	0.01
	Mite	0.16	0.80	0.04
	Anemone	0.06	0.21	0.01
	Fish Eggs	3.14	10.62	0.79
	Fish Larvae	0.69	1.00	0.18

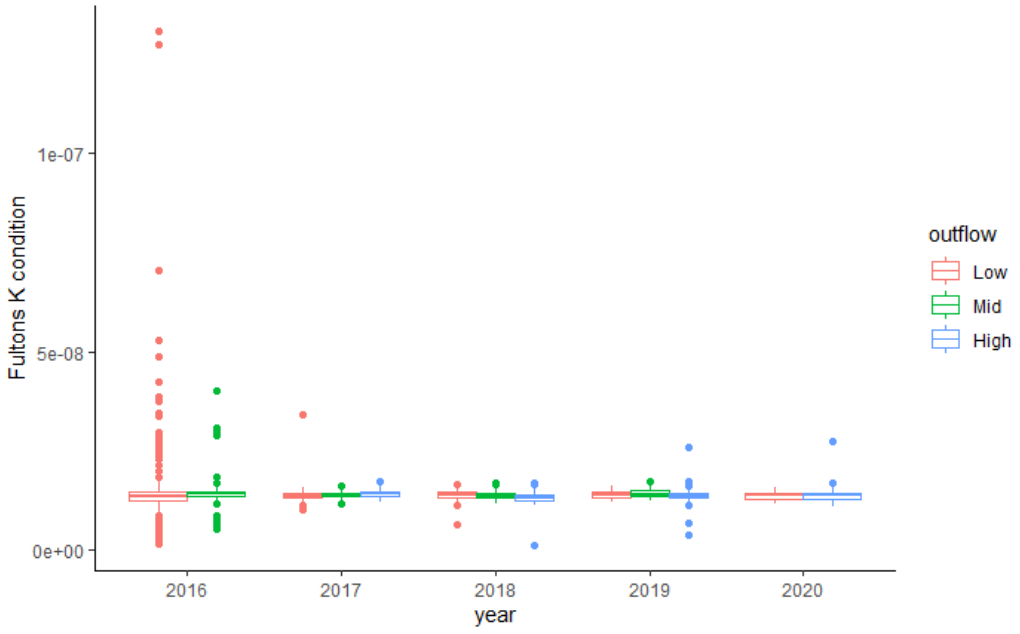

Figure 3.1 Fulton's K condition of Red Snapper across the five years

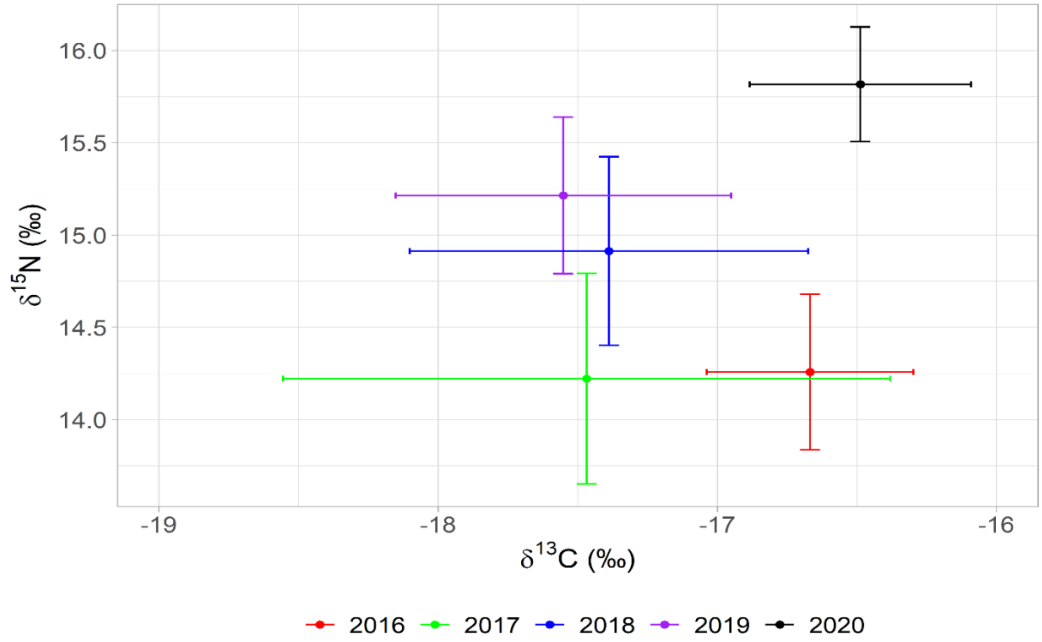

Figure 3.2 Red Snapper $\delta^{13}C$ versus $\delta^{15}N$ average stable isotopes values ± 1 standard deviation.

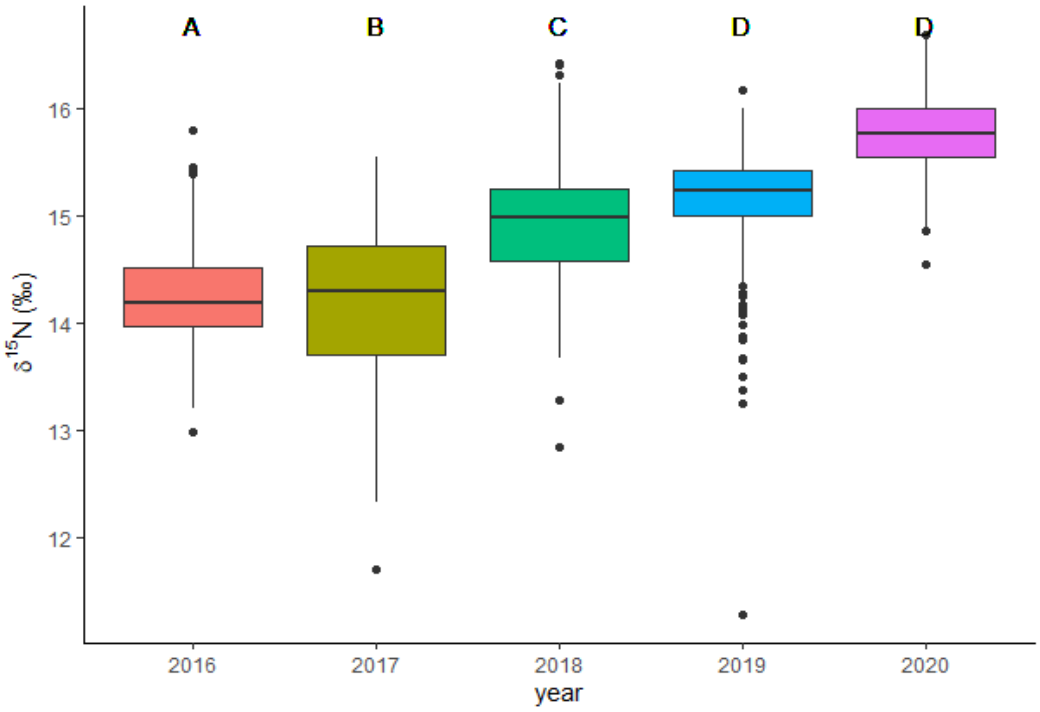

Figure 3.3 $\delta^{15}N$ of Red Snapper across the 5 year study. Letters indicate significance groups based on Tukey Post Hoc results.

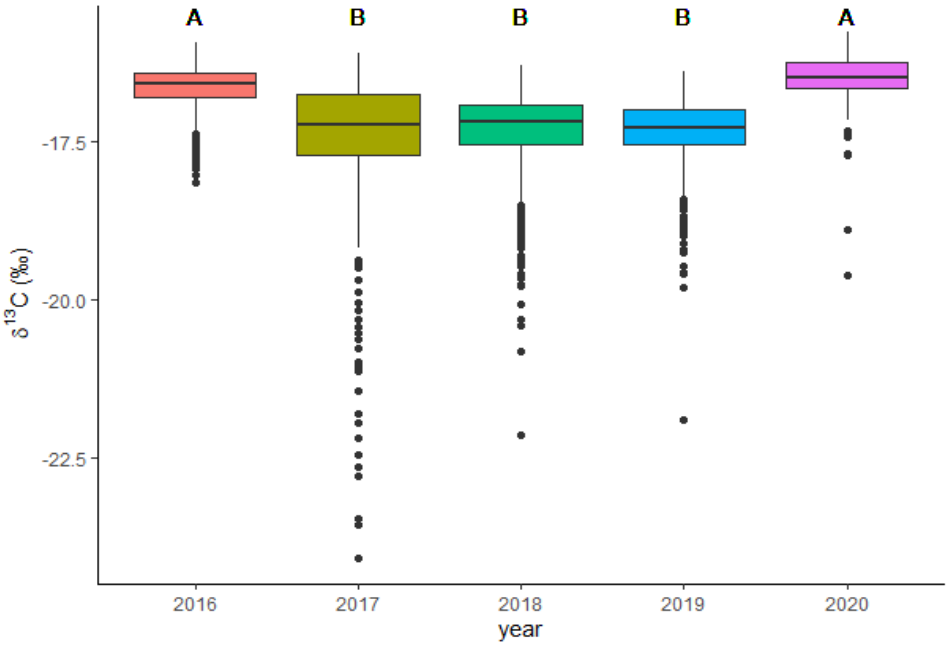

Figure 3.4 $\delta^{13}C$ of Red Snapper across the 5 year study. Letters indicate significance groups based on Tukey Post Hoc results.

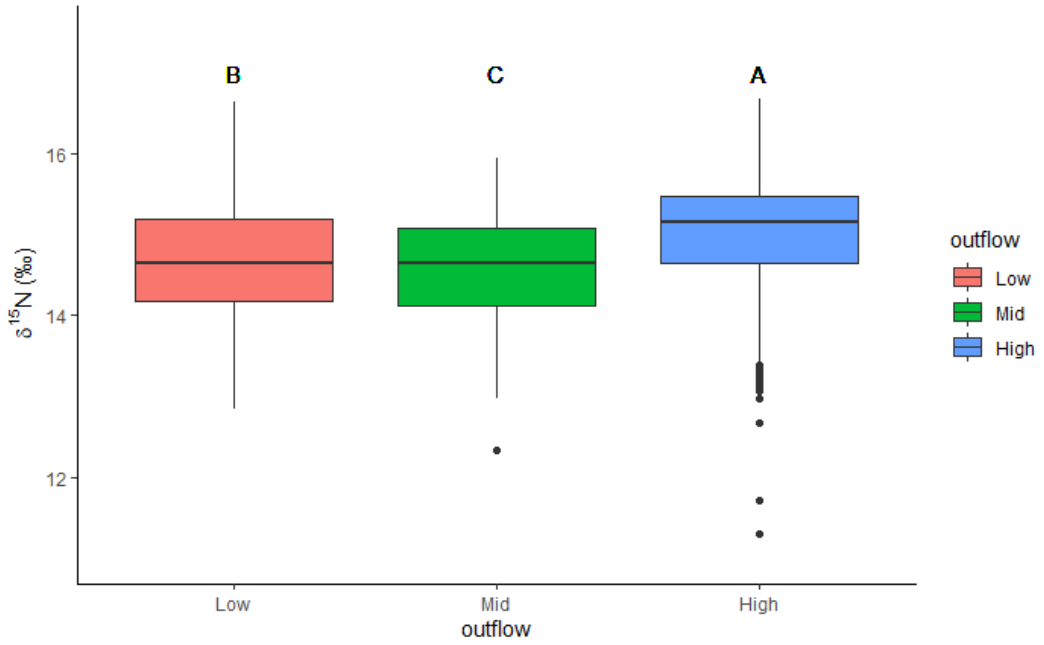

Figure 3.5 $\delta^{15}N$ of Red Snapper across the three outflow groups. Letters indicate significance groups based on Tukey Post Hoc results.

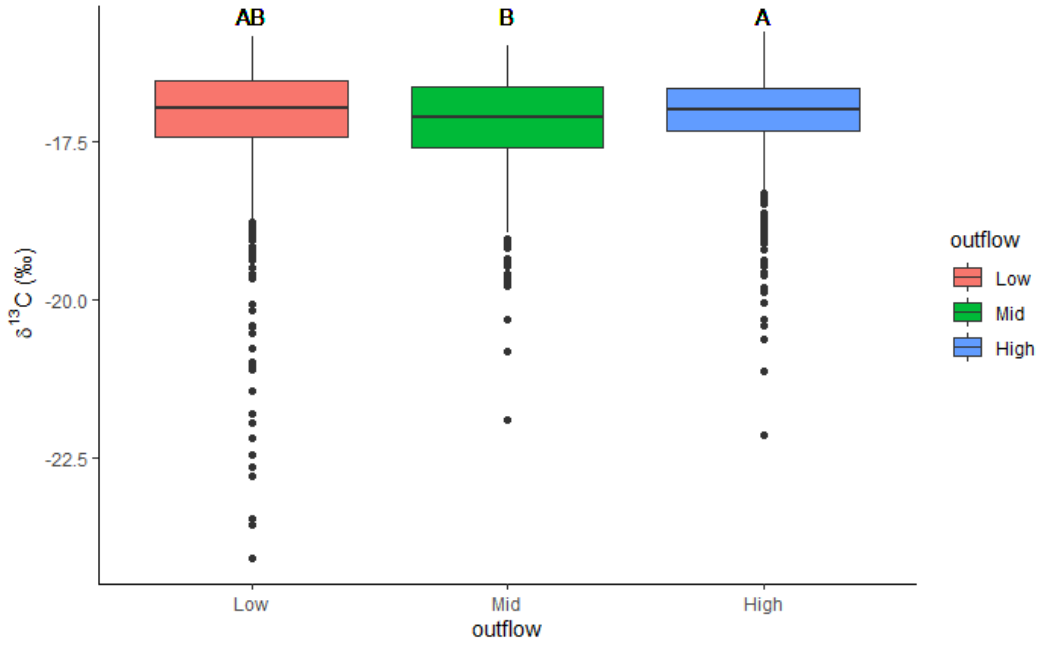

Figure 3.6 $\delta^{13}C$ of Red Snapper across the 3 outflow groups. Letters indicate significance groups based on Tukey Post Hoc results.

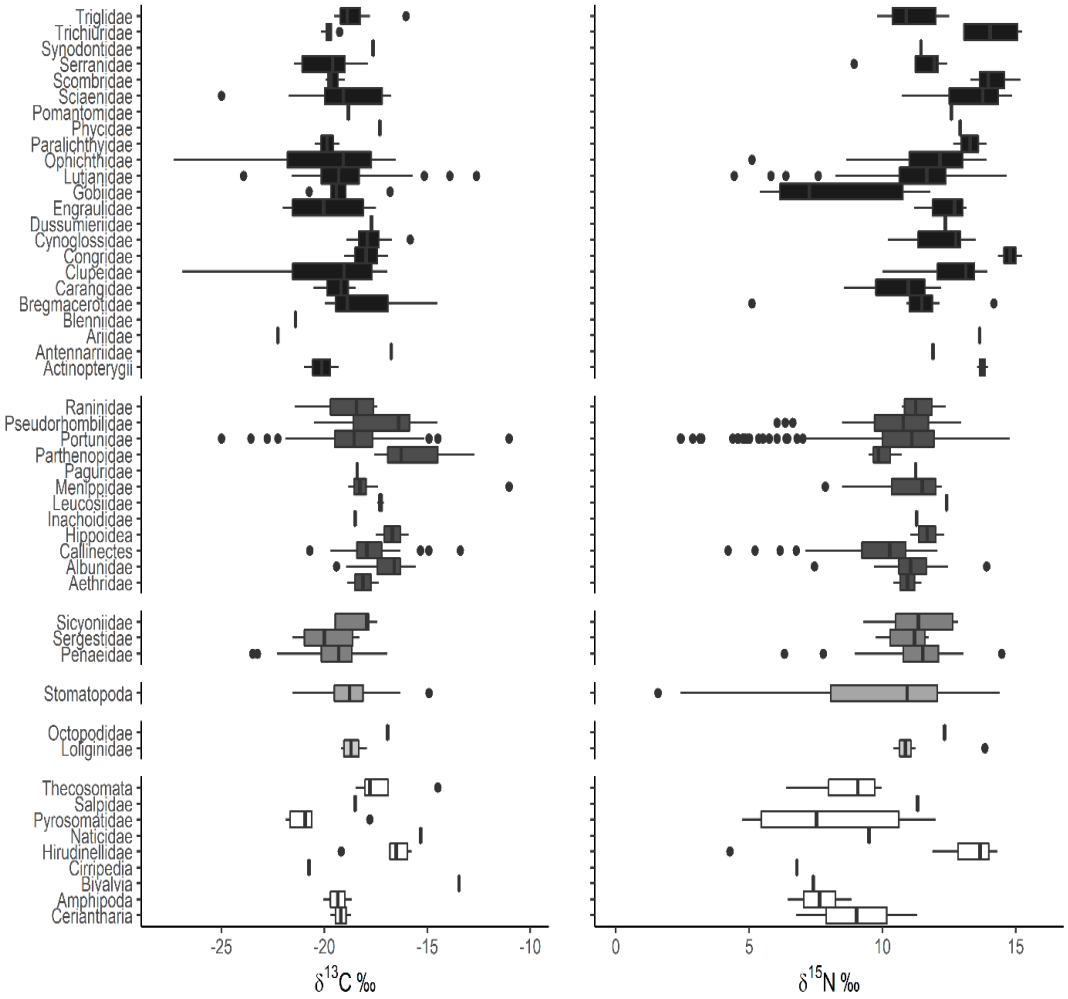

Figure 3.7 Isotope ranges of prey items found in Red Snapper from 2016 through 2020.

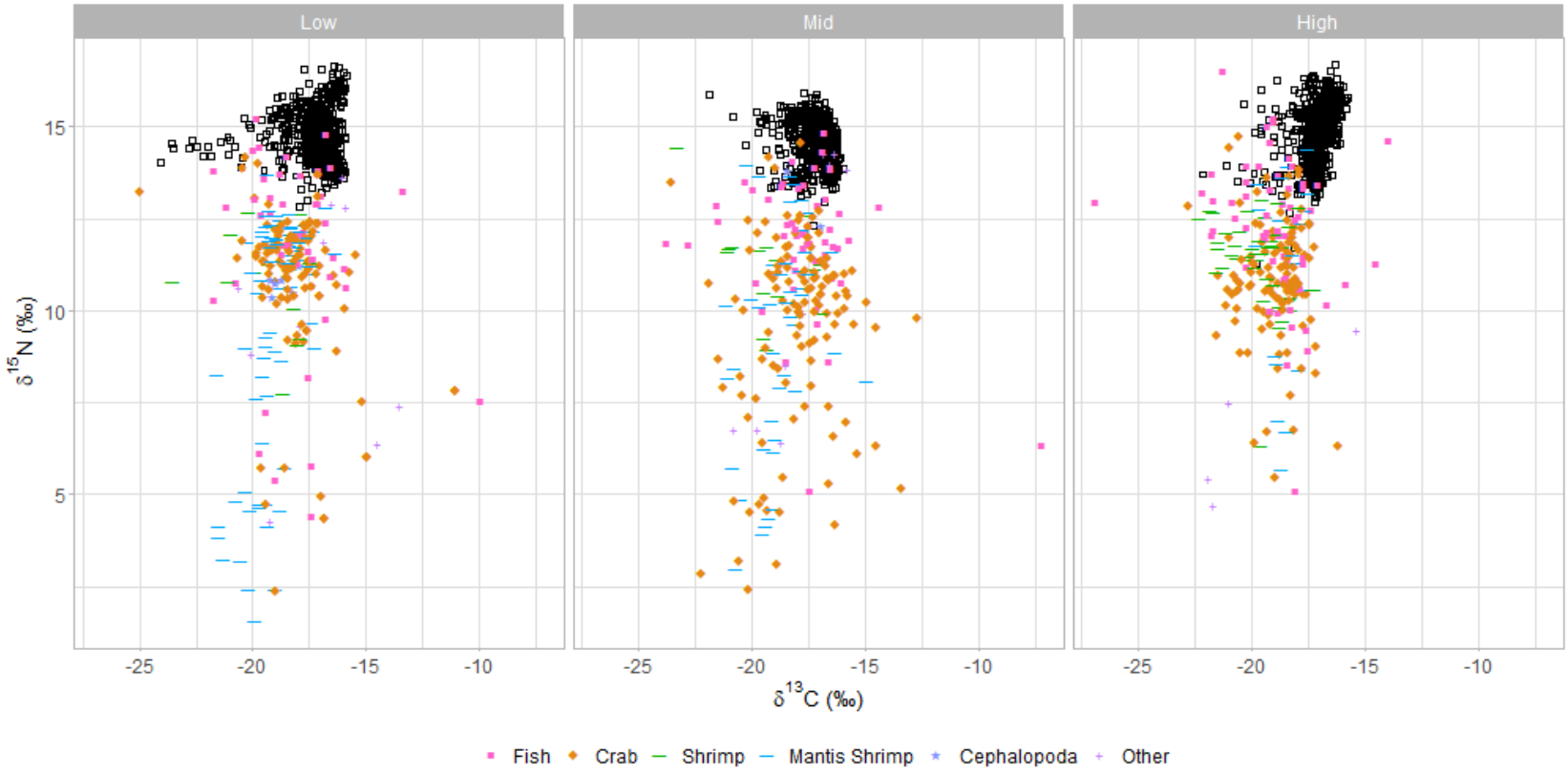

Figure 3.8 Predator and prey isotopes by river outflow group. Squares represent fish prey, diamonds, crab prey, dashes shrimp prey, stars, squids and octopus, and pluses indicate other types of prey genera that were less common in Red Snapper diet. Empty black squares indicate predator Red Snapper.

Figure 3.9 Predatory Red Snapper (open black squares), prey (colored symbols), POM (open grey circles), and zooplankton (closed black triangles) isotope values by river outflow group. Squares represent fish prey, diamonds, crab prey, dashes shrimp prey, stars, squids and octopus, and pluses indicate other types of prey genera that were less common in Red Snapper diet. Zooplankton were only collected in 2019.

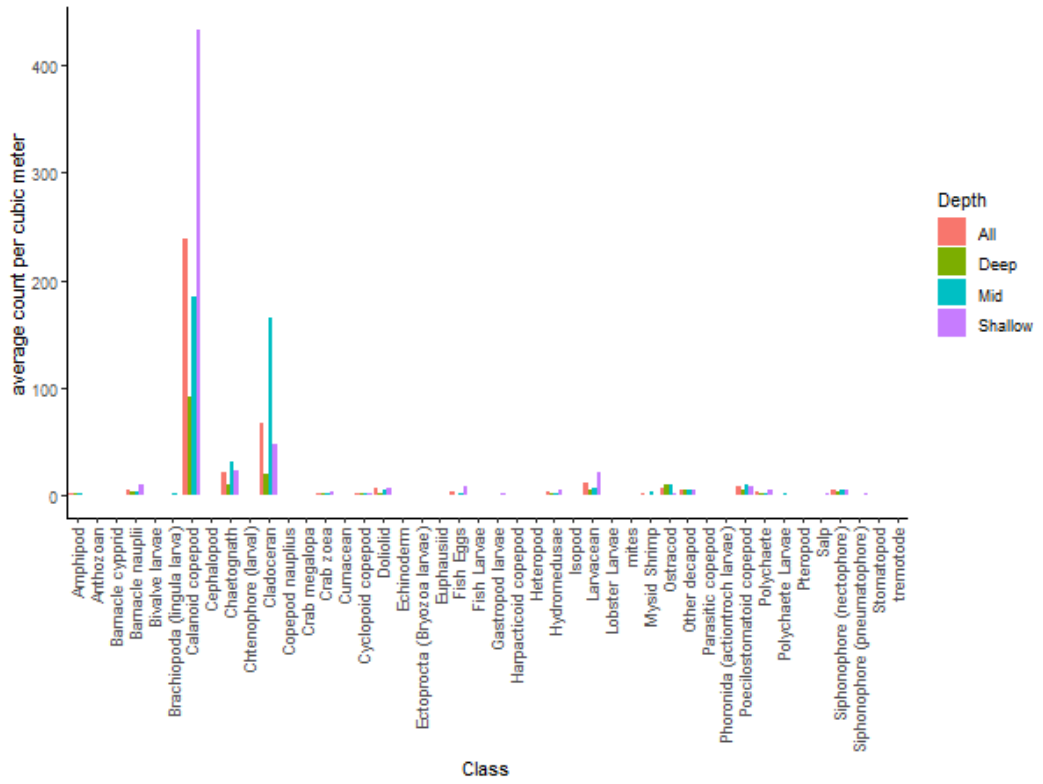

Figure 3.10 Plankton abundance by class in each depth strata.

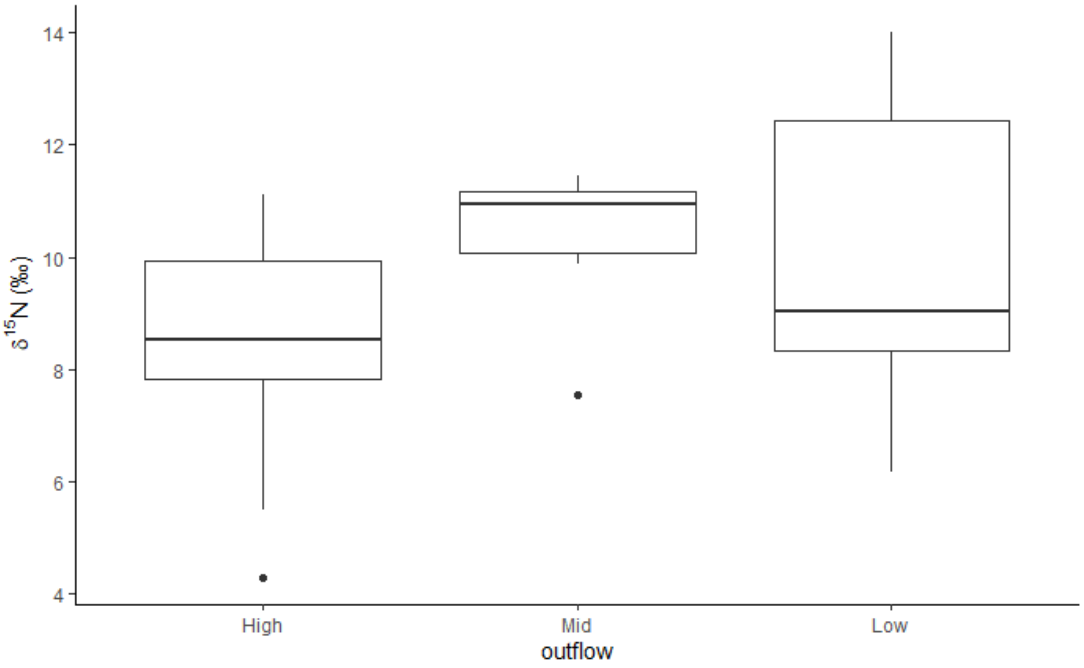

Figure 3.11 $\delta^{15}N$ values of zooplankton by outflow regime.

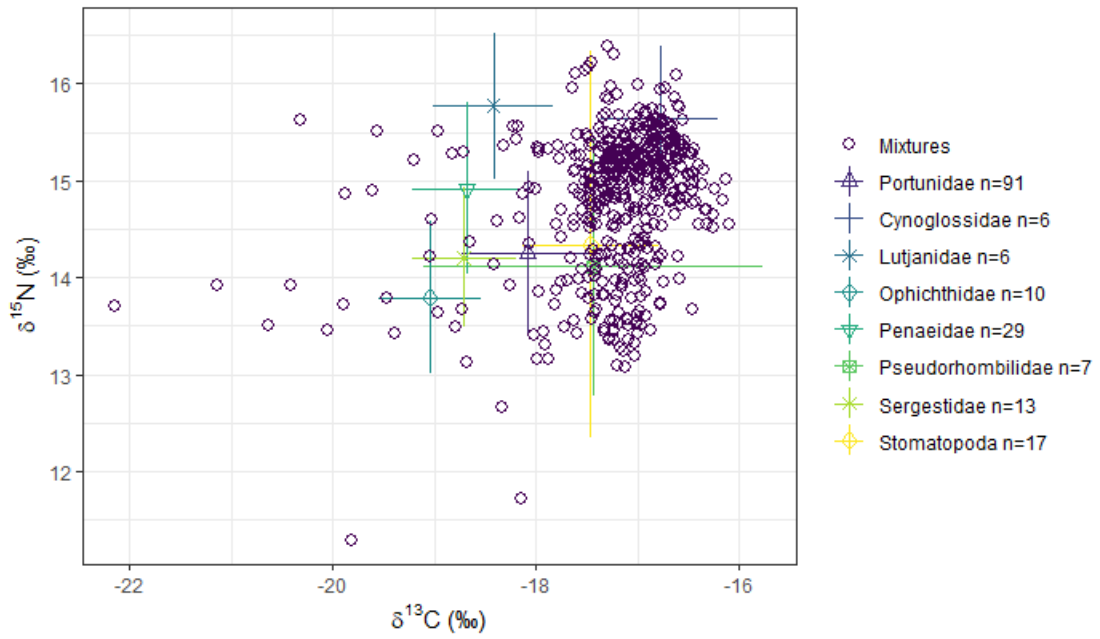

Figure 3.12 Biplot of Red Snapper and prey under high outflow conditions. Prey have been corrected using trophic enrichment factors and error bars indicate one standard deviation around the mean of the prey item.

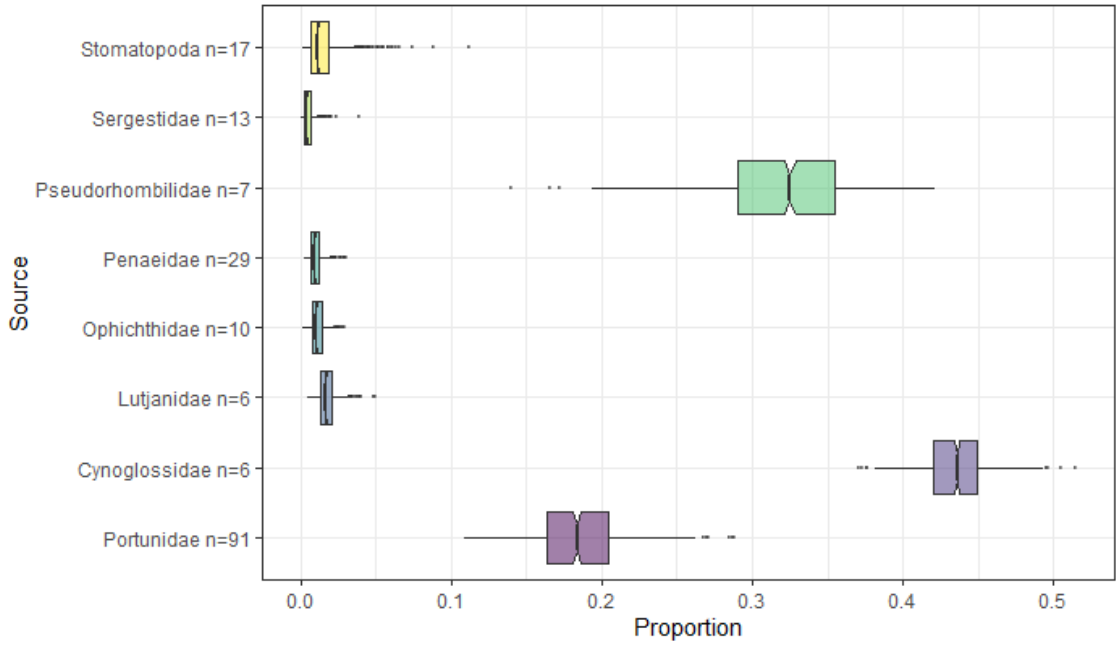

Figure 3.13 Dietary proportion contribution of prey to Red Snapper diet under the high outflow condition.

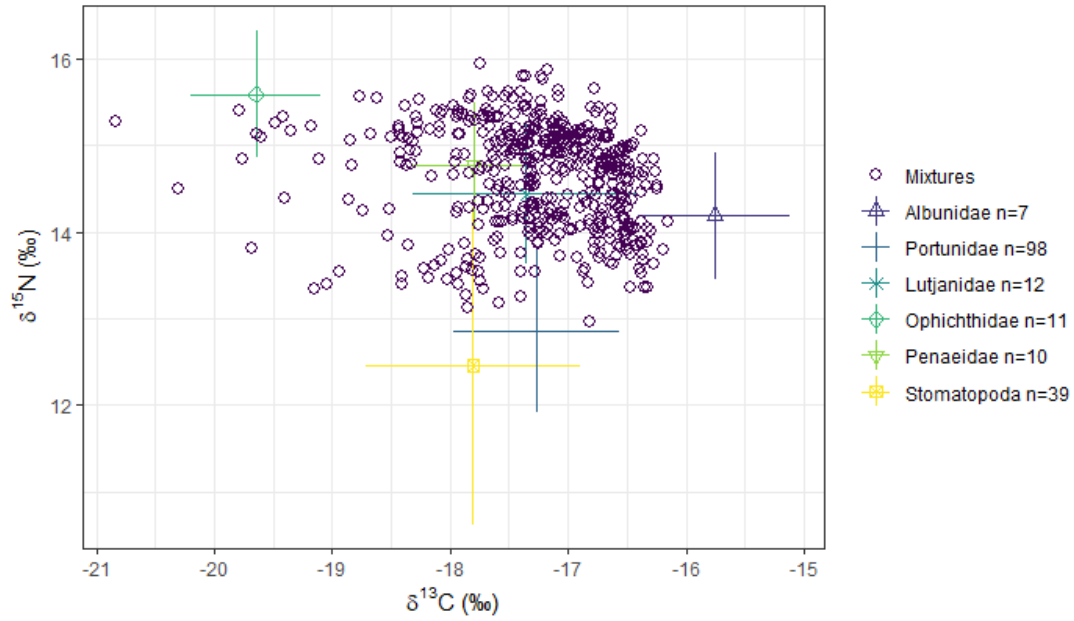

Figure 3.14 Biplot of Red Snapper and prey under mid outflow conditions. Prey have been corrected using trophic enrichment factors and error bars indicate one standard deviation around the mean of the prey item.

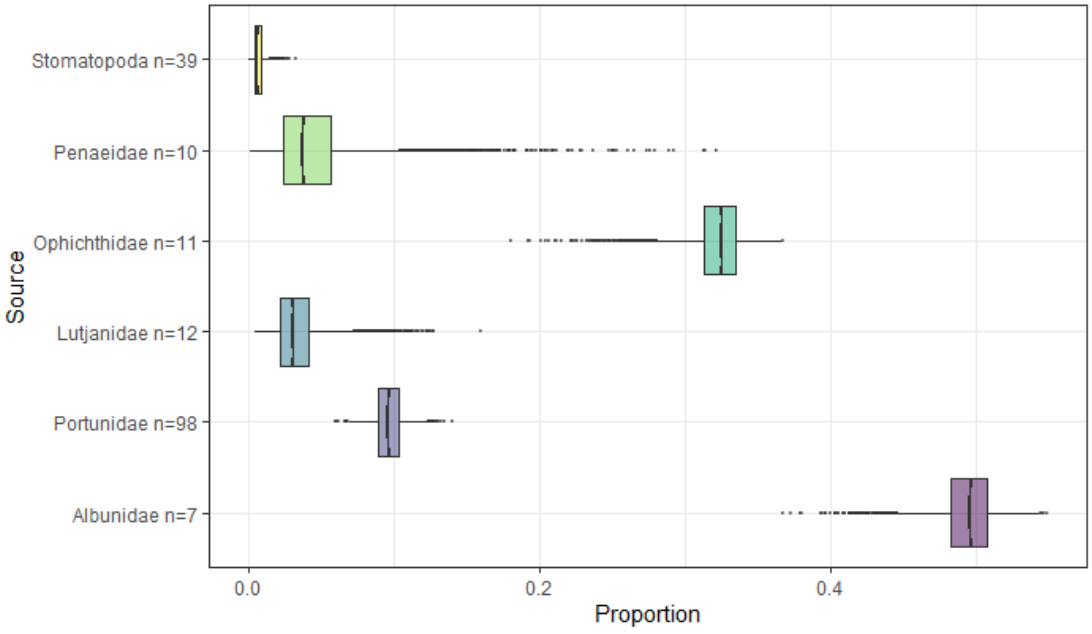

Figure 3.15 Dietary proportion contribution of prey to Red Snapper diet under the mid outflow condition.

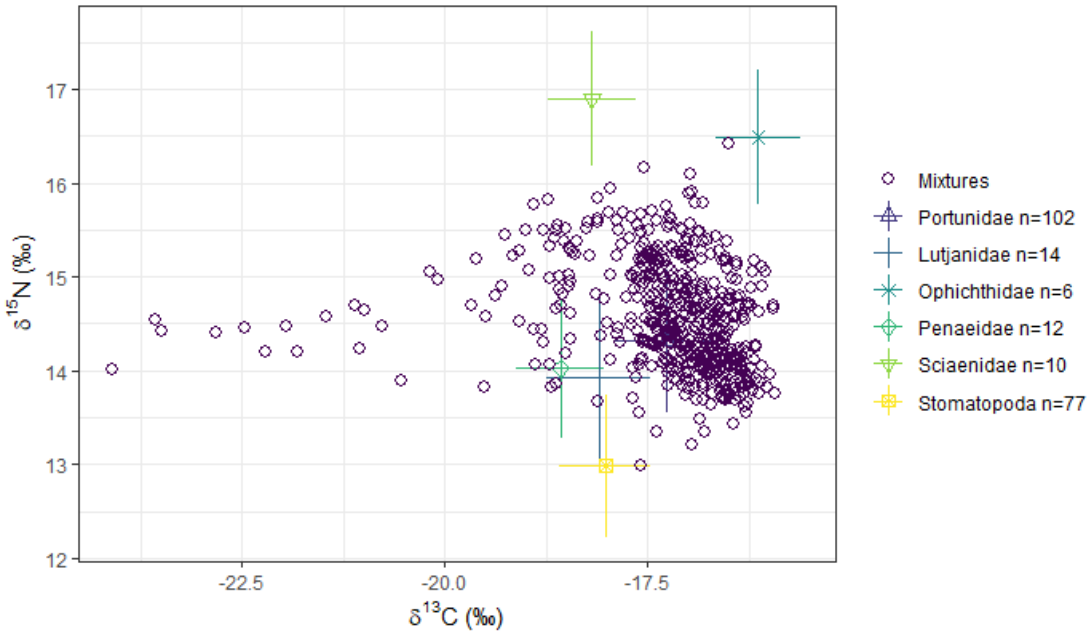

Figure 3.16 Biplot of Red Snapper and prey under Low outflow conditions. Prey have been corrected using trophic enrichment factors and error bars indicate one standard deviation around the mean of the prey item.

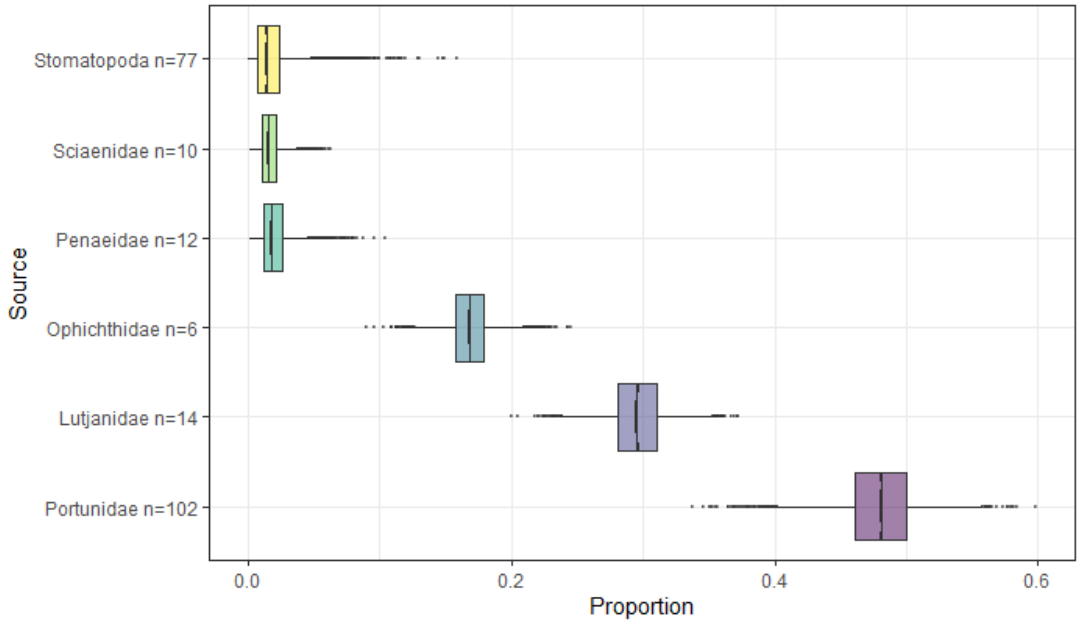

Figure 3.17 Dietary proportion contribution of prey to Red Snapper diet under the low outflow condition.

CHAPTER IV – AGING AND BULK STABLE ISOTOPE ANALYSIS OF RED SNAPPER EYE LENSES

4.1 Abstract

Red Snapper are an important fishery in the northern Gulf of Mexico that has been impacted by overexploitation. Since the late 1990's management efforts have succeeded in restoring the population to a less threatened state but continued efforts to better manage Red Snapper stocks are still underway. In this study eye lens lamina were analyzed to determine if they were suitable for aging by comparison to otolith based age estimates. Some variability between researcher counts (71.6% agreement within one year) and low agreement with otolith ages (78.4% agreement within one year) resulted in the recommendation that eye lenses not be used as a primary aging tool. However, these results do validate previous studies' findings that number of eye lens lamina does correlate with age. Stable isotope analysis of the lens lamina showed significant ontogenetic dietary change in Red Snapper with $\delta^{13}C$ and $\delta^{15}N$ increasing from the core to ~3-4 mm from the core and remaining consistent afterwards. This indicated a shift away from more terrestrially influenced near shore environments used as juvenile habitat coincident with an increase in trophic level. Stable isotopes of muscle tissue of each fish was compared to the outermost layer of the eye lens and found to be similar, though eye lenses did have higher variability. Future analysis of eye lens tissue of Red Snapper may therefore be used for comparison to older studies using muscle tissue without need of analyzing both tissue types.

4.2 Introduction

4.2.1 Aging

Fish contain many known aging structures including scales, the cleithrum, spines, rays, the vertebral column, and most commonly used, otoliths, but eye lenses also have the potential to be used as an aging structure and already have been used as age indicators for several species including squid and sharks (Wallace et al. 2014; Tzadik et al. 2017; Meath et al. 2019). Fish eye lenses are spheres, formed by the successive layering of fine fibers that run circumferentially from an anterior pole to an apex on the anterior side forming layers similar to an onion (Nicol 1989). As the fish grows new layers, or lamina, fibers form on the outside of the lens as live cells undergo attenuated apoptosis that destroys the organelles and genetic material of the cell, preventing continued protein synthesis but preserving existing crystalline proteins (Quaeck-Davies et al. 2018; Peebles and Hollander 2020). This process continues over the life of the fish and has been found to result in a lens weight that is correlated with standard length in carp (Carlton and Jackson 1968), and with standard length and scale aging in freshwater drum (Burkett and Jackson 1971). More recently, Quaeck-Davies et al. (2018) showed that accretion of lens material was linearly proportional to somatic growth in *A. carbo*, *C. rupestris*, *L. nasus*, and *S. acanthias*. Though currently eye lenses of teleost do not contain known age markers (Vecchio et al. 2021), lamina of lenses have been shown to be laid down over a consistent period of time similar to otoliths (Meath et al. 2019; Peebles and Hollander 2020). These studies however relied on the delamination of the layers of lens rather than eye lens sectioning similar to otoliths.

4.2.2 Stable Carbon and Nitrogen Isotopes

The eye lenses of fish are metabolically inactive and the lamina can be separated and studied individually (Berman 1991; Dahm et al. 2007; Wride 2011; Wallace et al. 2014; Tzadik et al. 2017). The organic protein matrix of the lens means that stable isotopes of carbon and nitrogen atoms in the proteins can be analyzed to determine the isotopic history of an individual fish over time back to its pre-juvenile phase in approximately annual increments with each layer of the lens (Tzadik et al. 2017; Nicol 1989). As the different lens layers form, they retain the $\delta^{13}C$ and $\delta^{15}N$ values indicative of the fish's feeding and movement patterns at the time of formation. With this timeline of isotope values for individual fish, we can determine when ontogenetic shifts in habitat and diet occur and at approximately what age if movement is great enough for there to be a shift in basal resources (Wallace et al. 2014). Stable carbon and nitrogen isotope analysis of fish eye lenses has already proved to be useful in determining resource use in several teleost species in the northern Gulf of Mexico (Tzadik et al. 2017) including invasive lionfish (Jackson et al. 2011; Curtis et al. 2020), hogfish (Faletti and Stallings 2021), tilefish and Red Grouper (Vecchio and Peebles 2020). The core of eye lenses has also been used to determine natal resource use for Black Sea Bass, Gag, Red Grouper, and Red Snapper off the Florida coast (Vecchio et al. 2021). Using eye lenses for stable isotope analysis may prove to be superior to simple muscle tissue isotope testing as collecting one fish will allow the analysis of diet and habitat over many life stages rather than just the integrated time period (months), captured by muscle tissue.

The large number of samples collected during a long-term monitoring project examining Red Snapper diet in and around the Mississippi Bight, is ideal for determining

if eye lens isotope data is suitable for management decisions such as setting catch limits based on age structure or setting up protections for potential diet items that are used across a fish's life. In this study we determined if the number of laminae present in the eye lens of Red Snapper correlate with the number of layers present in the otoliths of the same fish, analyzed the isotope values of successive lens layers, and compare the outer eye lens laminae stable isotope values to muscle tissue. We hypothesized that the outer eye lens isotope values would be comparable to muscle tissue, which would allow for comparison to previous studies completed using muscle tissue without the need to sample as many fish. We also hypothesize that stable isotope values in Red Snapper eye lens layers will reflect ontogenic habitat and diet shifts that are known to occur as these fish mature (Vecchio and Peebles 2020).

4.3 Methods

As part of a National Fish and Wildlife Foundation grant focused on quantifying reef fish abundances and trophic dynamics in the NGOM, we collected fish from bare bottom water control sites and reef fish habitats (artificial reefs and oil/gas rigs) from the study region discussed in chapter 1. Sagittal otoliths were removed from the Red Snapper and the left otolith was used for age assessment and the other was archived. Otolith processing and aging methodologies followed guidelines provided in the Gulf State Marine Fisheries Commission's *A Practical Handbook for Determining the Ages of Gulf of Mexico and Atlantic Coast Fishes, Third Edition: GSMFC Publication No. 300* (VanderKooy et al. 2020). Otolith annuli counts were

conducted by 3 experienced, independent readers and consensus was reached on final ages. A simple and novel method to age the lenses was developed for this study. The eye lenses used for aging comparison were dissected from the eye while frozen and sliced through the center from pole to pole using a scalpel under a dissection stereomicroscope. The back of the sliced half was removed similarly so a section of approximately 1-3 mm remained. Sections were not mounted in resin as an otolith would be, due to issues with shrinking of the lens during drying causing delamination and crumbling of layers. The left eye of each fish caught in 2019 and 2020 was collected and frozen at -20°C. Previous work determined there was no difference between the isotopes in the left and right eyes of a variety of NGOM species, including Red Snapper (Wallace et al. 2014). A subset of eye lenses from 2019 were analyzed for carbon and nitrogen stable isotope values (n=28) to assess resource use and trophic changes, while another subset from 2020 was analyzed for potential as an aging tool and compared to otolith derived ages (n=88). Eyes selected for stable isotope analysis were from a relatively wide range of muscle tissue isotope values, sizes, habitat types, depths at collection, and latitude of collection in 2019, while eyes analyzed for age comparison to otoliths were randomly selected from fish collected in 2020.

A photograph was taken of the lens section while still partially frozen under both transmitted and reflected light using a Nikon SMZ1500 stereoscopic zoom microscope with a Nikon digital sight DSFi2 camera and Nikon Digital Sight DS-U3 microscope camera controller interfaced with a PC through a FireWire 800 interface (Fig. 3.1). A central core was identified, and continuous rings were counted by the primary researcher 3 times and verified by a secondary independent reader skilled in otolith analysis.

Average of the lamina counts were then compared to otolith derived ages within one year to determine accuracy of eye lens aging using correlations and t-tests.

The eye lenses used for stable isotope analysis were dissected from the eye while frozen and individual lamina of the lens were dissected using a scalpel and forceps under a dissection stereomicroscope (Wallace et al. 2014). The diameter of the lens and the thickness of each layer was measured (in millimeters) using a digital micrometer as each layer was removed. A relative laminar position from the center of the lens was then calculated as thickness of the layer over diameter of the lens before the layer was removed. Individual lens layers were then air dried, placed in scintillation vials and stored in a desiccator until being packed (0.3 to 0.7 mg of material) in tin capsules for stable isotope analysis. If there was not enough material from the innermost (core) layer for the analysis, the layer was combined with the next layer out from the center. Samples were analyzed in duplicate for %C, %N and $\delta^{13}C$, $\delta^{15}N$ values with a Thermo Finnegan Delta V Advantage stable isotope ratio mass spectrometer coupled to a Costech 4010 elemental analyzer via a Thermo Conflo IV interface. The results were analyzed in R studio using the packages NichRover (Lysy et al. 2014; Swanson et al. 2015) and SIBER (Jackson et al. 2011). Lenses were grouped for analysis by distance from the center of the lens using the relative laminar position. Isotopic niche space of each lamina group was defined as the standard ellipse areas (SEA) using the central 40% probability region in isotopic space (Jackson et al. 2011). After niche space was determined, niche overlap was analyzed to determine if resource use changes with fish age. The isotope values of the outer most layer of the eye lenses was also compared to the muscle tissue isotope

values for each fish and a t-test was used to determine if isotope values of these two tissue types were different.

4.4 Results

4.4.1 Aging

There was a 30% agreement in eye lens aging estimates between the two counters but a 71.6% agreement within one year in number of layers present between the two sets of counts. A paired two tailed t-test determined the counts to be significantly different between the two counters (p=0.005). However, the average number of layers from these counts and the biological age of the fish determined from otolith analysis were not significantly different (p=0.312) and agreed in age within one year of 78.4% (Table 1). This result was the same for the counts from the primary counter (p=0.503) and the secondary counter (p=0.315) separately. Eye lenses were consistently counted to have more layers than otoliths between both counters, which may be due to counting of a currently accreting layer.

Despite the non-significant difference between otolith and eye lens aging results, the correlation between the average of the counts and biological age determined from otoliths was poor (r^2 = 0.136; Fig. 3.2; Table 3.1) but was stronger than the correlation between the average count of lens lamina with total length (mm) (r^2=0.11) or weight (kg) (r^2=0.079) of the fish indicating that faster growing fish are likely not accreting more layers than slower growing fish of the same age.

4.4.2 Stable isotopes

In total 28 eye lenses were dissected and a total of 266 layers were analyzed for $\delta^{13}C$ and $\delta^{15}N$. After grouping dissected layers by distance from the core, 50 layers were incorporated in the core group, 91 layers in the first group, 64 layers in the second, 28 in the third, 23 in the fourth, 2 in the fifth, and 1 in the sixth. The fifth and sixth layers were added to the fourth group as these represented adults based on otolith ages. Three layers were removed from the study as not enough material was present for analysis. $\delta^{13}C$ values ranged from -20.72 to -15.00‰ and became significantly higher until 2-3 mm where they plateaued at approximately -17‰ (Fig. 3.3). $\delta^{15}N$ ranged from 11.07 to 16.83 and continued to increase until approximately 4 -5 mm then plateaued at approximately 16‰ (Fig. 3.3). Significant isotopic variability was found in juveniles for both $\delta^{13}C$ and $\delta^{15}N$ (Fig. 3.3). This range can be seen in Fish 6221, 6127, 6170, and 6243 (Figure 3.4), but fish 6201 remains consistently more enriched in ^{13}C than the others.

The isotope niche space of each successive eye lens group increased in both $\delta^{13}C$ and $\delta^{15}N$ (Fig. 3.5). The core group was the largest with a SEA of 2.20 ‰^{2}. Group 1 encompassed an area of 1.48 ‰^{2}, group 2 an area of 1.52 ‰^{2}, group 3 an area of 1.23 ‰^{2}, and group 4 an area of 1.46 ‰^{2}. With increasing distance from the center of the core of the lens, the groups became more consistent with each other in both SEA size and location in isotope space. The probability of overlap between groups became larger as fish became older, with adult groups having almost no probability of overlap with natal groups and a small probability of overlap with juvenile groups (Table 3.2).

Muscle tissue of each fish was compared to the outermost eye lens lamina to determine if these two tissues produced similar results. Neither $\delta^{13}C$ nor $\delta^{15}N$ was

significantly different according to paired, two-tailed T-tests (p= 0.070 and p=0.223 respectively), though there was more variability in eye lenses isotope values compared to muscle tissue (Fig. 3.6).

4.5 Discussion

Eye lenses have long been known to accrete new layers over a fish's life, but only recently have been used for stable isotope analysis (Nicol 1989; Wallace et al. 2014; Tzadik et al. 2017). The benefit of being able to use eye lens layers from different time periods of a single fish's life for stable isotope analysis is that resource use can be ascertained over time and the general age of changes in diet and/or habitat can be determined. Therefore, fewer fish and less sampling effort is required to attain large amounts of data required for ecosystem based management (McCormack et al. 2019). While the differences between the eye lens and otolith age estimates were not significantly different, the correlation was not strong enough for eye lens aging analysis to be recommended as a primary aging tool. Consistent overcounting of eye lens layers compared to otolith annuli may be due to accretion of currently crystalizing cells around the outermost layer of the hardened nucleus (Fig. 3.1 panels D and E). Results do support the continued accretion of layers over time proportional to the age of the fish, rather than by size of the fish, and can thus be used as a general ageing tool (within a year), similar to using scales, spines, or vertebra for some species, if otoliths are not available or are too small to be accurately aged. Other types of aging also require specialized tools whereas this technique only requires a dissection scope and forceps. It may also be useful when age length relationships plateau after a certain age.

Red Snapper are known to utilize a variety of habitats with varying riverine impact, which have varying carbon and nitrogen isotope baselines depending on the dominant basal resources present and the amount of nutrients and organic matter delivered by rivers. This results in a large range of $\delta^{13}C$ values for juveniles which tend to become less variable as fish age and undergo ontogenetic migrations from inner shelf to outer shelf habitats (Szedlmayer and Lee 2004; Gallaway et al. 2009). Stable isotope analysis of eye lenses indicated significant habitat/dietary shifts over the life of Red Snapper in our study. There was an increase in $\delta^{13}C$ with laminar distance from the core, indicating a shift in the base of Red Snapper diet from more freshwater influenced habitats when young, to marine, phytoplankton supported habitats when older. An increase in $\delta^{15}N$ with increasing laminar distance from the core suggests these fish are feeding at a higher trophic level at older ages. Across the NGOM, Red Snapper have been shown to move from low relief juvenile habitats closer to shore to more complex offshore reef adult habitats at approximately age two (Gallaway et al. 2009; Szedlmayer and Lee 2004). These results strongly agree with this habitat shift that is well documented in the literature, clearly capturing distinct resource use between younger fish and older fish (Wells et al. 2008; Brewton et al. 2020; Rooker et al. 2004; Geary et al. 2007; Dance and Rooker 2019). Dance and Rooker (2019) used models of environmental parameters on Red Snapper abundance to determine that juveniles were most abundant in 10-40m of depth and abundance declined with movement east of the Mississippi River Delta, while adults were most abundant at the shelf edge from 100-150 m deep, decreasing eastward into Florida, with overall Red Snapper relative abundance increasing with movement eastward and offshore. They also determined that predicted high quality juvenile habitat

declined from Louisiana to Florida with movement away from the Mississippi River Delta. This was further supported on a smaller spatial scale by (Powers et al. 2018), who used a multigear survey off the coat of Alabama and found that juvenile Red Snapper were most abundant in the ~20-40 m depth range while adults were further offshore. The $\delta^{13}C$ values of POM, a proxy for phytoplankton which form the base of the food web in marine ecosystems, has been shown to become more depleted during higher riverine outflow (Cai et al. 2015). This isotopic change in the base of the food web can be reflected in the eye lenses (Peebles and Hollander 2020). Stable isotope values for the core of the eye lenses (indicative of natal habitats and diet), are completely separated in isotope space from adult fish with periods of transition between the two extremes. Based on $\delta^{13}C$ values, most younger fish examined were feeding in more freshwater influenced regions and then move offshore where they integrate into the adult population. In this study region, more marine dominated habitats like those found around the barrier islands may also be utilized by some juveniles, while others seem to be using more fresh water influenced areas. The use of more marine influenced habitats for some juvenile Red Snapper is demonstrated by fish 6201 which appears to have used more marine based resources throughout its entire life rather than utilizing more riverine influenced habitats (Fig 3.4).

The comparison between muscle tissue and the outer most eye lens layer shows that they are isotopically similar. Turnover times of different tissue types can vary such that they capture different time periods of the organism's diet (Vander Zanden et al. 2015). In large fish, muscle tissue has a slow tissue turnover rate compared to other tissue types such as plasma, blood cells and liver integrating diet over several months to a

year (Thomas and Crowther 2015). Eye lenses however, have no turnover time once they are formed being metabolically inactive (Wallace et al. 2014; Quaeck-Davies et al. 2018; Peebles and Hollander 2020). A study in 2018 showed an initial lag time in the incorporation of dietary isotopes into the eye lenses of captive Red Drum of approximately 16 days (Granneman 2018). This fast incorporation time may lead to higher variability compared to muscle tissue that integrates isotopes over longer periods of time.

4.6 Conclusion

Due to the growing need to understand habitat use and dietary shifts throughout a fish's life for better whole ecosystem management of important fisheries species, it is important to have the ability to elucidate dietary shifts over time for managed fish stocks. Red Snapper in Mississippi state and adjacent federal waters are exposed to an extremely dynamic environment. The ability to gather lifetime data from eye lenses of one fish rather than requiring larger harvests to sample across cohorts decreases the take required for fisheries analysis and allows researchers to study dietary and habitat changes over time in a different and in some ways, a more efficient manner. This study has shown that though eye lenses are not particularly useful as a primary aging tool however the successive layering of lens lamina over time is consistent enough to determine a general age and allow stable isotope analysis of a single fish at various ecologically and ontogenetically important time periods. Stable isotope analysis of Red Snapper eye lenses typically shows the distinct difference in resource use by Red Snapper over their life. The outermost eye lens lamina isotopes matched relatively well with the muscle isotope

data for the same fish, indicating that muscle tissue from previous studies can be used comparably to eye lens data in future, and does not require the analysis of both tissues to compare to older studies.

Table 4.1 Lamina counts for given eye lenses from figure 3.2 as compared to otolith aging results.

Eye lens	Average count of lamina	Biological age from otolith
A	4	4
B	4.5	3.83
C	5.25	4.92
D	3.75	3.0
E	3.75	3.17
F	3.75	3.92

Table 4.2 Matrix of the average isotopic niche overlap (%) for each pair of lens groups. Results represent the median posterior probability that the group listed on the left will be found in the niche space of the group listed across the top.

	core	1	2	3	4
core		20.9981	11.7509	3.0889	2.248
1	21.3064		24.7823	7.5052	5.6857
2	10.9023	24.0906		24.3763	24.3801
3	5.8421	15.6728	35.0027		40.1922
4	2.261	9.684	25.8114	32.1196	

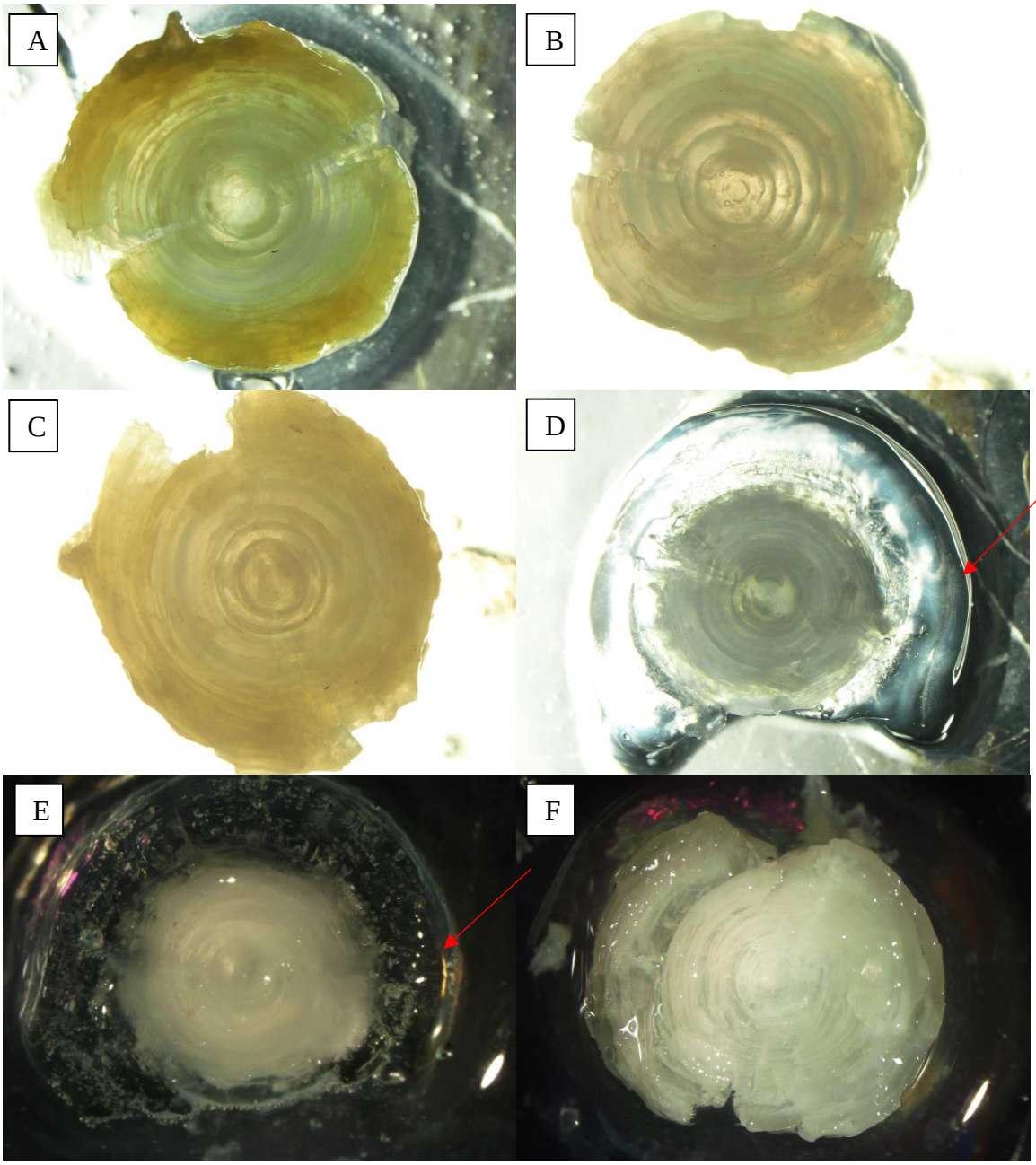

Figure 4.1 Eye lens images used for aging. Panels A, B, and C are taken under transmitted light, panels D, E, and F are taken under reflected light. Counts for given images as compared to their otolith results are in table below. Red arrows indicate outer most gelatinous layer where current year layer is forming.

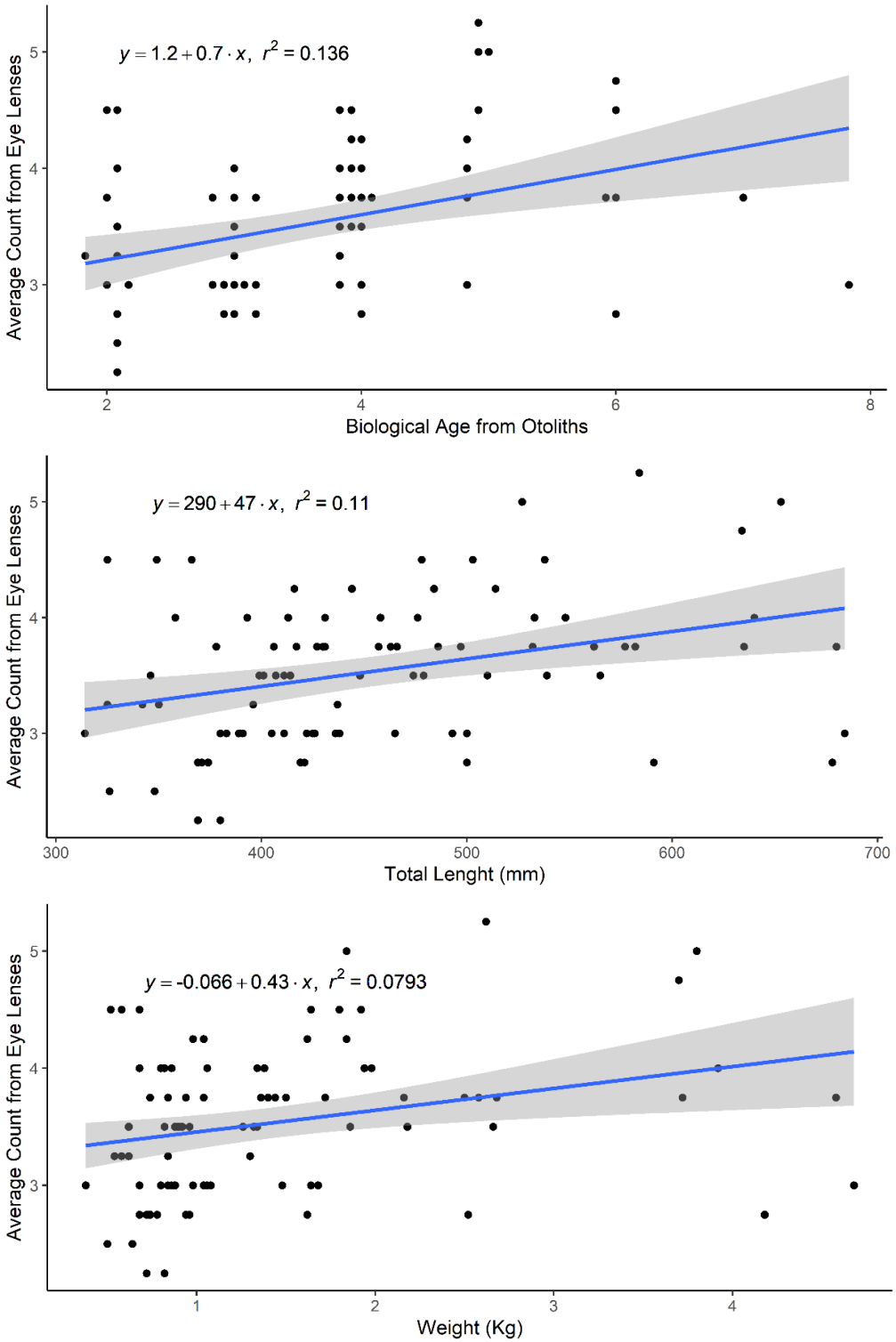

Figure 4.2 Correlation between average count of eye lenses and biological age determined from otoliths, total length of the fish (mm) and weight of the fish (kg).

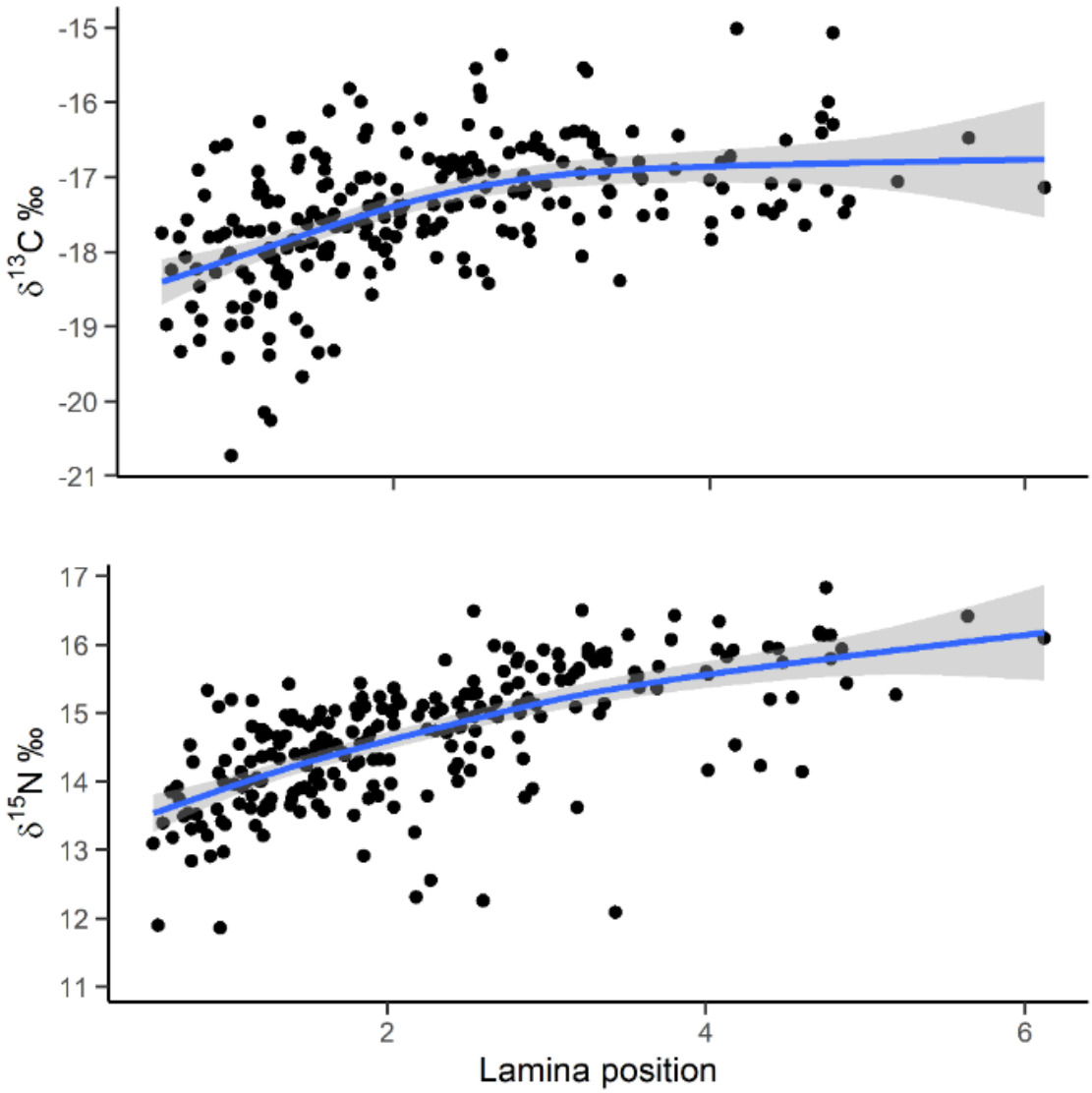

Figure 4.3 Stable isotope values of eye lenses relative to position from the core with fitted generalize linear model trendline (gray shading = 95% confidence interval).

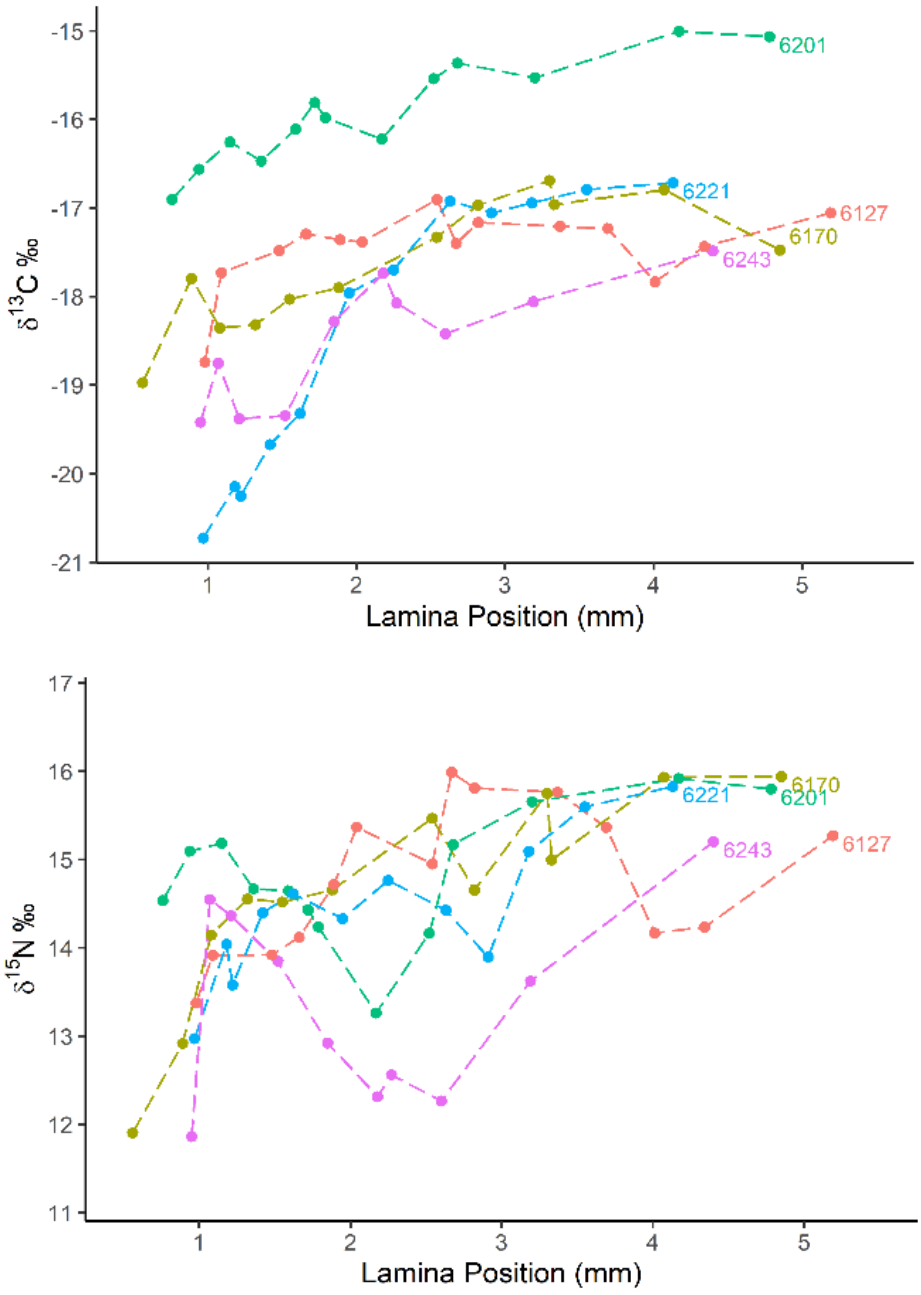

Figure 4.4 Stable isotope values by lamina position of 5 of the oldest Red Snapper analyzed.

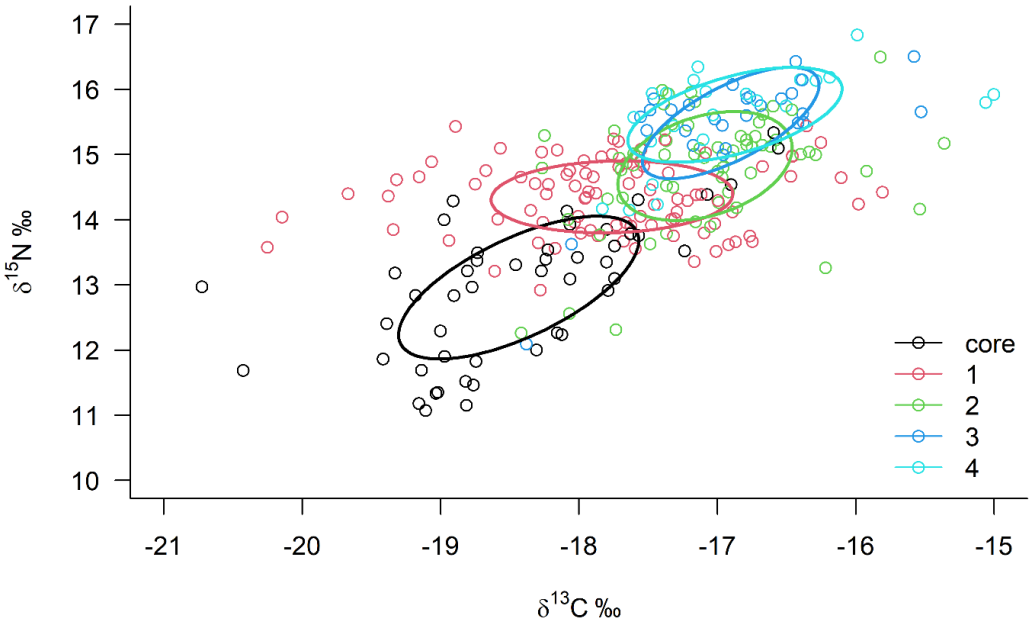

Figure 4.5 Isotope niche space of successive lamina of Red Snapper with associated standard eclipse areas. Ellipses represent 40% of the total area of the data.

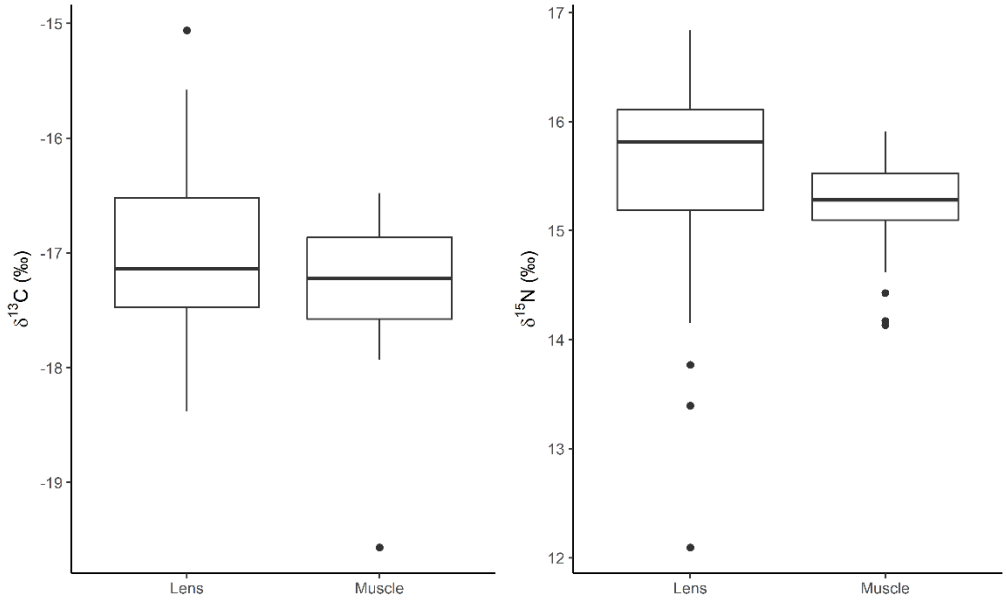

Figure 4.6 Comparison of stable isotope values between the outermost lens and muscle tissue.

CHAPTER V – SUMMARY

Over the course of this study, we have shown that river outflow impacts the basal resources of the Red Snapper food web, altering carbon sources and in turn impacting prey isotopes and Red Snapper themselves. In the Mississippi Bight, the Mississippi River has long been the primary focus for freshwater impact, however, this study, along with others (Dzwonkowski et al. 2018; Sanial et al. 2019) shows that multiple rivers in the region are significant contributors to nutrient and particulate organic matter delivery. Furthermore, these water quality parameters appear to interact in highly dynamic ways, including the dissolved nutrients being taken up by phytoplankton, breakdown of the phytoplankton derived organic particulate material as it sinks or undergoes various diagenic processes, resuspension of previously processed particulates from the sediments, etc. While in the bottom waters particulate organic matter pool seem to be primarily impacted by Mississippi River outflow, in the surface water they were found to be primarily impacted by the delayed outflow from the Mobile. Nutrients however were reversed with the Mississippi River impacting nutrients in the surface waters and the Mobile impacting them in the bottom. The inclusion of the Mobile River as an important source of freshwater, nutrients and POM to the study region is therefore important when studying the impact of these rivers on the ecology of the area.

While the changes in POM stable isotope values which represent the base of the food web did not appear to alter Red Snapper diet significantly, the trends found in POM and zooplankton isotopes related to river outflow did seem to be reflected in the isotope values of Red Snapper and their prey. Futhermore the body condition changes in Red Snapper by different outflow regimes, though not significant to suggest that more

dynamic, moderate to low outflow regimes produce higher Red Snapper condition. Under these conditions diet changed enough to be reflected in the bulk isotopes of the muscle tissue of Red Snapper, though different diet analysis techniques did not agree on how diet changed.

The increased river flow predicted under various climate change scenarios due to increased precipitation in the upper Mississippi and Ohio river basins (Jha et al. 2006), as well as more frequent and longer openings of river diversions for flood control, suggest that higher outflow is much more likely to be the new normal in the future (Driessen and van Ledden 2013). It is therefore imperative that mangers understand how habitat use and dietary shifts will impact Red Snapper in the future. Red Snapper in Mississippi state and adjacent federal waters are exposed to an already extremely dynamic environment and the ability to gather lifetime data from the eye lenses of one fish rather than requiring larger harvests to sample across cohorts decreases the take required for fisheries analysis and allows researchers to study dietary and habitat changes over time in a more efficient manner. This study has shown that though eye lenses are not particularly useful as a primary aging tool the successive layering of lens lamina over time is consistent enough to determine a general age and allow stable isotope analysis of a single fish at various ecologically and ontogenetically important time periods.

Many studies state that Red Snapper are generalist predators, but studies by Tranecki and Patterson (2015), Wells et al. (2008) and others, as well as this study show that their diet is influenced by changes to the prey assemblage and that prey assemblage or diet preferences is impacted by freshwater sources in their home regions. By studying how prey of Red Snapper are impacted by these environmental changes, we can better

understand how the fishery will change in the future, and using stable isotope analysis of the eye lens, we can more effectively see how individual fish are impacted by that change over time.

APPENDIX A – STABLE ISOTOPES OF ALL EYE LENS LAMINA BY LAMINA POSITION AND INDIVIDUAL FISH

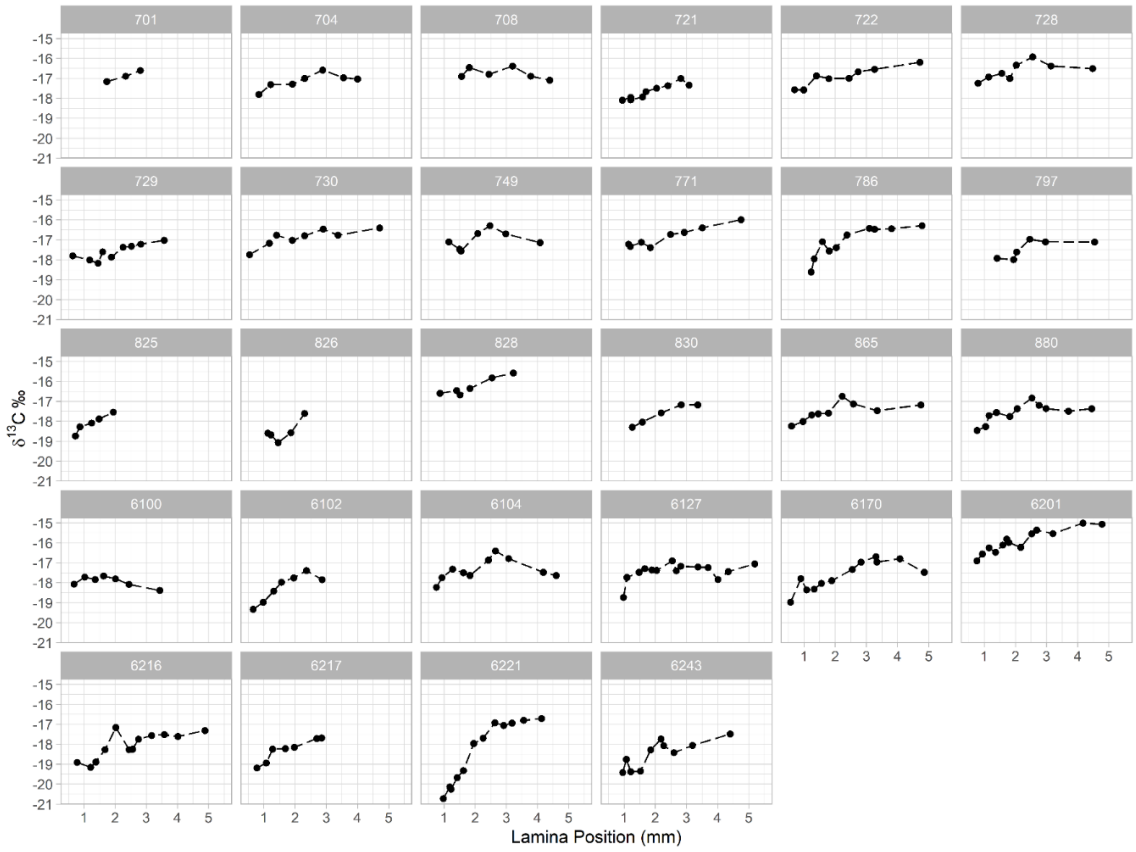

Figure A.1 $\delta^{13}C$ values by lamina position of all Red Snapper analyzed.

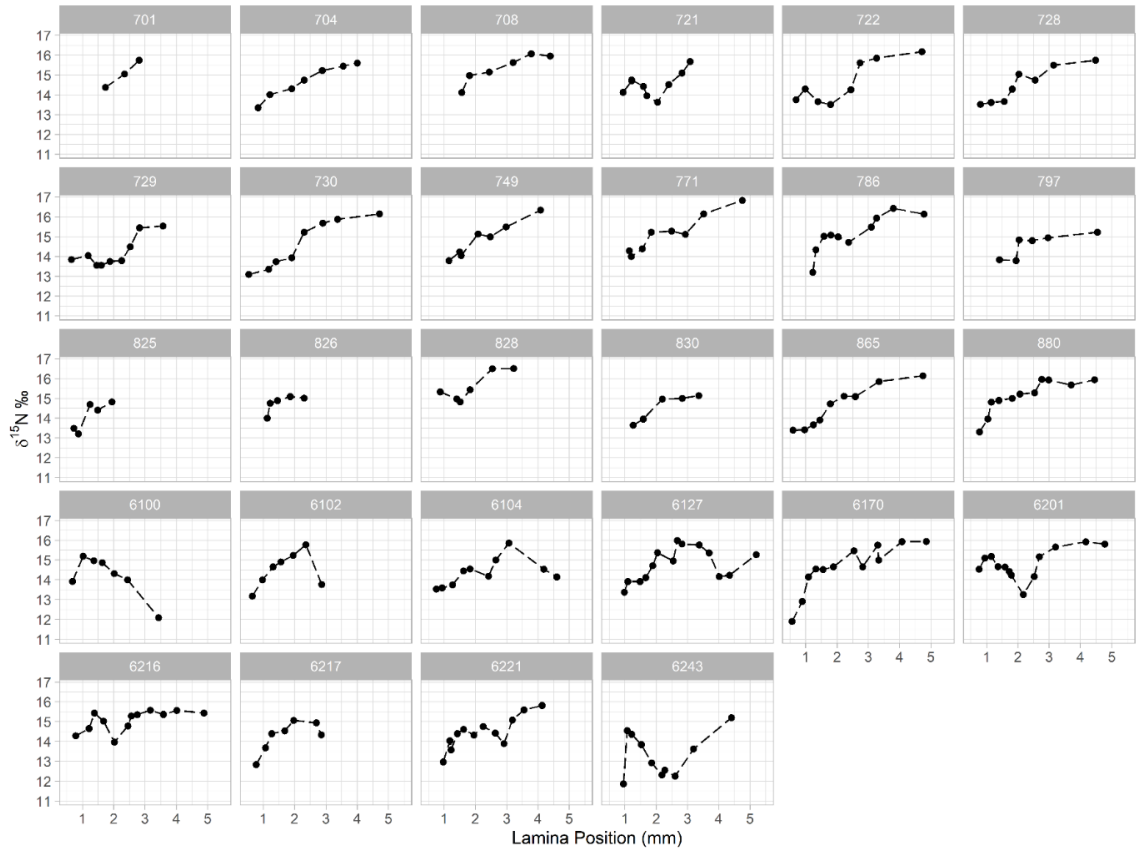

Figure A.2 $\delta^{15}N$ values by lamina position of all Red Snapper analyzed.

LITERATURE CITED

Aulenbach BT, Buxton HT, Battaglin WA, Coupe RH (2007) Streamflow and nutrient fluxes of the Mississippi–Atchafalaya River basin and sub-basins for the period of record through 2005. U.S. Geological Survey.

Bargu S, Justic D, White JR, Lane R, Day J, Paerl H, Raynie R (2019) Mississippi River diversions and phytoplankton dynamics in deltaic Gulf of Mexico estuaries: A review. Estuar Coast Shelf Sci 221:39–52.

Bargu S, White JR, Li C, Czubakowski J, Fulweiler RW (2011) Effects of freshwater input on nutrient loading, phytoplankton biomass, and cyanotoxin production in an oligohaline estuarine lake. Hydrobiologia 661:377–389.

Battaglin WA, Kendall C, Chang CCY, Silva SR, Campbell DH (2001) Chemical and isotopic evidence of nitrogen transformation in the Mississippi River, 1997-98. Hydrol Process 15:1285–1300.

Berman ER (1991) Biochemistry of the eye. Springer US, Boston, MA.

Bianchi TS, DiMarco SF, Cowan JH, Hetland RD, Chapman P, Day JW, Allison MA (2010) The science of hypoxia in the Northern Gulf of Mexico: a review. Sci Total Environ 408:1471–1484.

Bianchi TS, Mitra S, McKee BA (2002) Sources of terrestrially-derived organic carbon in lower Mississippi River and Louisiana shelf sediments: implications for differential sedimentation and transport at the coastal margin. Mar Chem 77:211–223.

Bianchi TS, Wysocki LA, Schreiner KM, Filley TR, Corbett DR, Kolker AS (2011) Sources of terrestrial organic carbon in the mississippi plume region: evidence for the importance of coastal marsh inputs. Aquat Geochem 17:431–456.

Box GEP, Cox DR (1964) An analysis of transformations. Journal of the Royal Statistical Society: Series B (Methodological) 26:211–243.

Braman RS, Hendrix SA (1989) Nanogram nitrite and nitrate determination in environmental and biological materials by vanadium(III) reduction with chemiluminescence detection. Anal Chem 61:2715–2718.

Breitburg DL, Craig JK, Fulford RS, Rose KA, Boynton WR, Brady DC, Ciotti BJ, Diaz RJ, Friedland KD, Hagy JD, Hart DR, Hines AH, Houde ED, Kolesar SE, Nixon SW, Rice JA, Secor DH, Targett TE (2009) Nutrient enrichment and fisheries exploitation: interactive effects on estuarine living resources and their management. Hydrobiologia 629:31–47.

Brewton RA, Downey CH, Streich MK, Wetz JJ, Ajemian MJ, Stunz GW (2020) Trophic ecology of Red Snapper *Lutjanus campechanus* on natural and artificial reefs: interactions between annual variability, habitat, and ontogeny. Mar Ecol Prog Ser 635:105–122.

Burkett RD, Jackson WB (1971) The eye lens as an age indicator in freshwater drum. American Midland Naturalist 85:222.

Busst GMA, Britton JR (2017) Tissue-specific turnover rates of the nitrogen stable isotope as functions of time and growth in a cyprinid fish. Hydrobiologia 805:1–12.

Cai Y, Guo L, Wang X, Aiken G (2015) Abundance, stable isotopic composition, and export fluxes of DOC, POC, and DIC from the Lower Mississippi River during 2006-2008. J Geophys Res Biogeosci 120:2273–2288.

Cai Y, Guo L, Wang X, Mojzis AK, Redalje DG (2012) The source and distribution of dissolved and particulate organic matter in the Bay of St. Louis, northern Gulf of Mexico. Estuar Coast Shelf Sci 96:96–104.

Carlton WG, Jackson WB (1968) The eye lens as an age indicator in carp. Copeia 1968:633.

Carpenter JS (1965) A Review of the Gulf of Mexico Red Snapper Fishery. U.S. Department of the Interior, Fish and Wildlife Service, Bureau of Commercial Fisheries, the University of Wisconsin - Madison.

Carpenter KE (2002a) The Living Marine Resources Of The Western Central Atlantic (fao Species Identification Guides For Fishery Purposes). Food & Agriculture Organization Of The United Nations, Rome.

Carpenter KE (2002b) The Living Marine Resources Of The Western Central Atlantic (fao Species Identification Guide For Fishery Purposes). Fao.

Childs CR, Rabalais NN, Turner RE, Proctor LM (2002) Sediment denitrification in the Gulf of Mexico zone of hypoxia. Mar Ecol Prog Ser 240:285–290.

Cowie GL, Hedges JI (1994) Biochemical indicators of diagenetic alteration in natural organic matter mixtures. Nature 369:304–307.

Curtis JS, Albins MA, Peebles EB, Stallings CD (2020) Stable isotope analysis of eye lenses from invasive lionfish yields record of resource use. Mar Ecol Prog Ser 637:181–194.

Dagg MJ, Breed GA (2003) Biological effects of Mississippi River nitrogen on the northern Gulf of Mexico—a review and synthesis. Journal of Marine Systems 43:133–152.

Dahm R, Schonthaler HB, Soehn AS, van Marle J, Vrensen GFJM (2007) Development and adult morphology of the eye lens in the zebrafish. Exp Eye Res 85:74–89.

Dance MA, Rooker JR (2019) Cross-shelf habitat shifts by Red Snapper (*Lutjanus campechanus*) in the Gulf of Mexico. PLoS ONE 14:e0213506.

Day JW, Lane RR, D'Elia CF, Wiegman ARH, Rutherford JS, Shaffer GP, Brantley CG, Kemp GP (2016) Large infrequently operated river diversions for Mississippi delta restoration. Estuar Coast Shelf Sci 183:292–303.

Dinnel SP, Schroeder WW, Wiseman WJ (1990) Estuarine-Shelf Exchange Using Landsat Images of Discharge Plumes. Journal of Coastal Research 6:789–799.

Dorado S, Rooker JR, Wissel B, Quigg A (2012) Isotope baseline shifts in pelagic food webs of the Gulf of Mexico. Mar Ecol Prog Ser 464:37–49.

Dortch MS, Zakikhani M, Noel MR, Kim S-C (2007) Application of a Water Quality Model to Mississippi Sound to Evaluate Impacts of Freshwater Diversions. U.S. Army Engineer Research and Development Center, Vicksburg, MS.

Driessen TLA, van Ledden M (2013) The large-scale impact of climate change to Mississippi flood hazard in New Orleans. Drink Water Eng Sci 6:81–87.

Dzwonkowski B, Fournier S, Reager JT, Milroy S, Park K, Shiller AM, Greer AT, Soto I, Dykstra SL, Sanial V (2018) Tracking sea surface salinity and dissolved oxygen on a river-influenced, seasonally stratified shelf, Mississippi Bight, northern Gulf of Mexico. Continental Shelf Research 169:25–33.

Dzwonkowski B, Greer AT, Briseño-Avena C, Krause JW, Soto IM, Hernandez FJ, Deary AL, Wiggert JD, Joung D, Fitzpatrick PJ, O'Brien SJ, Dykstra SL, Lau Y, Cambazoglu MK, Lockridge G, Howden SD, Shiller AM, Graham WM (2017) Estuarine influence on biogeochemical properties of the Alabama shelf during the fall season. Continental Shelf Research 140:96–109.

Dzwonkowski B, Park K, Collini R (2015) The coupled estuarine-shelf response of a river-dominated system during the transition from low to high discharge. J Geophys Res Oceans 120:6145–6163.

Dzwonkowski B, Park K, Kyung Ha H, Graham WM, Hernandez FJ, Powers SP (2011) Hydrographic variability on a coastal shelf directly influenced by estuarine outflow. Continental Shelf Research 31:939–950.

Everett AG, Szedlmayer ST, Gallaway BJ (2020) Movement patterns of Red Snapper *Lutjanus campechanus* based on acoustic telemetry around oil and gas platforms in the northern Gulf of Mexico. Mar Ecol Prog Ser 649:155–173.

Fahay MP (1983) Guide to the early stages of marine fishes occurring in the western north Atlantic Ocean, Cape Hatteras to the southern Scotian shelf. J Northw Atl Fish Sci 4:3–423.

Faletti ME, Stallings CD (2021) Life history through the eyes of a hogfish: trophic growth and differential juvenile habitat use from stable isotope analysis. Mar Ecol Prog Ser 666:183–202.

Fischer A, Baker MS, Wilson CA (2004) Red snapper (*Lutjanus campechanus*) demographic structure in the northern Gulf of Mexico based on spatial patterns in growth rates and morphometrics. Fish Bull 102:593–603.

Fitzhugh GR, Kline WC, Porch CE, Gardner CL (2019) Improving the Historical Baseline of the Gulf of Mexico Red Snapper, *Lutjanus campechanus*, Fishery. In: *Red snapper biology in a changing world*. Szedlmayer ST, Bortone SA (eds) CRC Press, p 201–231

France RL, Peters RH (1997) Ecosystem differences in the trophic enrichment of 13C in aquatic food webs. Can J Fish Aquat Sci 54:1255–1258.

Fry B, Justić D, Riekenberg P, Swenson EM, Turner RE, Wang L, Pride L, Rabalais NN, Kurtz JC, Lehrter JC, Murrell MC, Shadwick EH, Boyd B (2015) Carbon Dynamics on the Louisiana Continental Shelf and Cross-Shelf Feeding of Hypoxia. Estuaries Coast 38:703–721.

Fry B (2006a) Isotope notation and measurement. In: *Stable Isotope Ecology*. Springer New York, New York, NY, p 21–39

Fry B (2006b) Using stable isotope tracers. In: *Stable Isotope Ecology*. Springer New York, New York, NY, p 40–75

Gallaway BJ, Szedlmayer ST, Gazey WJ (2009) A Life History Review for Red Snapper in the Gulf of Mexico with an Evaluation of the Importance of Offshore Petroleum Platforms and Other Artificial Reefs. Reviews in Fisheries Science 17:48–67.

Geary B, Mikulas J, Rooker J (2007) Patterns of Habitat Use by Newly Settled Red Snapper in the Northwestern Gulf of Mexico. American Fisheries Society Symposium.

Goodyear P (1993) Red Snapper in U.S. Waters of the Gulf of Mexico 1992 Assessment. Southeast Fisheries Center Miami Laboratory Coastal Resources Division.

Goolsby DA, Battaglin WA, Aulenbach BT, Hooper RP (2000) Nitrogen flux and sources in the Mississippi River Basin. Sci Total Environ 248:75–86.

Goolsby DA, Battaglin WA, Aulenbach BT, Hooper RP (2001) Nitrogen input to the Gulf of Mexico. J Environ Qual 30:329–336.

Goolsby DA, Battaglin WA, Lawrence GB, Artz RS, Aulenbach BT, Hooper RP, Keeney DR, Stensland GJ (1999) Flux and Sources of Nutrients in the Mississippi–Atchafalaya River Basin Topic 3 Report for the Integrated Assessment on Hypoxia in the Gulf of Mexico . National Oceanic and Atmospheric Administration, Silver Spring, Maryland.

Granneman J (2018) Evaluation of trace-metal and isotopic records as techniques for tracking lifetime movement patterns in fishes. Doctoral dissertation

Gulf of Mexico Fishery Management Council (2004) Final Amendment 22 to the reef fish fishery management plan to set Red Snapper sustainable fisheries act targets and thresholds, set a rebuilding plan, and establish bycatch reporting methodologies for the reef fish fishery. Gulf of Mexico Fishery Management Council, Tampa, Florida.

Gulf of Mexico Fishery Management Council (2007) Joint Amendment 27 to the Reef Fish Fishery Management Plan and Amendment 14 to the Shrimp Fishery Management Plan. Gulf of Mexico Fishery Management Council.

Gulf of Mexico Fishery Management Council (2017) Minimum Stock Size Threshold (MSST) Revision for Reef Fish Stocks with Existing Status Determination Criteria Final Amendment 44 to the Fishery Management Plan for the Reef Fish Resources of the Gulf of Mexico.

Gunter G (1963) The Fertile Fisheries Crescent. Mississippi Academy of Sciences 9:286–290.

Handy SM, Deeds JR, Ivanova NV, Hebert PDN, Hanner RH, Ormos A, Weigt LA, Moore MM, Yancy HF (2011) A single-laboratory validated method for the generation of DNA barcodes for the identification of fish for regulatory compliance. J AOAC Int 94:201–210.

Hendrix JP, Hulet WH, Greenberg MJ (1981) Salinity tolerance and the responses to hypoosmotic stress of the bay squid Lolliguncula brevis, a euryhaline cephalopod mollusc. Comparative Biochemistry and Physiology Part A: Physiology 69:641–648.

Henrichs SM (1992) Early diagenesis of organic matter in marine sediments: progress and perplexity. Marine Chemistry 39:119–149.

Hoellein TJ, Bruesewitz DA, Richardson DC (2013) Revisiting Odum (1956): A synthesis of aquatic ecosystem metabolism. Limnol Oceanogr 58:2089–2100.

Hutchinson GE (1957) Concluding Remarks: Cold Spring Harbor symposium. Quant Biol 22:415–477.

Hypoxia Task Force (2016) The Mississippi/Atchafalaya River Basin (MARB). https://www.epa.gov/ms-htf/mississippiatchafalaya-river-basin-marb

Jackson AL, Inger R, Parnell AC, Bearhop S (2011) Comparing isotopic niche widths among and within communities: SIBER - Stable Isotope Bayesian Ellipses in R. J Anim Ecol 80:595–602.

Jackson GD, Forsythe JW, Hixon RF, Hanlon RT (1997) Age, growth, and maturation of Lolliguncula brevis (Cephalopoda: Loliginidae) in the northwestern Gulf of Mexico with a comparison of length-frequency versus statolith age analysis. Can J Fish Aquat Sci 54:2907–2919.

Jaxion-Harm J, Szedlmayer ST (2015) Depth and artificial reef type effects on size and distribution of Red Snapper in the northern Gulf of Mexico. North American Journal of Fisheries Management 35:86–96.

Jha M, Arnold JG, Gassman PW, Giorgi F, Gu RR (2006) Climate change sensitivity assessment on upper Mississippi River basin stream flows using SWAT. J Am Water Resources Assoc 42:997–1015.

Justić D, Rabalais NN, Turner RE (2005) Coupling between climate variability and coastal eutrophication: Evidence and outlook for the northern Gulf of Mexico. J Sea Res 54:25–35.

Justić D, Rabalais NN, Turner RE (1996) Effects of climate change on hypoxia in coastal waters: A doubled CO_2 scenario for the northern Gulf of Mexico. Limnol Oceanogr 41:992–1003.

Kendall C, Silva SR, Kelly VJ (2001) Carbon and nitrogen isotopic compositions of particulate organic matter in four large river systems across the United States. Hydrol Process 15:1301–1346.

Layman CA, Araujo MS, Boucek R, Hammerschlag-Peyer CM, Harrison E, Jud ZR, Matich P, Rosenblatt AE, Vaudo JJ, Yeager LA, Post DM, Bearhop S (2012) Applying stable isotopes to examine food-web structure: an overview of analytical tools. Biol Rev Camb Philos Soc 87:545–562.

Lee S-A, Kim T-H, Kim G (2020) Tracing terrestrial versus marine sources of dissolved organic carbon in a coastal bay using stable carbon isotopes. Biogeosciences 17:135–144.

Lohrenz SE, Redalje DG, Cai W-J, Acker J, Dagg M (2008) A retrospective analysis of nutrients and phytoplankton productivity in the Mississippi River plume. Continental Shelf Research 28:1466–1475.

Lysy M, Stasko AD, Swanson HK (2014) NicheROVER: (Niche) (R)egion and Niche (Over)lap Metrics for Multidimensional Ecological Niches. R.

Macpherson M (2001) Integrating Ecosystem Management Approaches Into Federal Fishery Management Through The Magnuson-Stevens Fishery Conservation And Management Act. Ocean & Coastal L J 6:1–32.

Madigan DJ, Litvin SY, Popp BN, Carlisle AB, Farwell CJ, Block BA (2012) Tissue turnover rates and isotopic trophic discrimination factors in the endothermic teleost, pacific bluefin tuna (Thunnus orientalis). PLoS ONE 7:e49220.

McCawley J, Cowen JH (2007) Seasonal and Size Specific Diet and Prey Demand of Red Snapper on Alabama Artificial Reefs. American Fisheries Society Symposium 60:77–104.

McCawley JR, Cowan JH, Shipp RL (2006) Feeding Periodicity and Prey Habitat Preference of Red Snapper, *Lutjanus campechanus* (Poey, 1860) on Alabama Artificial Reefs. goms 24.

McCormack SA, Trebilco R, Melbourne-Thomas J, Blanchard JL, Fulton EA, Constable A (2019) Using stable isotope data to advance marine food web modelling. Rev Fish Biol Fish 29:277–296.

Mceachran J, Fechhelm JD (1998) Fishes Of The Gulf Of Mexico, Vol. 1: Myxiniformes To Gasterosteiformes, 1st ed. University Of Texas Press, Austin.

McEachran JD, Fechhelm JD (2006) Fishes of the Gulf of Mexico, Volume 2: Scorpaeniformes to Tetraodontiformes, Illustrated. University of Texas Press, Austin.

Meath B, Peebles EB, Seibel BA, Judkins H (2019) Stable isotopes in the eye lenses of Doryteuthis plei (Blainville 1823): Exploring natal origins and migratory patterns in the eastern Gulf of Mexico. Continental Shelf Research 174:76–84.

Milliman JD (2001) Delivery and fate of fluvial water and sediment to the sea: a marine geologist's view of European rivers. Sci Mar 65:121–132.

Mitsch WJ, Day JW, Zhang L, Lane RR (2005) Nitrate-nitrogen retention in wetlands in the Mississippi River Basin. Ecol Eng 24:267–278.

Murphy RR, Curriero FC, Ball WP (2010) Comparison of spatial interpolation methods for water quality evaluation in the Chesapeake Bay. J Environ Eng 136:160–171.

Nash RDM, Valencia AH, Geffen AJ (2006) The Origin of Fulton's Condition Factor—Setting the Record Straight. Fisheries 31.

Nicol JAC (1989) The Eyes of Fishes. Oxford Science Publications, Oxford.

Nielsen SS (1998) Pigment Analysis. In: *Instructor's manual for food analysis: second edition*. Nielsen SS (ed) Springer US, Boston, MA, p 67–69

Nunnally CC, Rowe GT, Thornton DCO, Quigg A (2013) Sedimentary oxygen consumption and nutrient regeneration in the northern Gulf of Mexico hypoxic zone. Journal of Coastal Research 63:84–96.

Odum EP (1980) The status of three ecosystem-level hypotheses regarding salt marsh estuaries: Tidal subsidy, outwelling, and detritus-based food chains. In: *Estuarine Perspectives*. KENNEDY VS (ed) Academic Press, p 485–495

Osborne J (2010) Improving your data transformations: Applying the Box-Cox transformation. University of Massachusetts Amherst.

Parnell AC (2019) Simmr: A Stable Isotope Mixing Model. R.

Parra SM, Sanial V, Boyette AD, Cambazoglu MK, Soto IM, Greer AT, Chiaverano LM, Hoover A, Dinniman MS (2020) Bonnet Carré Spillway freshwater transport and corresponding biochemical properties in the Mississippi Bight. Continental Shelf Research 199:104114.

Peebles EB, Hollander DJ (2020) Combining Isoscapes with Tissue-Specific Isotope Records to Recreate the Geographic Histories of Fish. In: *Scenarios and responses to future deep oil spills: fighting the next war*. Murawski SA, Ainsworth CH, Gilbert S, Hollander DJ, Paris CB, Schlüter M, Wetzel DL (eds) Springer International Publishing, Cham, p 203–218

Peterson BJ, Fry B (1987) Stable Isotopes in Ecosystem Studies. Annu Rev Ecol Syst 18:293–320.

Porch CE, Fitzhugh GR, Linton BC (2013) Modeling the dependence of batch fecundity and spawning frequency on size and age for use in stock assessments of red snapper in U.S. Gulf of Mexico waters. SEDAR, North Charleston, SC.

Post DM (2002) USING STABLE ISOTOPES TO ESTIMATE TROPHIC POSITION: MODELS, METHODS, AND ASSUMPTIONS. Ecology 83:703–718.

Powers SP, Drymon JM, Hightower CL, Spearman T, Bosarge GS, Jefferson A (2018) Distribution and Age Composition of Red Snapper across the Inner Continental Shelf of the North-Central Gulf of Mexico. Trans Am Fish Soc 147:791–805.

Quaeck-Davies K, Bendall VA, MacKenzie KM, Hetherington S, Newton J, Trueman CN (2018) Teleost and elasmobranch eye lenses as a target for life-history stable isotope analyses. PeerJ 6:e4883.

Quiñones-Rivera ZJ, Wissel B, Justić D, Fry B (2007) Partitioning oxygen sources and sinks in a stratified, eutrophic coastal ecosystem using stable oxygen isotopes. Mar Ecol Prog Ser 342:69–83.

Rabalais NN, Turner RE, Dortch Q, Justic D, Bierman VJ, Wiseman WJ (2002) Nutrient-enhanced productivity in the northern Gulf of Mexico: past, present and future. In: *Nutrients and Eutrophication in Estuaries and Coastal Waters: Proceedings of the 31st Symposium of the Estuarine and Coastal Sciences Association (ECSA), held in Bilbao, Spain, 3–7 July 2000*. Orive E, Elliott M, de Jonge VN (eds) Springer Netherlands, Dordrecht, p 39–63

Rabalais NN, Turner RE, Justić D, Dortch Q, Wiseman WJ, Gupta BKS, Justic D (1996) Nutrient changes in the Mississippi River and system responses on the adjacent continental shelf. Estuaries 19:386.

Rabalais NN, Turner RE (2019) Gulf of Mexico hypoxia: past, present, and future. Limnology and Oceanography Bulletin 28:117–124.

Rahav E, Bar-Zeev E, Ohayon S, Elifantz H, Belkin N, Herut B, Mulholland MR, Berman-Frank I (2013) Dinitrogen fixation in aphotic oxygenated marine environments. Front Microbiol 4:227.

Redfield AC (1958) The biological control of chemical factors in the environment. Am Sci 46:230A, 205–221.

Rester JK (2015) SEAMAP Environmental and biological atlas of the Gulf of Mexico 2013. Gulf States Marine Fisheries Commission.

Richards WJ (ed) (2005) Early stages of Atlantic fishes. CRC Press.

Ricker WE (1978) Computation and interpretation of biological statistics of fish populations (Bulletin of the Fisheries Research Board of Canada), Reprint. Minister of Supply Canada.

Rooker JR, Landry AM, Geary BW, Harper JA (2004) Assessment of a shell bank and associated substrates as nursery habitat of post settlement Red Snapper. Estuar Coast Shelf Sci 59:653–661.

Russell M, Montagna P (2007) Spatial and Temporal Variability and Drivers of Net Ecosystem. Estuaries Coast 30:137–153.

Sanial V, Shiller AM, Joung D, Ho P (2019) Extent of Mississippi River water in the Mississippi Bight and Louisiana Shelf based on water isotopes. Estuar Coast Shelf Sci 226:106196.

Santschi PH, Oktay SD, Cifuentes L (2007) Carbon isotopes and iodine concentrations in a Mississippi River delta core recording land use, sediment transport, and dam building in the river's drainage basin. Mar Environ Res 63:278–290.

Schiller RV, Kourafalou VH, Hogan P, Walker ND (2011) The dynamics of the Mississippi River plume: Impact of topography, wind and offshore forcing on the fate of plume waters. J Geophys Res 116.

Schlacher TA, Connolly RM, Skillington AJ, Gaston TF (2009) Can export of organic matter from estuaries support zooplankton in nearshore, marine plumes? Aquat Ecol 43:383–393.

Simonsen KA, Cowan JH, Boswell KM (2015) Habitat differences in the feeding ecology of red snapper (Lutjanus campechanus, Poey 1860): a comparison between artificial and natural reefs in the northern Gulf of Mexico. Environ Biol Fishes 98:811–824.

Strickland JDH, Parsons TR (1972) A Practical Handbook of Seawater Analysis, 2nd ed. Stevenson JC (ed) Ottawa.

Stumpf RP, Gelfenbaum G, Pennock JR (1993) Wind and tidal forcing of a buoyant plume, Mobile Bay, Alabama. Continental Shelf Research 13:1281–1301.

Swanson HK, Lysy M, Power M, Stasko AD, Johnson JD, Reist JD (2015) A new probabilistic method for quantifying n-dimensional ecological niches and niche overlap. Ecology 96:318–324.

Syväranta J, Lensu A, Marjomäki TJ, Oksanen S, Jones RI (2013) An empirical evaluation of the utility of convex hull and standard ellipse areas for assessing population niche widths from stable isotope data. PLoS ONE 8:e56094.

Szedlmayer S, Lee J (2004) Diet shifts of juvenile Red Snapper (*Lutjanus campechanus*) with changes in habitat and fish size. Fishery bulletin 102:366–375.

Szedlmayer ST, Brewton RA (2019) Diet Analyses of Red Snapper, Lutjanus campechanus, Based on DNA Barcoding from Artificial Reefs in the Northern Gulf of Mexico. In: *Red snapper biology in a changing world*. Szedlmayer ST, Bortone SA (eds) CRC Press, p 143–165

Tarnecki JH, Patterson WF (2015) Changes in red snapper diet and trophic ecology following the deepwater horizon oil spill. Marine and Coastal Fisheries 7:135–147.

Thayer GW, Govoni JJ, Connally DW (1983) Stable carbon isotope ratios of the planktonic food web in the northern Gulf of Mexico. Bulletin of marine science 33:247–256.

Thomas SM, Crowther TW (2015) Predicting rates of isotopic turnover across the animal kingdom: a synthesis of existing data. J Anim Ecol 84:861–870.

Topolski MF, Szedlmayer ST (2004) Vertical distribution, size structure, and habitat associations of four blenniidae species on gas platforms in the northcentral gulf of mexico. Environ Biol Fishes 70:193–201.

Trefry JH, Metz S, Nelsen TA, Trocine RP, Eadie BJ (1994) Transport of particulate organic carbon by the Mississippi River and its fate in the Gulf of Mexico. Estuaries 17:839.

Turner RE, Rabalais NN, Alexander RB, McIsaac G, Howarth RW (2007) Characterization of nutrient, organic carbon, and sediment loads and concentrations from the Mississippi River into the northern Gulf of Mexico. Estuaries Coast 30:773–790.

Turner RE, Rabalais NN, Swenson EM, Kasprzak M, Romaire T (2005) Summer hypoxia in the northern Gulf of Mexico and its prediction from 1978 to 1995. Mar Environ Res 59:65–77.

Tzadik OE, Curtis JS, Granneman JE, Kurth BN, Pusack TJ, Wallace AA, Hollander DJ, Peebles EB, Stallings CD (2017) Chemical archives in fishes beyond otoliths: A review on the use of other body parts as chronological recorders of microchemical constituents for expanding interpretations of environmental, ecological, and life-history changes. Limnol Oceanogr Methods 15:238–263.

VanderKooy S, Carroll J, Elzey S, Gilmore J, Kipp J (eds) (2020) A Practical Handbook for Determining the Ages of Gulf of Mexico and Atlantic Coast Fishes, 3rd ed. Gulf States Marine Fisheries Commission.

Vander Zanden MJ, Clayton MK, Moody EK, Solomon CT, Weidel BC (2015) Stable isotope turnover and half-life in animal tissues: a literature synthesis. PLoS ONE 10:e0116182.

Vecchio JL, Ostroff JL, Peebles EB (2021) Isotopic characterization of lifetime movement by two demersal fishes from the northeastern Gulf of Mexico. Mar Ecol Prog Ser 657:161–172.

Vecchio JL, Peebles EB (2020) Spawning origins and ontogenetic movements for demersal fishes: An approach using eye-lens stable isotopes. Estuar Coast Shelf Sci 246:107047.

Wallace AA, Hollander DJ, Peebles EB (2014) Stable isotopes in fish eye lenses as potential recorders of trophic and geographic history. PLoS ONE 9:e108935.

Wang X-C, Chen RF, Gardner GB (2004) Sources and transport of dissolved and particulate organic carbon in the Mississippi River estuary and adjacent coastal waters of the northern Gulf of Mexico. Mar Chem 89:241–256.

Wells RJD, Cowan JH, Fry B (2008) Feeding ecology of Red Snapper *Lutjanus campechanus* in the northern Gulf of Mexico. Mar Ecol Prog Ser 361:213–225.

Whitfield AK (1996) Fishes and the environmental status of South African estuaries. Fish Manag Ecol 3:45–57.

Wride MA (2011) Lens fiber cell differentiation and organelle loss: many paths lead to clarity. Philos Trans R Soc Lond B Biol Sci 366:1219–1233..